

DESY, August 2006, TESLA-FEL 2006-05

# **Layout Considerations on the 25GeV / 300kW Beam Dump of the XFEL Project**

**M. Maslov<sup>1)</sup>, M. Schmitz<sup>2)</sup>, V. Sychev<sup>1)</sup>**

<sup>1)</sup> IHEP, Protvino, Russia, <sup>2)</sup> DESY, Hamburg, Germany

# Layout Considerations on the 25GeV / 300kW Beam Dump of the XFEL Project

M. Maslov<sup>1)</sup>, M. Schmitz<sup>2)</sup>, V. Sychev<sup>1)</sup>

<sup>1)</sup> IHEP, Protvino, Russia, <sup>2)</sup> DESY, Hamburg, Germany

## Table of Contents

Abstract .....	2
1 Introduction .....	2
2 Basic Layout Considerations.....	4
2.1 Dump Core Material Selection.....	6
2.1.1 Remarks on Spot Size Limit.....	9
2.2 Radial Layout .....	10
2.2.1 Homogeneous radial Layout using one Material .....	10
2.2.2 Segmented radial Layout with Graphite Core.....	14
2.3 Back Stopper .....	17
2.3.1 Further Optimization of Dump Length .....	19
3 Baseline Design of the 25GeV / 300kW Dump with slow Sweeping.....	20
3.1 Consequences of slow Sweeping a pulsed Beam.....	23
3.1.1 Reasonable Choice of Sweeping Frequency .....	24
3.1.2 Analysis of Stresses and Temperatures in the Dump.....	27
3.1.2.1 Without Beam Sweep .....	29
3.1.2.2 With Beam Sweep .....	30
3.2 Heat Transfer at the Graphite-Copper Boundary .....	38
3.2.1 Pressed Contact .....	38
3.2.2 Brazed Contact .....	41
4 Alternative Dump Designs without slow Sweeping .....	41
4.1 Pyrolytic Graphite Dump Core .....	42
4.2 Upstream Spoilers .....	45
4.3 Segmented Graphite Dump Core .....	48
4.3.1 Energy Deposition in the segmented Dump Core.....	49
4.3.2 Heat Extraction in the segmented Dump Core.....	53
4.3.3 Longitudinal Temperature Profiles of the segmented Dump Layout.....	55
5 Comparative Summary.....	58
A Fundamentals on Energy Deposition in an Electron Dump.....	60
A.1 Electromagnetic Shower (EMS) Development.....	60
A.1.1 Longitudinal Characterization.....	62
A.1.2 Radial Characterization .....	63
B Fundamentals on Dump Heating.....	66
B.1 Instantaneous Heating .....	69
B.2 Heat Diffusion .....	70
B.3 Average Heating.....	70
References .....	72

## **Abstract**

The European X-Ray Free Electron Laser (XFEL) project, which is currently under design at DESY, requires 3 beam dumps downstream of the accelerator. By means of energy deposition, temperature and mechanical stress calculations the layout of a solid edge cooled beam dump is presented. This dump is able to withstand a high cyclic impact, as induced by each subsequent bunch train of up to  $2.5 \cdot 10^{13}$  electrons in combination with a large amount of dissipated power density ( $\approx 1.8 \text{ kW/cm}$ ) coming from a beam with an average power of up to 300kW at a variable energy up to 25GeV. The cyclic impact is faced by using graphite as a core material in the dump and setting a lower limit for the incoming beam size at  $\sigma_{\text{beam}} \geq 2 \text{ mm}$ . Introducing a slow (not within the bunch train) circular beam sweep answers the question of heat extraction.

Alternative layouts are investigated in order to avoid active beam sweeping. Unfortunately more severe risks and disadvantages are coming along with them. That is why these solutions are not regarded as reliable alternatives and the dump design with beam sweeping is considered to be the baseline solution, for which a technical layout is under way.

## **1 Introduction**

The XFEL facility phase 1 will be equipped with 3 beam dumps downstream of the linac. Two of them are housed in dedicated buildings (XSDU1 and XSDU2). During normal FEL operation they are obviously required to abort the electrons at the end of each of the two possible electron routes through the various undulators. A third dump station is located at the end of the linac tunnel (XTL) in the separation building (XS1). This dump will be used during commissioning of the linac and for machine protection in emergency cases. But even in regular FEL mode it is intended, that this dump takes those bunches, which are removed in the process of delivering special bunch patterns to the undulator beam lines, while identical bunch trains are accelerated in the linac in order to simplify its stable operation. These dumps are called main dumps. They are completely identical and their limits, which will be motivated in a moment, are specified in Table 1.

The linac, which drives the XFEL facility, is able to deliver trains of electron bunches in the energy range  $E_0$  up to 25GeV with a repetition rate  $\nu_t$  of up to 10Hz [1]. The maximum

$E_0$ , electron energy	$\leq 25 \text{ GeV}$
$P_{\text{ave}}$ , average beam power	$\leq 300 \text{ kW}$
$I_{\text{ave}}$ , average beam current	$\leq 40 \mu\text{A}$
$N_t$ , # of electrons per bunch train	$\leq 2.5 \cdot 10^{13} e^- \Leftrightarrow 4 \mu\text{C}$
$T_t$ , length of bunch trains	$\leq 0.8 \text{ ms}$
$\nu_t$ , repetition rate of bunch trains	$\leq 10 \text{ Hz}$
$W_t$ , energy carried in one bunch train	$\leq 100 \text{ kJ}$
required beam size at dump entrance resp. window	$\sqrt{\sigma_{x,\text{min}} \cdot \sigma_{y,\text{min}}} \geq 2 \text{ mm}$
relative energy leakage	$\leq 1 \%$
lifetime	$\approx 10 \text{ to } 20 \text{ years}$

*Table 1:* Specification of the main beam dumps for the XFEL.

population within one bunch train will not exceed 4000 bunches, interspaced in time not less than  $T_{bb} = 200\text{ns}$  and carrying a maximum charge of  $1\text{ nC} (= 6.25 \cdot 10^9 e^-)$  each. Thus a bunch train is up to  $T_t \leq 0.8\text{ms}$  long and contains not more than  $N_t \leq 2.5 \cdot 10^{13}$  electrons ( $= 4\mu\text{C}$ ).

At maximum conditions the linac beam carries a substantial amount of average power  $P_{ave}$  of around  $1\text{MW} (40\mu\text{A} \cdot 25\text{GeV})$ , but the main dumps are specified to  $300\text{kW}$  only. This limit is a consequence of a more fundamental previously taken decision to use a solid absorber in order to avoid the complexity and the risks, which are associated with a liquid dump (e.g. water). As will be seen in this report, the  $300\text{kW}$  limit at the given beam energy is still a reasonable level to be taken by a graphite based solid absorber solution. Furthermore this power restriction is less severe than it might look like at the first sight, since it allows linac operation at the nominal parameters ( $20\text{GeV}$ , 3000 bunches with  $1\text{nC}$  each,  $10\text{Hz}$ ), if the beam is in average evenly distributed into the two beam lines. Actually an operation at almost maximum linac beam power is possible, if it is distributed more or less evenly amongst all 3 main dumps. In that sense control of the correct switchyard functioning plays an important role.

Independent of average power the main dump has to be capable of taking a full bunch train with a charge of  $4\mu\text{C}$ . As derived in annex B, the related heating is quasi instantaneous and depends on the size of the impinging beam. Hence the required lower spot size limit at the dump entrance as specified in Table 1 is already a result of the dump design. It should enable a safe and reliable long term operation over the whole lifetime of the facility, which is at least 10 years respectively more than  $10^9$  bunch train passages at  $10\text{Hz}$ .

For shielding reasons the absorber is placed approximately  $2\text{m}$  deep in a dead end hole of the surrounding concrete shield, which is part of the building, the dump is located in. All supplying infrastructure (cooling water pipes, temperature control cabling, ...) and the beam pipe have to be extended by this length of  $2\text{m}$ , in order to allow disconnection respectively connection outside of the concrete. The absorber itself together with this front extension represents one single part, the so called dump module. Installation and exchange in the XFEL facility requires the dump module not to exceed an overall length of  $6\text{m}$  (access shafts, transportation in the tunnel) a diameter of  $1\text{m}$  and a total weight of  $10\text{ tons}$  (cranes). Subtracting the  $2\text{m}$  length of the front part, results in a maximum of  $4\text{m}$  for the length of the pure absorber.

By means of simplified but conservative calculations, the next chapter 2 motivates the material selection and optimizes the radial as well as the longitudinal layout of a solid dump in terms of compactness but without exceeding heating or stress limits. Chapter 3 presents a more detailed analysis of this layout and emphasizes the key questions to be solved technically regarding heat extraction. While the baseline design operates with a slow circular beam sweeping system in order to dilute the heat source and reduce average heating in the dump, chapter 4 informs about alternative solutions, which avoid such an active system, but introduce other disadvantages. The summary in chapter 5 compares all presented options briefly and concludes the slow sweeping solution to be the most preferable.

The basis of all electron dump layout considerations is heating and correlated mechanical stress as a consequence of energy deposition by electromagnetic shower development. In chapters 2 to 4 the results of shower, heating and stress calculations are discussed in order to draw conclusions, but the analytical background of the most often used parameters, their interdependencies and the applied calculations or approximations can not be explained there in depth. For readers of this report, who are not that familiar in this field, it is recommended to study annex A and B first, where the required knowledge is summarized in detail and to which will be partially referred to during the discussion of results anyway.

## 2 Basic Layout Considerations

We are aiming for a cylindrical absorber of length  $L$ , which is water cooled at its outer radial surface at  $r=R$ . The temperature of the cooling water is called  $T_0$ . For the planned dump cooling system the forward and return water temperatures are expected to be  $40^\circ\text{C}$  and  $70^\circ\text{C}$  respectively. As an average value  $T_0$  can be set to about  $50^\circ\text{C}$ , which is generally used in the frame of this work unless otherwise stated, e.g. in section 3.1.2, where  $T_0=20^\circ\text{C}$  is assumed.

An edge cooled solid absorber for relatively high beam power is dominated by its heat extraction capabilities. The bulk part ( $\approx 90\%$ ) of the beam power is dissipated near the shower axis within one Molière radius and has to flow radially towards the cooled circumference. The less the power dissipated per unit length  $dP/dz$  and the radial thermal resistance of the layout are, the smaller the equilibrium temperature level inside of the dump will be. A small  $dP/dz$  can be achieved by stretching the shower when using materials of low mass density. A low radial thermal resistance is achieved by materials of high thermal conductivity and by making the radial distance towards the cooling water as small as possible, i.e. by reducing the radial thickness of the dump. Low density materials and small thickness are contradictory constraints in terms of energy capture, which requires a certain radial size of about  $R_{99\%} \approx 5 \cdot R_M$ .

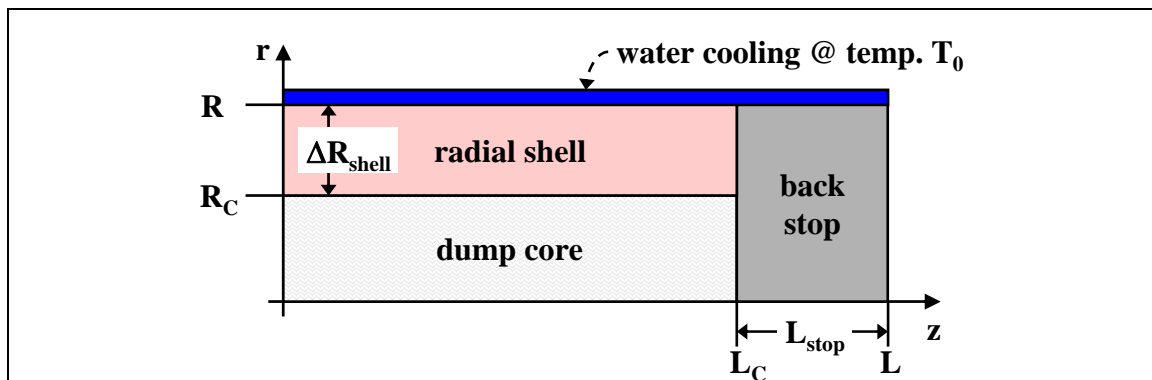


*Figure 1:* Schematic cylindrical layout of the desired edge cooled solid dump solution.

Combining thermal, energy capture and compactness constraints leads to a segmentation into a low  $\rho$  core embedded in a higher  $\rho$  radial shell of high thermal conductivity and in good thermal contact with the core material. By this means both, radial size and radial thermal resistance are reduced, while the radial tail of the shower is still captured. The longitudinal shower tail is captured by a backstop of again high  $\rho$  material behind the dump core and gains compactness in length. As a consequence the layout of the desired dump will look like as sketched in Figure 1.

According to the mentioned constraints, materials of interest for such a dump layout are graphite, aluminium and copper. They have good thermal properties, are available in larger quantities without problem and can be machined in an uncomplicated and non hazardous way. Table 2 summarizes their properties of interest. The first part shows the parameters, which are relevant for shower processes. As explained in annex A,  $R_{99\%}$  and  $L_{99\%}$  quantify the expected size of a non structured dump simply made out of one uniform material, in order to fulfil the 99% energy containment constraint independent of other aspects like e.g. heating. After that the melting temperature  $T_{\text{melt}}$  and a reasonable maximum operation temperature  $T_{\text{op}}$  are mentioned. In the case of Al and Cu such a limit is determined by the level beyond which they significantly lose their mechanical strength. Graphite should not be operated above temperatures of  $500^\circ\text{C}$  to  $600^\circ\text{C}$  when exposed to air. Beyond that level a slow chemical

reaction with the oxygen of the air would commence. But in a noble gas atmosphere or under vacuum, graphite can run up to much higher temperatures without problem.

The last block of parameters in Table 2 are related to mechanical stress development as a consequence of thermal expansion during heating processes. Especially the dump core is heavily affected by pulsed heating and therefore cyclic stress load. In that respect the endurance limit  $\sigma_u$  is the upper stress limit, which does not create damage or fatigue effects in the material after a certain number of mechanical cycles. The value stated here is valid for about  $10^7$  to  $10^8$  cycles. Since  $\sigma_u$  shows already a flat behaviour there, it is justified to apply this value also for our application, where more than  $10^9$  cycles are required, but material data is not available. The yield strength or plasticity limit, at which a non elastic elongation of 0.2% remains after relaxation, is called  $\sigma_{0.2}$ . The elastic modulus is named E, the coefficient of linear thermal expansion is expressed by  $\alpha$  and  $\nu$  is used for the Poisson number, which is the ratio between transversal elongation and longitudinal shrinkage in the presence of longitudinal compressive stress.

The specific heat capacity  $c$  and the thermal conductivity  $\lambda$  are displayed in Figure 2 and

	Graphite	Aluminium	Copper
A	12.01	26.98	63.54
Z	6	13	29
$\rho$ [g/cm <sup>3</sup> ]	1.71	2.7	8.96
$E_c$ [MeV]	75.9	40	18.8
$X_0$ [cm]	25.1	8.89	1.44
$R_M$ [cm]	7	4.7	1.6
$R_{99\%}$ [cm]	35	23.5	8
$L_{99\%}$ [cm]	383	159	30
$T_{melt}$ [°C]	3800	660	1083
$T_{op}$ [°C]	500 - 600 <sup>3)</sup>	$\leq 250$	$\leq 200$
E [GPa]	13 (11-15)	70	120
$\alpha$ [ $10^{-6}/K$ ]	7 (6-8)	26	17
$\sigma_{0.2}$ [MPa]	---	200 - 400	150 - 400
$\sigma_u$ [MPa]	60 <sup>1)</sup> / 30 <sup>2)</sup>	80 - 120	60 - 100
$\nu$	0.26	0.31	0.38

<sup>1)</sup> at compression / <sup>2)</sup> at tension; <sup>3)</sup> at normal air

*Table 2:* Required properties of the materials to be used for a solid beam dump design.

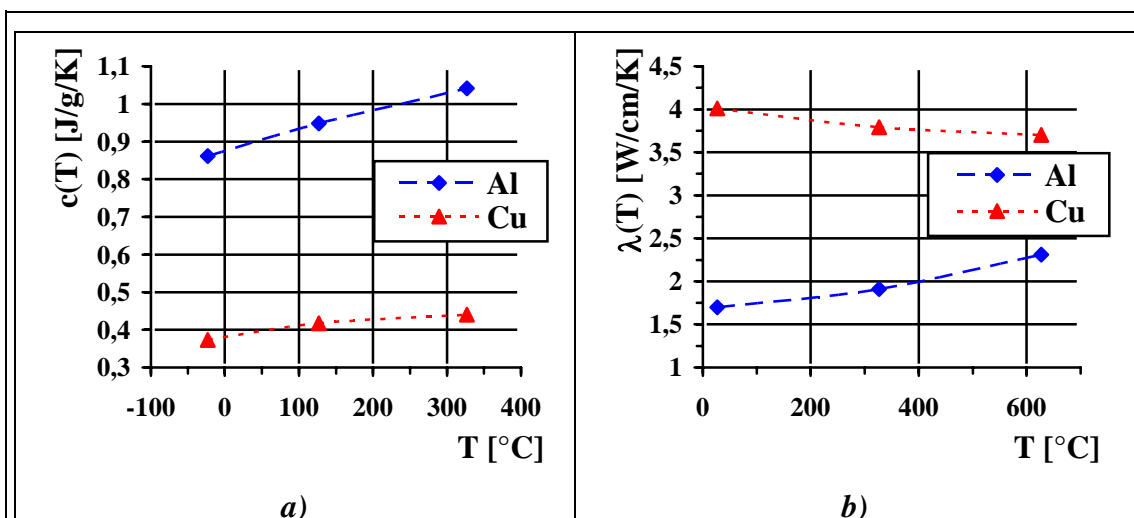


*Figure 2:* a) Specific heat capacity  $c(T)$  and b) thermal conductivity  $\lambda(T)$  of aluminium and copper as a function of temperature  $T$ .

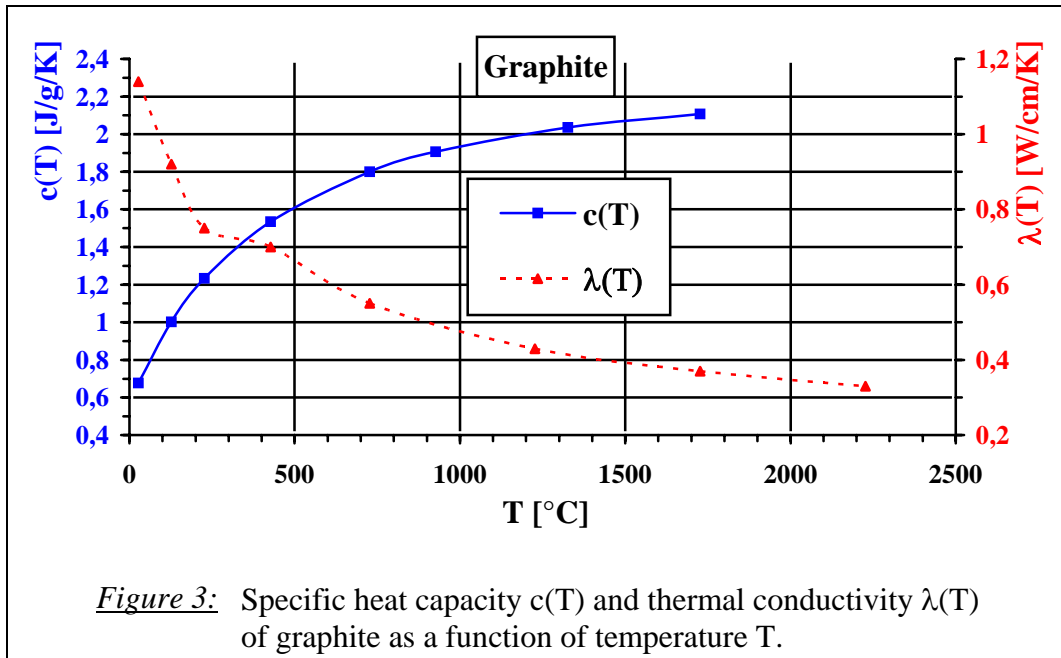


Figure 3 as a function of temperature. Especially for graphite this dependence is quite significant and the specific heat capacity can be fitted quite well by:

$$c(T) = 1.48 \frac{\text{J}}{\text{g} \cdot \text{K}} \cdot \left( 1.44 - e^{-T/511^\circ\text{C}} \right) \quad \text{for graphite} \quad \text{Equation 1}$$

It is not reasonable to do the same for the thermal conductivity of graphite, because it depends on the degree of graphitization and thus on the particular kind, that will be chosen. The given curve represents a typical behaviour qualitatively and quantitatively.

Based on the given material properties, the following sections solve the questions of material choice and dimensions of the desired dump layout as sketched in Figure 1. This solution meets the requirements as listed in Table 2 and is regarded as the baseline design, which is closer looked at in chapter 3.

As a main tool the monte carlo code MARS [2] is used to obtain the spatial distribution of deposited energy  $\varepsilon(r,z)$ , from which temperature profiles are derived by the methods explained in annex B.

## 2.1 Dump Core Material Selection

The dump core is intended to capture the bulk part of the energy, which is deposited by the EMS. Therefore the material of the core in combination with the radial heat flow is responsible for the equilibrium temperature level in the dump. Estimated by means of Equation 38 the maximum longitudinal power density dissipated by a 7.5GeV / 300kW beam in graphite, aluminium and copper is 1.84kW/cm, 4.6kW/cm and 27kW/cm respectively. As will be seen more evidently in section 2.2.1 the latter two values are out of question in terms of heat extraction. This is one reason why a material like graphite with low  $\rho$  and high  $E_c$  is preferred, but a more stringent condition comes from the pulsed beam operation.

The dump core is heavily affected by cyclic stress as a consequence of the instantaneous heating process due to the passage of each bunch train. In order to guarantee a long term operation without damage or fatigue effects, this cyclic stress has to stay below the endurance strength limit  $\sigma_u$  of the material. Since temperature jump and induced stress are correlated by thermal expansion, one can define a tolerable instantaneous temperature jump  $\text{tol}(\Delta T_{\text{inst}})$  for which the induced stress is just at the endurance limit:

$$\text{tol}(\Delta T_{\text{inst}}) = (1 - \nu) \cdot \frac{\sigma_u}{\alpha \cdot E} \quad \text{Equation 2}$$

Here  $\nu$  is the Poisson number,  $\sigma_u$  the endurance limit,  $\alpha$  the coefficient of linear thermal expansion and  $E$  the elastic modulus. This result can be obtained, when a cylindrical volume element is heated up by  $\text{tol}(\Delta T_{\text{inst}})$ , but can only expand longitudinally, while its radial dimensions are forced to stay constant [3]. Let us consider a volume element in the dump, where we find the maximum instantaneous temperature rise  $\text{max}(\Delta T_{\text{inst}})$ . The longitudinal instantaneous temperature profile is quite smooth compared to the radial one, as can be seen in the  $dE/dm$  profiles for graphite material in Figure 17 and Figure 18 b). That is why the longitudinal expansion will create negligible stress. The radial temperature profile is quite sharp and can be conservatively approximated by a step function. In other words our volume element is heated, while the radial neighbourhood stays cold and prevents our enclosed volume element to expand radially. In practice the situation is a little more relaxed, since the actual radial temperature profile is not step-like, but can be expressed by the Grindhammer function with the appropriate width (see Equation 43). In that sense Equation 2 is a conservative limit for our problem. According to the given assumptions the resulting stress is

	<b>Graphite</b>	<b>Aluminium</b>	<b>Copper</b>
$\text{tol}(\Delta T_{\text{inst}})$ [K]	480 <sup>1)</sup> / 240 <sup>2)</sup>	30 - 45	18 - 30
<b><math>\text{tol}(dE/dm)</math> [J/g] @ <math>T_i = 20^\circ\text{C}</math></b>	<b>580 / 240</b>	<b>30 - 45</b>	<b>7 - 12</b>
@ $E_0 = 25\text{GeV}$ , $N_t = 2.5 \cdot 10^{13} e^-$ , $\sigma_{\text{beam}} = 2\text{mm}$			
<b><math>N_t \cdot \text{max}(dE/dm)</math> [J/g]</b>	<b>248</b>	<b>520</b>	<b>1520</b>
$\text{max}(dE/dm)$ [GeV/g/e]	0.062	0.13	0.38

<sup>1)</sup> from compressive / <sup>2)</sup> from tensile endurance strength limit

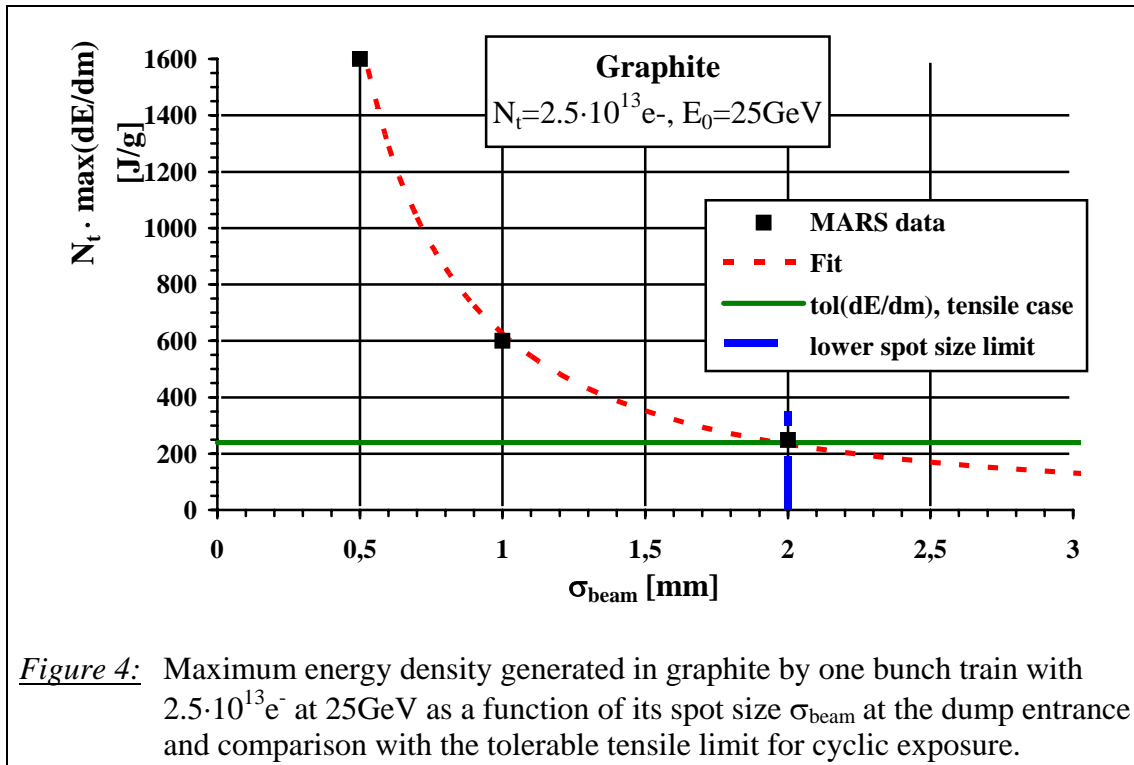
**Table 3:** Tolerable instantaneous temperature rise  $\text{tol}(\Delta T_{\text{inst}})$  and corresponding energy density  $\text{tol}(dE/dm)$  as derived from the endurance strength in comparison with the energy density as deposited by one bunch train populated with  $N_t = 2.5 \cdot 10^{13} e^-$  at  $E_0 = 25\text{GeV}$  and a size of  $\sigma_{\text{beam}} = 2\text{mm}$ .

purely compressive and not tensile.

Table 3 lists the tolerable instantaneous temperature jumps  $\text{tol}(\Delta T_{\text{inst}})$  for graphite, aluminium and copper together with the corresponding tolerable energy density  $\text{tol}(dE/dm)$ :

$$\text{tol}\left(\frac{dE}{dm}\right) = \int_{T=T_i}^{T_i + \text{tol}(\Delta T_{\text{inst}})} c(T) dT \quad \text{Equation 3}$$

Since  $c(T)$  increases with temperature  $T_i$  was set to  $20^\circ\text{C}$  in this table and is valid for the case, that a cold absorber is hit by one bunch train. The tolerable energy density has to be compared with the actual maximum energy density created by one bunch train. From explanations in annex A.1.2 especially from Equation 45 we know, that  $\text{max}(dE/dm)$  not only depends on the material properties, but also increases with rising energy  $E_0$  and falling size of the incoming beam. Figure 4 plots the maximum energy density  $N_t \cdot \text{max}(dE/dm)$  created by one bunch train of  $N_t = 2.5 \cdot 10^{13}$  electrons versus the size  $\sigma_{\text{beam}}$  of a radially round gaussian distributed beam at  $E_0 = 25\text{GeV}$ .



Although the induced stress is really dominated by compressive effects, the lower value of the tolerable energy density for cyclic applications as derived from the tensile endurance strength of 30MPa is indicated as a conservative limit in this figure too. Hence an operation below this limit of 240J/g requires a spot size of  $\sigma_{\text{beam}} \geq 2\text{mm}$  at the entrance of a graphite absorber. For the same conditions Table 3 lists also the energy density, which would occur in an aluminium or copper absorber. They exceed their tolerable limit by at least one order of magnitude and can not be used as a dump core material. That is the main reason why the high thermal and mechanical stress limits in combination with its low density and relatively good thermal conductivity, make graphite the most preferred material to be used in a core of a solid dump for pulsed beams with high pulse charge and high power.

Table 4 gives an overview of the parameters relevant for heating in a graphite absorber. For a constant bunch population the maximum spatial energy density occurs at the highest possible energy, which is 25GeV and determines instantaneous heating processes. At a constant average beam power of  $P_{\text{ave}} = 300\text{kW}$  one notes, that the maximum longitudinal power density is generated in the 7.5GeV case, since the shower is shorter there than at 25GeV. Below 7.5GeV the power of 300kW can not be achieved anymore, because the average beam current is limited to  $I_{\text{ave}} \leq 40\mu\text{A}$  according to the specifications in Table 1.

That is why the 7.5GeV / 40 $\mu\text{A}$  respectively 7.5GeV / 300kW situation determines the maximum average heat load and is relevant when dealing with heat extraction and equilibrium temperature level calculations. On the other hand maximum instantaneous heating and cyclic stress is expected at the high energy 25GeV condition. Especially for a low average temperature level  $T_i$  in the absorber, a more severe cyclic stress situation develops due to the growth of specific heat capacity with increasing temperature. Therefore a beam operation with low repetition rate but fully populated bunch trains is regarded to be the worst case for instantaneous heating and related cyclic stress. In Table 4 the maximum instantaneous temperature rise is calculated for a graphite absorber being “cold” (20°C) and around its maximum operation temperature at 420°C as well as at an intermediate temperature of 220°C.

<b>Parameters of a Graphite absorber relevant for heating</b>								
@ max. spatial energy density per one e- and for $N_t = 2.5 \cdot 10^{13}$					@ max. longitudinal energy density per one e- and for $P_{ave} = 300kW$			
$E_0$	z-pos. = $t_E$	$\max\left(\frac{dE}{dm}\right)$	$N_t \cdot$ $\max\left(\frac{dE}{dm}\right)$	$\Rightarrow$ $\max(\Delta T_{inst})$ @ $T_i [^\circ C] =$ <b>20 / 220 / 420</b>	z-pos. = $t_{max}$	$\max\left(\frac{dE}{dz}\right)$	$I_{ave}$	$\max\left(\frac{dP}{dz}\right)$
[GeV]	[cm]	[GeV/g]	[J/g]	[K]	[cm]	[GeV/cm]	[ $\mu A$ ]	[W/cm]
<b>7.5</b>	<b>45</b>	<b>0.025</b>	<b>100</b>	<b>115 / 80 / 65</b>	<b>95</b>	<b>0.046</b>	<b>40</b>	<b>1840</b>
<b>20</b>		<b>0.051</b>	<b>204</b>	<b>210 / 150 / 130</b>	<b>121</b>	<b>0.112</b>	<b>15</b>	<b>1680</b>
<b>25</b>	<b>75</b>	<b>0.062</b>	<b>248</b>	<b>240 / 180 / 150</b>	<b>130</b>	<b>0.138</b>	<b>12</b>	<b>1650</b>

*Table 4:* Parameters of a graphite absorber relevant for instantaneous and average heating processes.

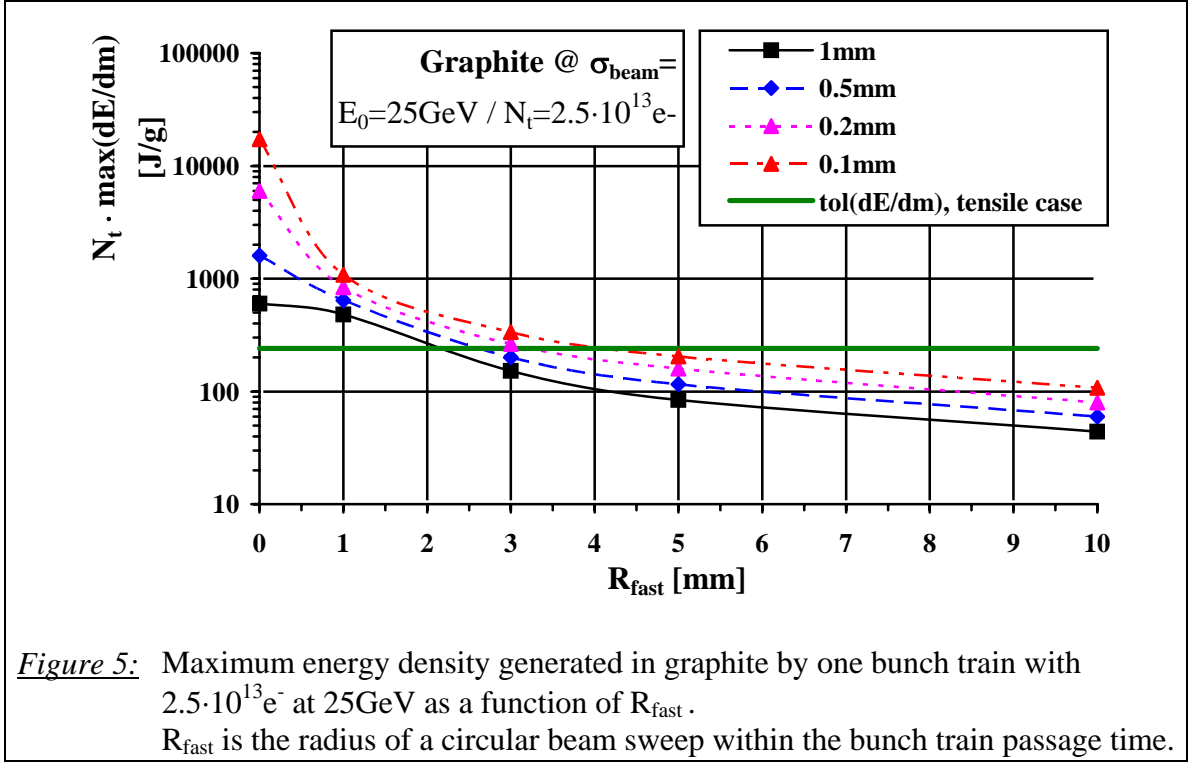
Finally it has to be emphasized, that for a beam size of  $\sigma_{beam} = 2mm$  the maxima of instantaneous and average heating do not coincide in space, but take place at a different depth in the absorber. Hence summing up the values  $\max(\Delta T_{inst})$  and  $\max(\Delta T_{eq})$  overestimates the maximum total temperature rise in the material.

### 2.1.1 Remarks on Spot Size Limit

For a graphite based absorber core the spot size of the incoming beam has to be  $\sigma_{beam} \geq 2mm$ , if the bunch trains are populated with  $2.5 \cdot 10^{13} e^-$ . This keeps the tolerable energy density generated by one bunch train below the conservative long term cyclic operation limit of 240J/g. If that beam size can not be achieved by beam optics, one could think about distributing the bunches of a train within the bunch train passage time of  $T_t \approx 0.8ms$  by active sweeping methods. A pair of orthogonal deflectors located upstream of the dump and driven by a sine- and cosine-like current of frequency  $\nu_{fast} \geq 1/T_t \approx 1kHz$ , places the individual bunches of each train on a circle with radius  $R_{fast}$  around the center of the dump axis. This does not affect the beam size  $\sigma_{beam}$ , but enlarges the effective spot size of a bunch train and therefore reduces the bunch train induced energy density in the absorber. Figure 5 shows the latter value as a function of the fast sweeping radius and compares it with the tolerable limit of 240J/g. For beams with a size down to  $\sigma_{beam} = 0.1mm$  a sweep radius of up to about  $R_{fast} \approx 5mm$  is required in order to achieve similar instantaneous loads as for the unswept 2mm beam.

This plot assumes no temporal structure within the bunch train, i.e. the total charge of  $N_t$  electrons is distributed evenly in time over the bunch train length  $T_t$ . This is justified if the spatial distance between subsequent bunches on the sweep circle is smaller than their transverse size  $\sigma_{beam}$ . For  $R_{fast} = 5mm$  the sweep circle is  $2\pi R_{fast} = 31mm$  long and 2000 bunches are thus separated each from another by only  $16\mu m$ . Hence  $\sigma_{beam} \geq 0.1mm$  as used in the graph fulfils the above assumptions.

Going further down with beam size means, that at some stage the tolerable energy density limit of 240J/g is already deposited by one single bunch. In that case a sweeping with  $\nu_{fast} \approx 1/T_t$  does not help anymore, because it will not apply different deflection to the electrons of a sub-picosecond long bunch, which would require (non existing) systems with sweeping frequencies in the THz range !



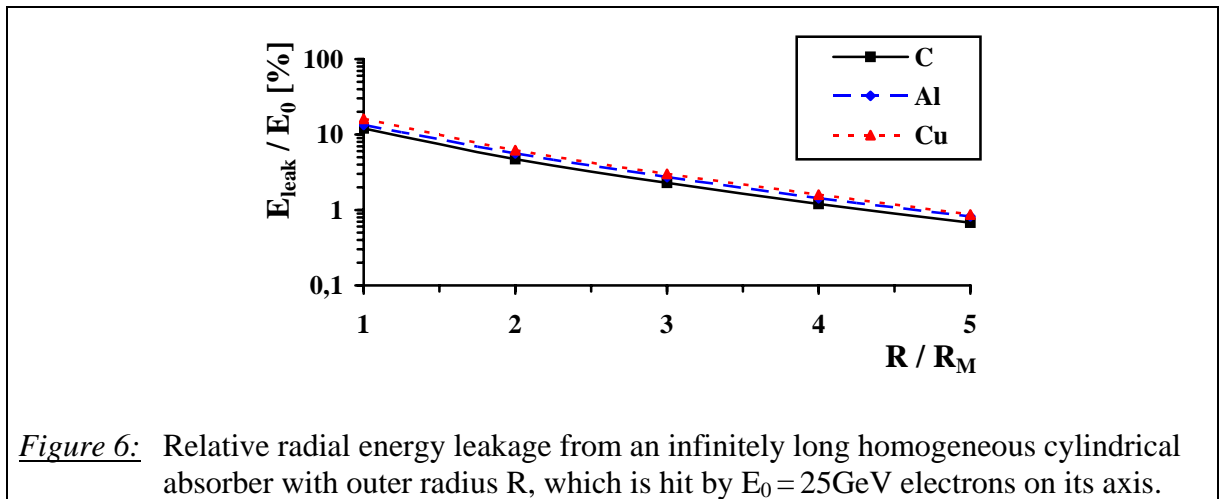
## 2.2 Radial Layout

On the one hand the radial layout has to guarantee that the amount of radial energy leakage does not exceed the desired value of 1%. Figure 6 displays the results of MARS simulations. Here the relative fraction of energy leaking through the radial surface of an infinitely long homogeneous cylindrical absorber is calculated for graphite, aluminium and copper as a function of its radial size in units of Molière radii. The absorber is hit by 25GeV electrons on its axis. Therefore the absorber needs a radial thickness of  $R_{99\%} \approx 5 \cdot R_M$  between shower axis and outer radius  $R$ , as already known from Equation 40.

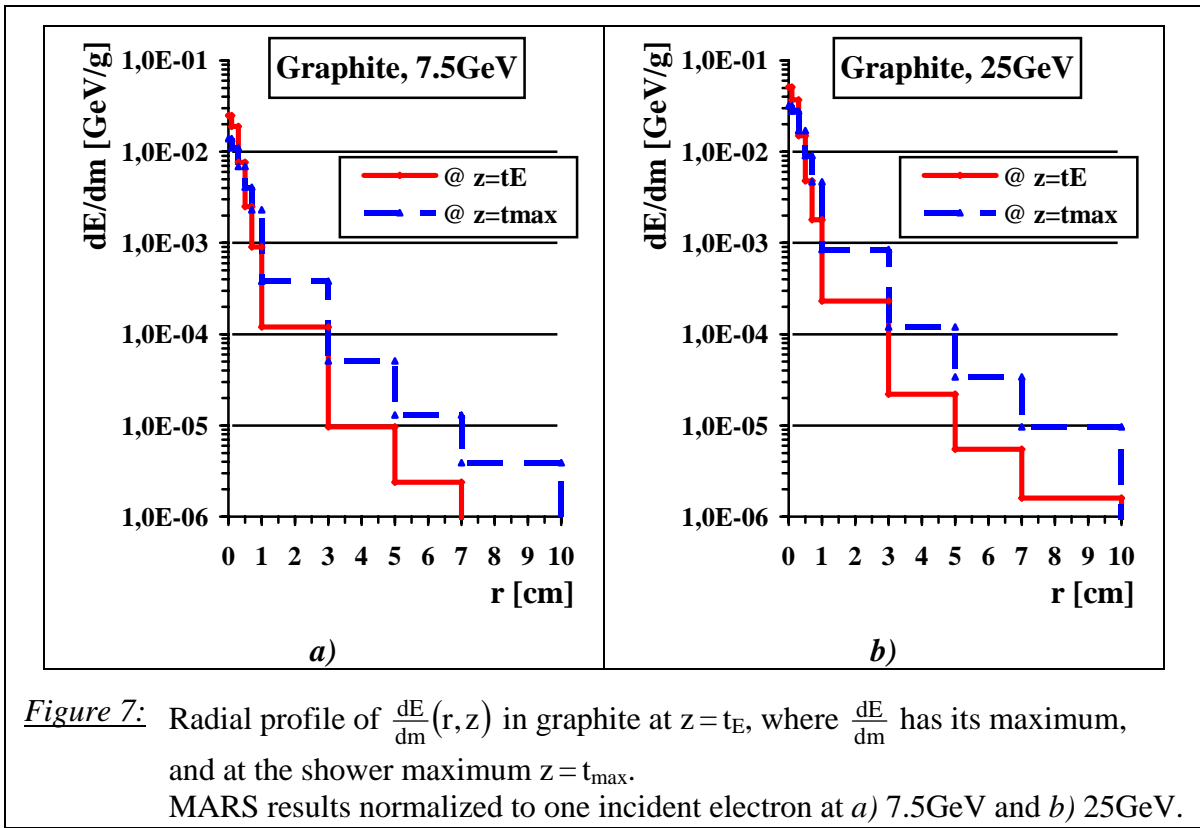
On the other hand a radial structure of low thermal resistance is aimed at, in order to extract the large amount of power radially from the axis towards the water cooled radial circumference at a moderate and tolerable equilibrium temperature drop.

### 2.2.1 Homogeneous radial Layout using one Material

As a first and very simple approach the dump should have no radial structure. That means a shell as indicated in Figure 1 does not exist and the dump consists uniformly out of one



material, namely graphite, with an outer radius of  $R_{99\%} = 5R_M = 35\text{cm}$ . Figure 7 shows the radial profile  $\frac{dE}{dm}(r, z)$  at  $z = t_E$ , where it has its maximum and at the shower maximum  $z = t_{\max}$ . These profiles are presented for 7.5GeV as well as for 25GeV and are normalized to one incident electron. Fitting these profiles by the sum of two Gauss distributions (see Equation 42) results in characteristic widths for both energies of about  $\sigma_1(t_E) \approx 2.8\text{mm}$  and  $\sigma_1(t_{\max}) \approx 3.9\text{mm}$  for the narrow core, which is relevant when dealing with the question of instantaneous heating and  $\sigma_2(t_{\max}) \approx 10\text{mm}$  for the broad part, which carries most of the deposited energy. In order to get the radial temperature profile  $T_{\text{eq}}(r, z)$ , which builds up in a given longitudinal slice of the absorber between the radius  $r$  and the outer radius  $R$  as a consequence of a time independent heat source and pure radial heat flow, the exact profile from the shower simulation was taken and integrated numerically according to Equation 63 in annex B.3. The situation is sketched in Figure 8 a). As discussed previously, the highest equilibrium temperature level is always expected at the shower maximum  $z = t_{\max}$  and in our



application the 7.5GeV / 40 $\mu$ A situation gives a maximum of dissipated power there.

Therefore the energy density profile  $\frac{dE}{dm}(r, z = t_{\max})$  at 7.5GeV in Figure 7 a) is used together with 40 $\mu$ A of average beam current to derive the worst case equilibrium temperature profile in a pure graphite dump with a radius of 35cm as shown in Figure 8 b). The cooling water temperature of  $T_0 = 50^\circ\text{C}$  and the temperature drop  $\Delta T_{\rightarrow w}$ , which builds up across the boundary from graphite to water, is also included. This heat transfer is assumed to take place over the whole surface area of  $dA = 2\pi R \cdot dz$  with a realistic coefficient of  $K_{\rightarrow w} = 0.4\text{W/cm}^2/\text{K}$ . In that case

$$\Delta T_{\rightarrow w} = \frac{1}{K_{\rightarrow w}} \cdot \frac{dP}{dA} = \frac{1}{K_{\rightarrow w}} \cdot \frac{1}{2\pi \cdot R} \cdot \frac{dP}{dz} \quad \text{Equation 4}$$

gives about 21K for  $R=35\text{cm}$  and  $dP/dz=1840\text{kW/cm}$ . As a consequence of the large power density of about  $1840\text{kW/cm}$ , the narrow radial profile of heat impact and the quite long radial path of  $35\text{cm}$  towards the heat sink a significant temperature of almost  $2500^\circ\text{C}$  builds up at the axis of the graphite dump. Since we are aiming at maximum temperature levels of less than  $500^\circ\text{C}$ , a pure graphite dump is not acceptable and additional measures have to be taken.

Still without introducing a radial shell of another material, in which the graphite core is embedded, one can reduce the average temperature by means of dilution of the heat source. Most of the temperature drop is generated near the shower axis at small  $r$ . Here already most of the heat is dissipated but has to flow through a relatively small radial area of  $dA=2\pi R \cdot dz$  only, which results in a large heat flux density and thus temperature drop. But the cross

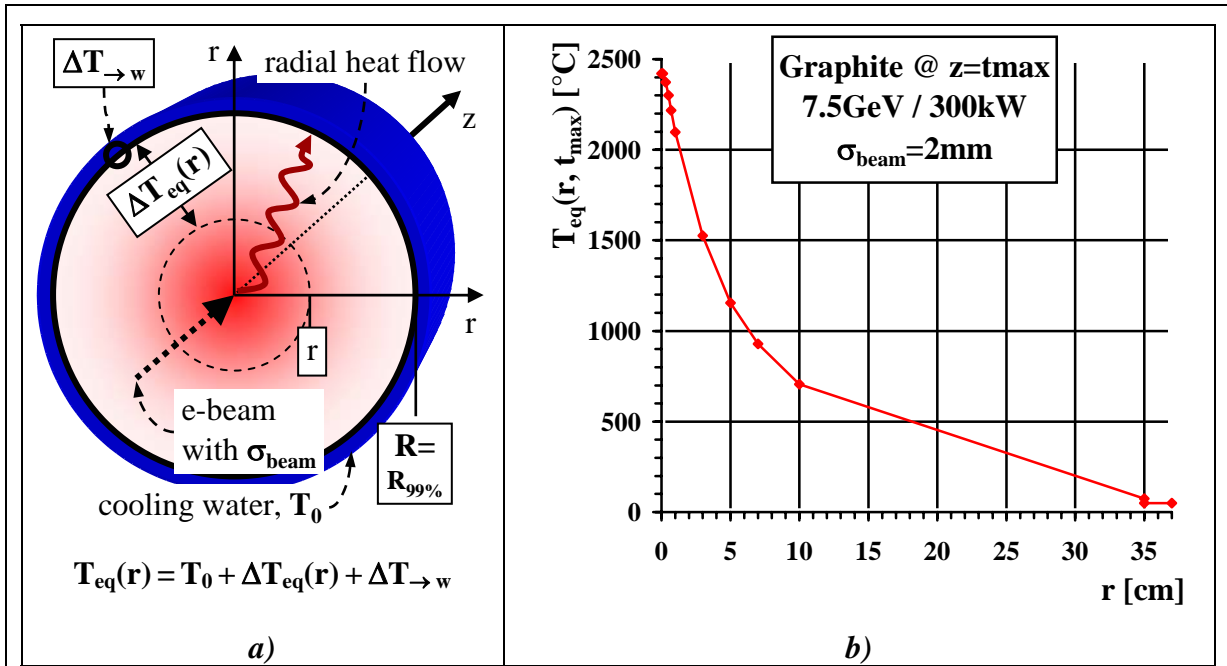


**Figure 8:** a) Sketch of radial heat flow and correlated equilibrium temperature drop in a longitudinal slice of a homogeneous cylindrical dump.  
b) Numerically calculated equilibrium temperature profile  $T_{\text{eq}}(r)$  at the shower maximum of a pure graphite dump with outer radius  $R = 35\text{cm}$ . A  $7.5\text{GeV} / 300\text{kW}$  beam with  $\sigma_{\text{beam}} = 2\text{mm}$  hits axially on the dump. Thermal conductivity of graphite according to Figure 3. Heat transfer at graphite→water boundary  $K_{\rightarrow w} = 0.4\text{W/cm}^2/\text{K}$  and  $T_0 = 50^\circ\text{C}$ .

section for heat flux can be increased if the beam does not enter on the axis of the absorber, but is distributed (swept) around it with a radius of  $R_s$ .

For rough estimations Equation 67 is applied to calculate the equilibrium temperature drop  $\Delta T_{\text{eq}}(R_s, R, t_{\text{max}})$  between the sweep radius and the outer radius of a homogeneous absorber, which is now increased to  $R = R_s + R_{99\%}$  in order to fulfil the energy leakage constraint. Hence:

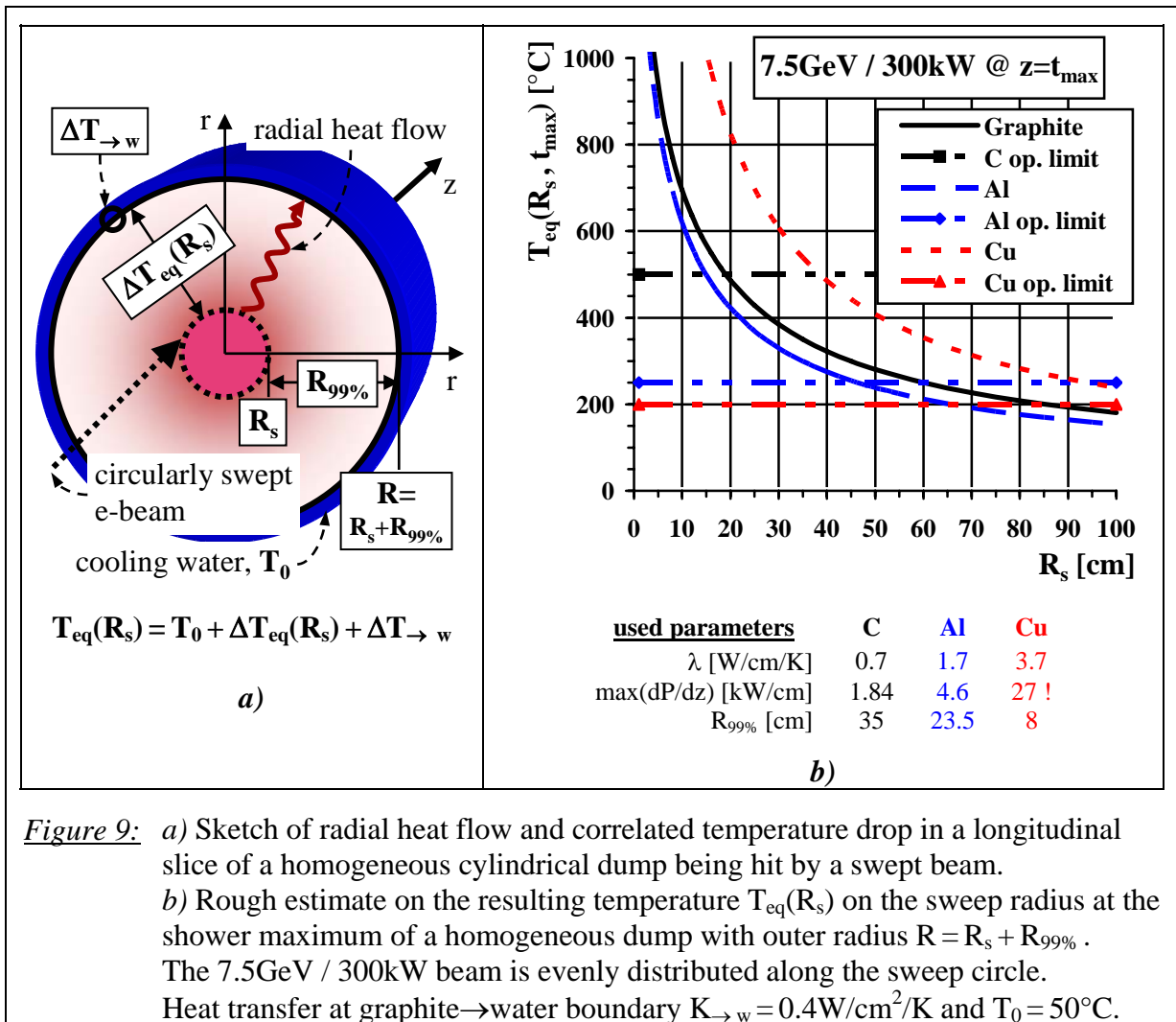
$$\Delta T_{\text{eq}}(R_s, R, t_{\text{max}}) = \frac{1}{2\pi \cdot \lambda} \cdot \max\left(\frac{dP}{dz}\right) \cdot \ln\left(\frac{R_s + R_{99\%}}{R_s}\right) \quad \text{Equation 5}$$

Figure 9 a) illustrates this situation. A perfect homogeneous distribution of beam power on the sweep circle is assumed and the radial extension of the energy deposition is neglected in

the limit of  $\sigma(z) \ll R_s$ . In that case the radial equilibrium temperature profile has a constant value within the sweep circle ( $0 \leq r \leq R_s$ ) and then falls logarithmically for  $r > R_s$ . Under these assumptions Equation 5 determines the maximum average temperature in the dump. This value is plotted in Figure 9 b) for graphite, aluminium and copper as a function of the sweep radius  $R_s$ , again including  $T_0 = 50^\circ\text{C}$  and  $K_{\rightarrow w} = 0.4 \text{W/cm}^2/\text{K}$ . The required parameters are listed there too.  $R_{99\%}$  is taken from Table 2, a temperature independent but conservative value of the thermal conductivity is assumed and  $\max(dP/dz)$  is estimated by Equation 38 for the relevant  $7.5\text{GeV} / 40\mu\text{A}$  case.

Figure 9 explains very impressively, that heat extraction is one of the most challenging issues at the given beam parameters. In order to bring the average heating below the level of reasonable operation limits, as inserted by means of horizontal lines in the graph as well, sweep radii of more than 45cm and 100cm are necessary to operate a pure aluminium respectively copper absorber. Therefore it is not reasonable to install neither Al nor Cu on the shower axis right at the beginning of a dump. They are not suited to handle the cyclic load of the beam, as was explained in section 2.1, but even for a non pulsed dc-beam these materials are obviously out of question.

Although graphite and aluminium show a similar behaviour in the plot of Figure 9 because their ratio between  $\max(dP/dz)$  and the thermal conductivity  $\lambda$  differs not too much, graphite is allowed to be operated up to  $500^\circ\text{C}$  in our case, while the limit for aluminium was set at about half that value. The required sweep radius when using a pure graphite dump would be around  $R_s \geq 20\text{cm}$ . Nevertheless in terms of the implied diameter of the beam pipe ( $\geq 300\text{mm}$ )



**Figure 9:** a) Sketch of radial heat flow and correlated temperature drop in a longitudinal slice of a homogeneous cylindrical dump being hit by a swept beam. b) Rough estimate on the resulting temperature  $T_{eq}(R_s)$  on the sweep radius at the shower maximum of a homogeneous dump with outer radius  $R = R_s + R_{99\%}$ . The  $7.5\text{GeV} / 300\text{kW}$  beam is evenly distributed along the sweep circle. Heat transfer at graphite  $\rightarrow$  water boundary  $K_{\rightarrow w} = 0.4 \text{W/cm}^2/\text{K}$  and  $T_0 = 50^\circ\text{C}$ .

and that of the graphite dump ( $\geq 1.1\text{m}$ ), this is still not a favourable solution, but subject to further optimization by introduction of a surrounding shell of a different material as discussed in the following section.

### 2.2.2 Segmented radial Layout with Graphite Core

The previous sections explained that graphite is the most and only suitable material for a solid dump core, which will now be embedded in a surrounding shell material of higher density and better thermal conductivity than graphite. Here aluminium or copper are the right candidates to improve radial heat extraction while still catching the radial tail of the EMS.

The first question to be answered concerns the radial distance  $\Delta R$  between the inner radius of this shell and the shower axis. The closer the shell, the more of direct energy deposition from the beam will enter the shell and affects it with cyclic stress.

In that respect the graphite to shell junction is the most critical position. Keeping in mind, that a reliable long term stable heat contact is required here, where two materials of different thermal expansion meet, this boundary should not experience significant cyclic stress. Therefore  $\Delta R$  should be chosen, such that the instantaneous temperature rise  $\Delta T_{\text{inst}}$  generated by one bunch train at the graphite to shell boundary is at least one order of magnitude less than the tolerable limit  $\text{tol}(\Delta T_{\text{inst}})$  for cyclic load as listed in Table 3. The situation is sketched in Figure 10 a) and Figure 10 b) shows the result of MARS calculations for the maximum of  $\Delta T_{\text{inst}}$  in a Cu-shell as a function of  $\Delta R$ . The maximum is located in a depth of 1.3m to 1.5m for our conditions. For copper the 10% level of  $\text{tol}(\Delta T_{\text{inst}})$  is about 2K, thus  $\Delta R \geq 4\text{cm}$  is required. For relaxed beam steering and alignment tolerance of the dump in terms of position and tilt, a radial distance between shower axis in graphite and its boundary to the shell is chosen to be 5cm in the following.

Since  $5\text{cm} = 0.72R_M$  of graphite, this distance also agrees with the necessity, that the bulk

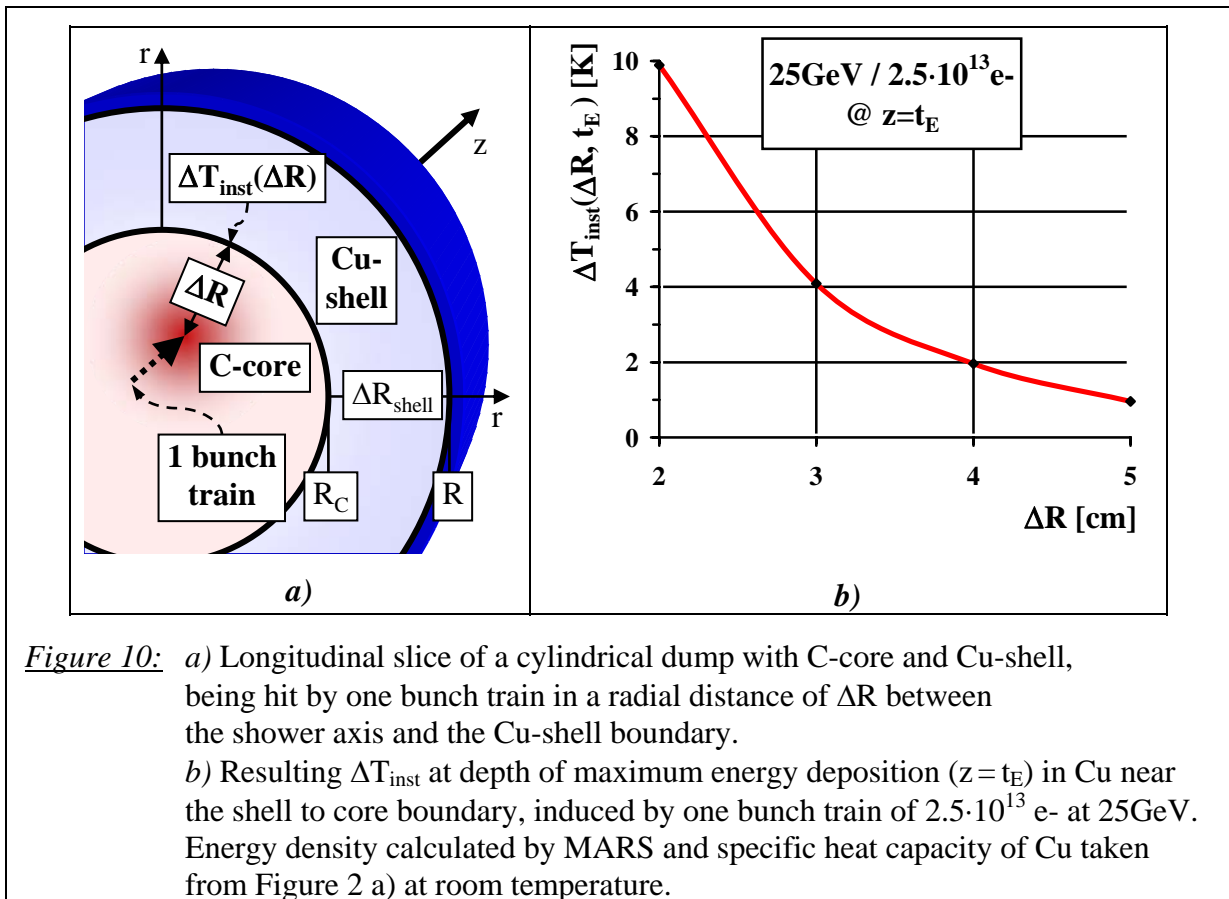


**Figure 10:** a) Longitudinal slice of a cylindrical dump with C-core and Cu-shell, being hit by one bunch train in a radial distance of  $\Delta R$  between the shower axis and the Cu-shell boundary. b) Resulting  $\Delta T_{\text{inst}}$  at depth of maximum energy deposition ( $z = t_E$ ) in Cu near the shell to core boundary, induced by one bunch train of  $2.5 \cdot 10^{13} e^-$  at 25GeV. Energy density calculated by MARS and specific heat capacity of Cu taken from Figure 2 a) at room temperature.

part of the power dissipation is reigned by the graphite core and the maximum value of about 1.8kW/cm is still valid for heat extraction considerations.

The thickness of the shell  $\Delta R_{shell}$  is chosen in order to build up a total material layer of  $5R_M = R_{99\%}$  between the sweep radius  $R_s$  and the outer radius  $R$ . Taking into account the contribution of 5cm graphite one gets  $\Delta R_{shell} = 4.3R_M$ . In a similar way as it was done in Figure 9 for the uniform geometry without shell, Figure 11 b) shows the impact of sweeping on the equilibrium heating for the segmented radial layout with an aluminium or copper shell as shown in Figure 11 a). As a result of the 1.84kW/cm power source being evenly distributed over the sweep circle and radial heat flow in graphite and shell material including the

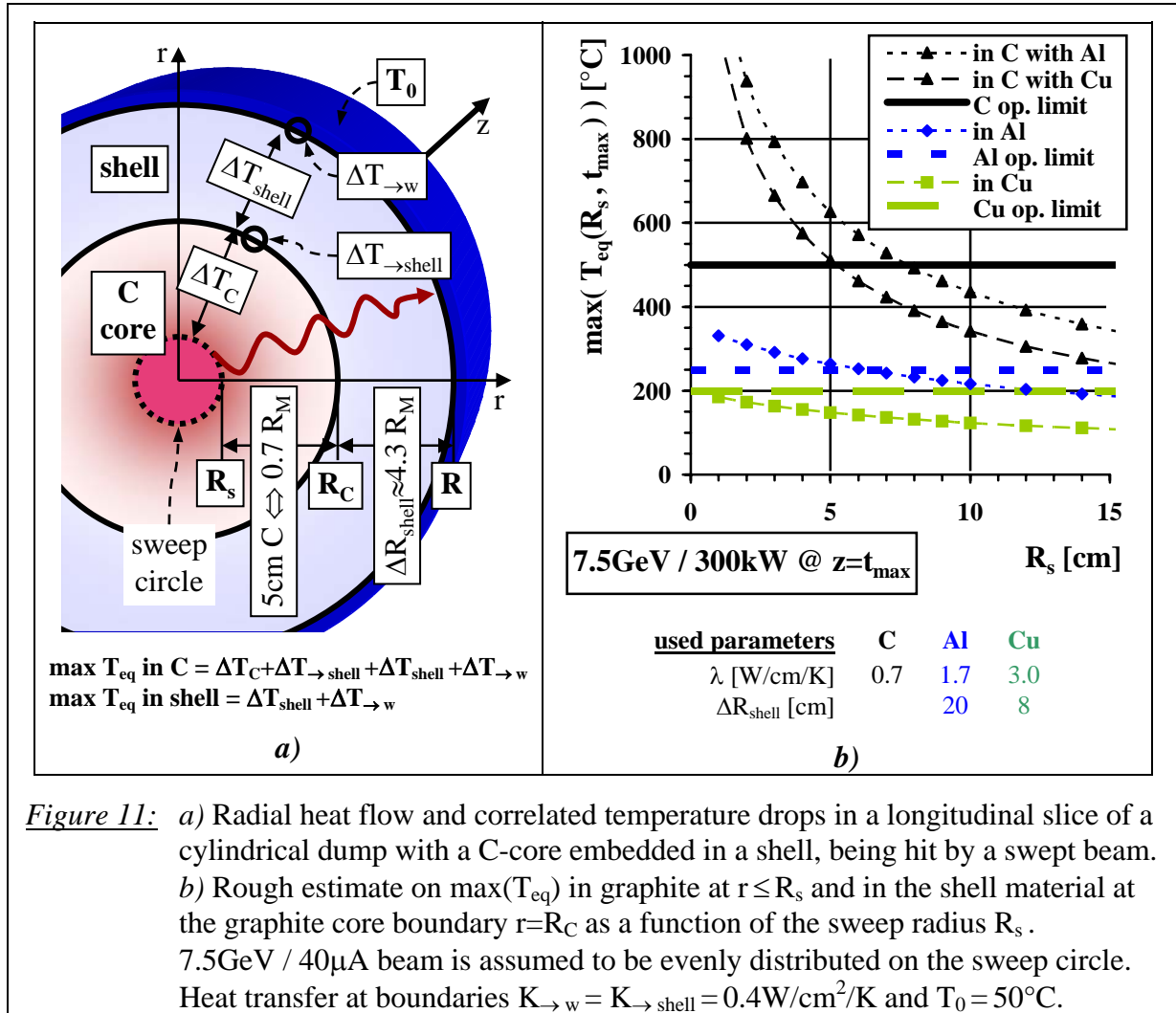


**Figure 11:** a) Radial heat flow and correlated temperature drops in a longitudinal slice of a cylindrical dump with a C-core embedded in a shell, being hit by a swept beam. b) Rough estimate on  $\max(T_{eq})$  in graphite at  $r \leq R_s$  and in the shell material at the graphite core boundary  $r = R_C$  as a function of the sweep radius  $R_s$ . 7.5GeV / 40μA beam is assumed to be evenly distributed on the sweep circle. Heat transfer at boundaries  $K_{\rightarrow w} = K_{\rightarrow shell} = 0.4W/cm^2/K$  and  $T_0 = 50^\circ C$ .

boundaries, the maximum equilibrium temperature in graphite inside the sweep circle  $r \leq R_s$  and in the shell material just at the boundary to graphite at  $r = R_C$  are plotted as a function of the sweep radius  $R_s$ .

These temperatures are compared with the maximum operation temperatures  $T_{op}$  from Table 2. For the C / Al design the graphite stays below 500°C for a sweep radius  $R_s \geq 8cm$ . In that case the aluminium shell operates at about 230°C, where its mechanical properties deteriorate significantly. The larger  $\rho/\lambda$  ratio of copper allows a smaller sweep radius of  $R_s \geq 5cm$  to satisfy the 500°C limit in the graphite core and achieves a safe value of 150°C as a worst case in the copper itself. This difference is not negligible in terms of sweeping effort and beam pipe dimensions. That is why the copper shell solution is very much preferred.

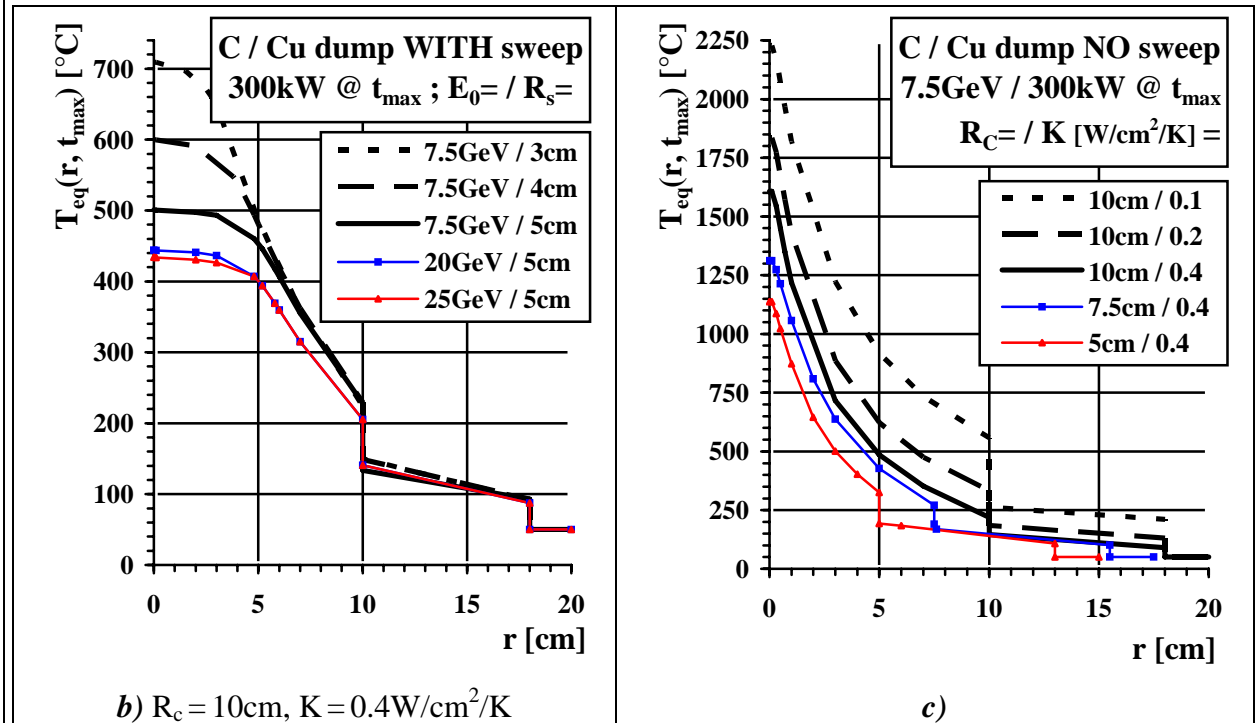
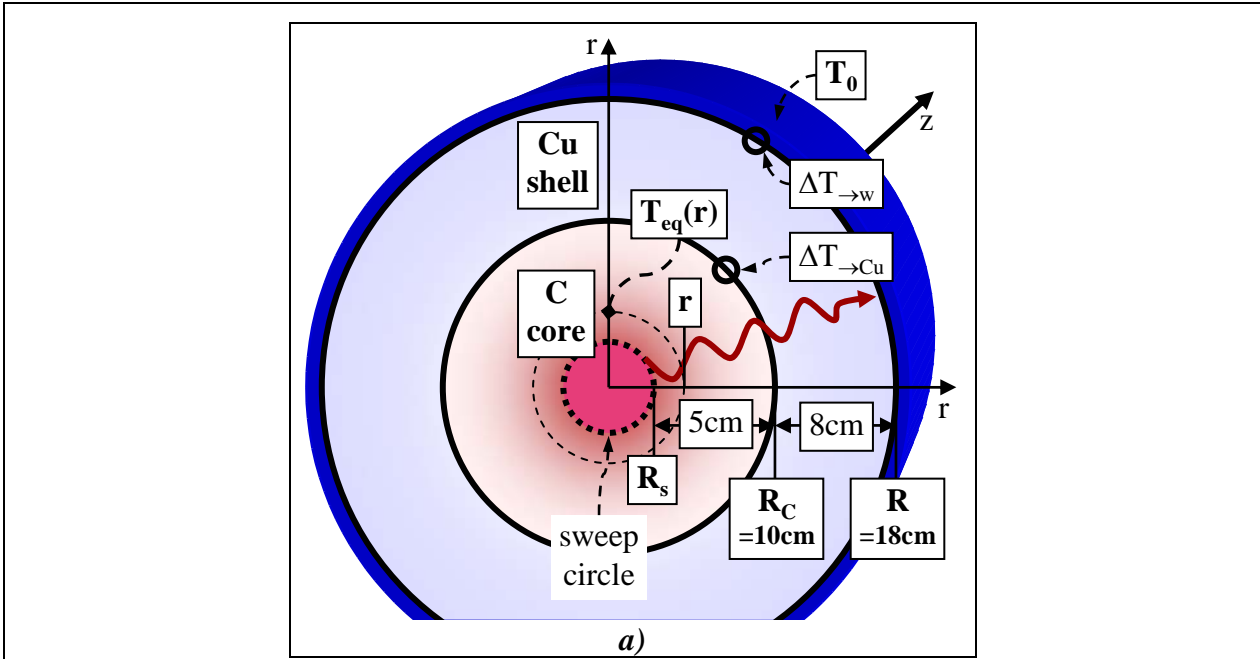


**Figure 12:** a) Sketch of a longitudinal slice of the preferred radial C / Cu dump layout. Numerically calculated equilibrium temperature profile  $T_{eq}(r)$  in the slice at the shower maximum of such a layout for a 300kW beam with  $\sigma_{beam} = 2\text{mm}$  which: b) is evenly distributed on sweep radius  $r = R_s$ . c) enters without sweep axially on the dump axis at  $r = 0$ . Thermal conductivity of graphite and copper taken from Figure 2 and Figure 3. Same heat transfer coefficient at both boundaries and  $T_0 = 50^\circ\text{C}$ .

Figure 12 a) sketches the radial layout of the preferred C / Cu design. The corresponding radial temperature profiles as derived from numerical integration of the stationary heat Equation 63 with an energy density profile gained from MARS calculations using a 300kW beam with a size of  $\sigma_{beam} = 2\text{mm}$  are shown for various cases of a swept or un-swept beam in Figure 12 b) and Figure 12 c) respectively. Normal operation should run with a sweep of

radius  $R_s = 5\text{cm}$ . Here the maximum temperature in graphite is  $500^\circ\text{C}$  and confirms the rough estimate quite well. Nevertheless deviating from the nominal sweep radius by about  $1\text{cm}$  results in a positive or negative change of about  $100\text{K}$ . The difference between  $500^\circ\text{C}$  and  $430^\circ\text{C}$  when going from  $7.5\text{GeV}/300\text{kW}$  to  $25\text{GeV}/300\text{kW}$  is mostly due to the reduced power density of  $1650\text{kW}/\text{cm}$  instead of  $1840\text{kW}/\text{cm}$ .

The profiles in the un-swept case indicate graphite temperatures around  $1600^\circ\text{C}$  for the nominal case, in which a transfer coefficient of at least  $0.4\text{W}/\text{cm}^2/\text{K}$  at both (C / Cu and Cu / water) heat junctions is assumed. Avoiding the oxidation risk of graphite make heat source dilution mechanisms like beam sweeping mandatory for such a design. The graphite core diameter can be reduced if beam sweeping is not applied, but still temperature falls only down to the level of about  $1200^\circ\text{C}$ , if the radius of the graphite core is  $5\text{cm}$  instead of  $10\text{cm}$ .

Last but not least the plots of different heat transfer coefficients emphasize again, that a good radial thermal contact at the boundaries towards copper and water is vital. Quantitatively speaking the maximum heat flux density through the C / Cu boundary at  $r = R_C = 10\text{cm}$  is in the order of  $1840 \frac{\text{kW}}{\text{cm}} \cdot \frac{1}{2\pi R_C} \approx 30\text{W}/\text{cm}^2$  and contributes already with a temperature drop of  $75\text{K}$  if the thermal contact has a quality as characterized by  $K_{\rightarrow\text{Cu}} = 0.4\text{W}/\text{cm}^2/\text{K}$ . Compared to the heat flux density, that can be achieved at the surface of a standard  $2\text{kW}$  electrical cooking plate of  $15\text{cm}$  diameter, the value at the C / Cu boundary is 3 times larger. Therefore section 3.2 discusses the problem of heat transfer at this contact more carefully.

### 2.3 Back Stopper

The preferred radial C / Cu layout as presented in the previous section weights about  $700\text{kg}$  per meter of length ( $54\text{kg}/\text{m}$  of graphite core and  $630\text{kg}/\text{m}$  of copper shell). Without further optimization the total length for energy capture must be about  $L_{99\%}$  of graphite, which is about  $3.8\text{m}$  and gives at least (without concrete front part and weight of copper cooling pipes) a weight of  $2.7$  tons.

A backstop behind the graphite core at  $z = L_C$  is introduced to shorten the dump. Again average and instantaneous heating constraints in this backstop determine how much the graphite core length can be reduced, before a material of higher density behind that suffers from too much energy deposition.

Radial heat extraction in a longitudinal slice of the C-core to Cu-shell section has to be

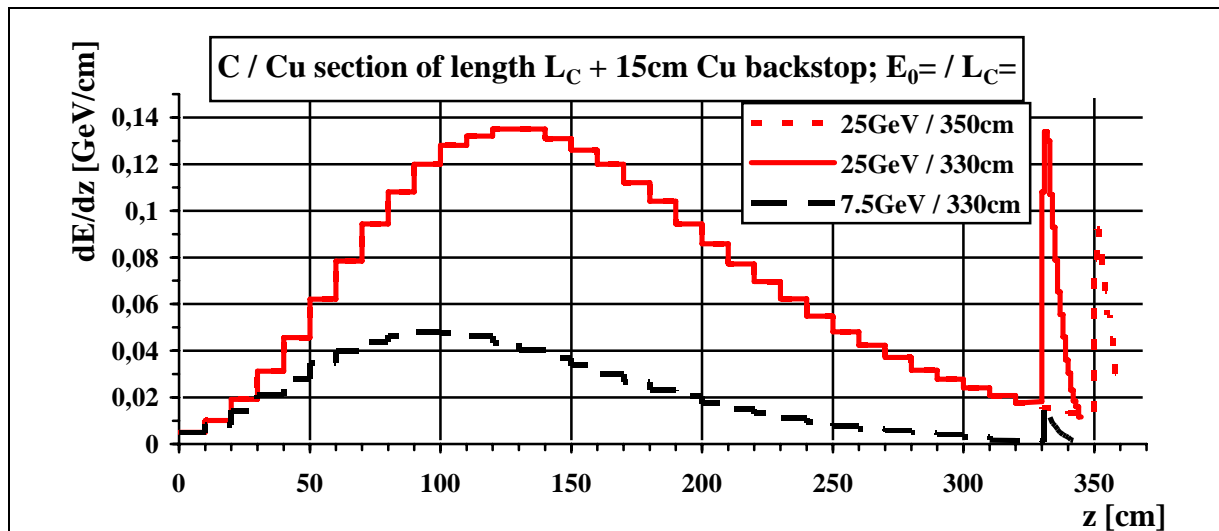
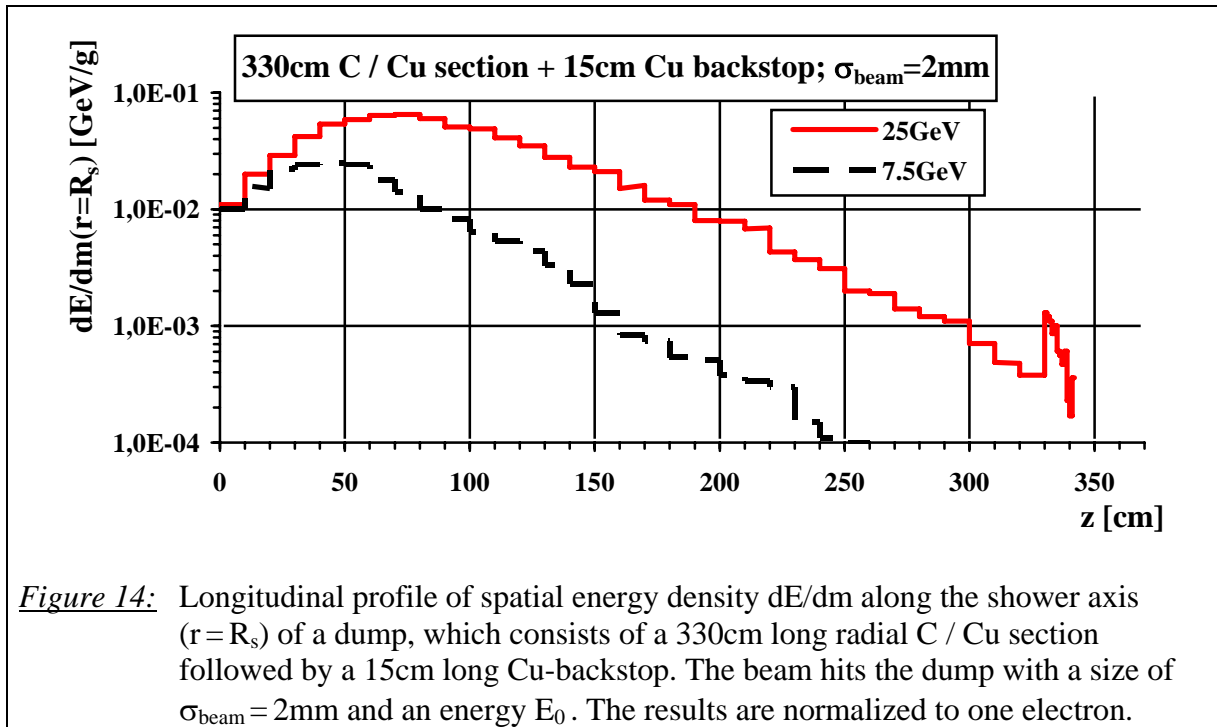


**Figure 13:** Longitudinal profile of deposited energy per unit length  $dE/dz$  induced by one electron of energy  $E_0$  in dump, which consists of the preferred radial C / Cu-layout of length  $L_C$  followed by a  $15\text{cm}$  long Cu-backstop.



solved technically anyhow, especially in terms of the C / Cu and Cu / water junctions at  $r = 10\text{cm}$  and  $r = 18\text{cm}$  respectively. Here the heat flux densities of  $30\text{W}/\text{cm}^2$  and  $16\text{W}/\text{cm}^2$  have to be handled near the shower maximum in the worst case of a longitudinal power density of  $1.8\text{kW}/\text{cm}$  generated by a  $7.5\text{GeV} / 300\text{kW}$  beam. These values will determine the technical layout and should neither be exceeded elsewhere, nor in the backstop. Otherwise this would at least affect the heat transfer situation at the boundary towards the cooling water. Here one absolutely has to keep a safe margin from effects like boiling crisis, which becomes relevant if the heat flux density is in the range of  $100\text{W}/\text{cm}^2$ . If taking the total surface area as transition cross section at the outer dump radius, as we always assume in this report, leads already to a level of around 20% of this critical limit.

Therefore the length of the C / Cu leading section is chosen just such long, that the value of longitudinal energy density in the adjacent backstop behind it does not exceed the value at the shower maximum in the leading section.

Using too many different materials in the dump design may introduce an additional technological challenge of having connections of various materials, especially in radial direction towards the cooling water. Hence a pure copper backstop of length  $L_{\text{stop}} = 15\text{cm}$  is considered first. Figure 13 shows the longitudinal energy density profile per one incident electron when this Cu-backstop is placed behind the C / Cu main part of length  $L_C = 350\text{cm}$  and  $330\text{cm}$  respectively. At  $25\text{GeV}$  the shower is longer and thus more energy is deposited in the backstop. This case requires the Cu-backstop to be installed not before a graphite core length of  $L_C = 330\text{cm}$ . At  $25\text{GeV}$  the energy density at the beginning of the Cu-backstop near  $z = 330\text{cm}$  peaks at  $0.134\text{GeV}/\text{cm}$ , which is  $1.6\text{kW}/\text{cm}$  at  $300\text{kW}$  ( $12\mu\text{A}$ ). For  $7.5\text{GeV}$  the corresponding value is  $0.0167\text{GeV}/\text{cm}$  for one electron and thus only  $0.67\text{kW}/\text{cm}$  at  $300\text{kW}$  ( $40\mu\text{A}$ ).

Figure 14 plots the spatial energy density profile per mass unit along the shower axis, as created by a beam with size  $\sigma_{\text{beam}} = 2\text{mm}$ , which enters such an absorber with  $L_C = 330\text{cm}$ . The result is normalized to one incident electron and given in units of  $\text{GeV}/\text{g}$ . While the  $7.5\text{GeV}$  case is practically not visible in the backstop, the maximum amount of  $0.0013\text{GeV}/\text{g}$  is deposited there by a  $25\text{GeV}$  beam. In terms of instantaneous heating as induced by one full charge bunch train, this number converts to  $5.2\text{J}/\text{g}$  or  $\Delta T_{\text{inst}} \approx 15\text{K}$  for a specific heat

capacity of copper of  $c(\text{Cu})=0.35\text{J/g/K}$ . This cyclic heating occurs fully in copper and not at a critical radial material junction. Thus the tolerable limit of 18K to 30K from Table 3 for cyclic load can be applied without restriction and is fulfilled here.

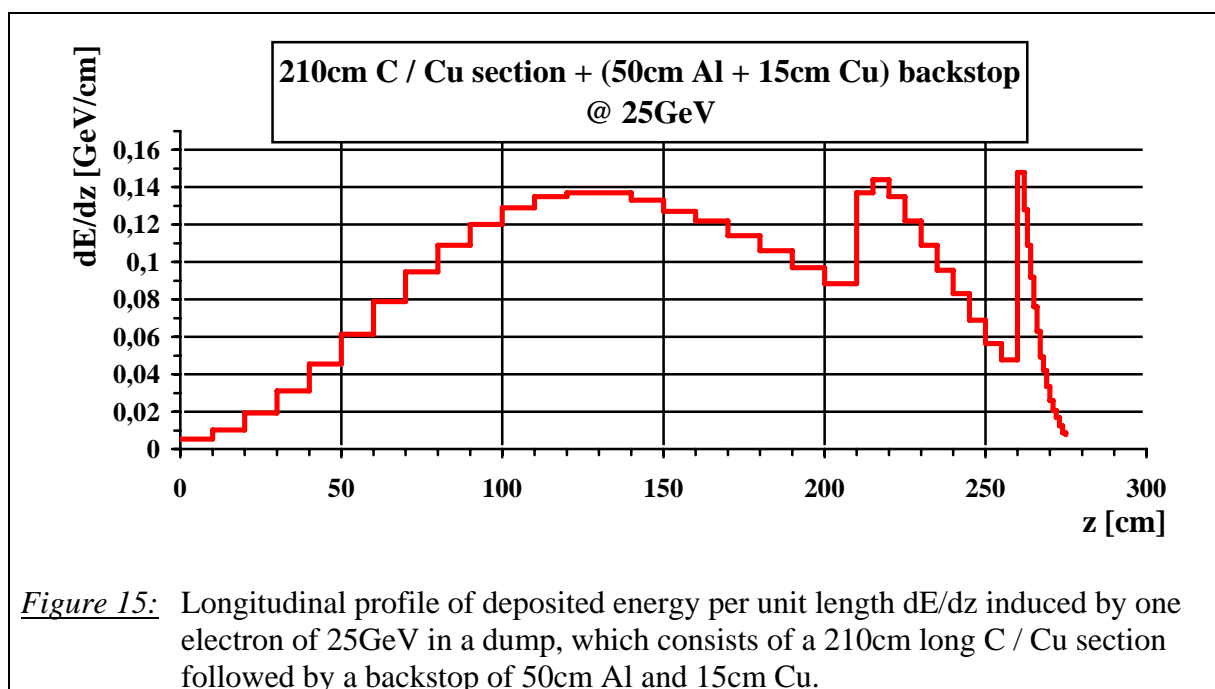
All in all, this absorber layout has a length of 345cm (330cm C / Cu-section + 15cm Cu-backstop) and a weight of 2.4 tons (2100kg Cu-shell, 180kg C-core, 140kg Cu-backstop). These have to be regarded as minimum values, since an additional radial copper thickness in order to implement cooling channels directly in the Cu-shell at  $r \geq 18\text{cm}$  will add as well as other material, which may be required to strengthen this structure mechanically. For the whole dump module including the 2m front part of shielding concrete another 500kg to 1000kg have to be taken into account additionally.

### 2.3.1 Further Optimization of Dump Length

A further reduction of length is possible if the backstop is longitudinally subdivided in materials of increasing density. This can be achieved by inserting a material like aluminium between the C / Cu section and the Cu-end. Optimized in a similar way as has been done for the pure Cu-backstop, Figure 15 shows the longitudinal energy density profile of such an C / Cu-Al-Cu layout if the total length of the backstop  $L_{\text{stop}}=L_{\text{Al}}+L_{\text{Cu}}$  is made up of a  $L_{\text{Al}}=50\text{cm}$  long Al cylinder followed by the already known  $L_{\text{Cu}}=15\text{cm}$  long Cu cylinder. Both have the same outer radius of 18cm as the preceding C / Cu section, which is in this case only 210cm long. For the 25GeV / 300kW operation the resulting maximum longitudinal power densities are 1.73kW/cm in the Al-middle part and 1.78kW/cm in the Cu-end part. Instantaneous temperature jumps within one bunch train have been calculated as well and are about 25K and 20K in the intermediate Al- and the Cu-end part respectively.

By insertion of the aluminium section it is possible to achieve a further reduction of the overall absorber length by about 70cm down to 275cm (210cm C / Cu + 50cm Al + 15cm Cu). The overall absorber weight is now about 1.8 tons (1400kg Cu-shell, 110kg C-core, 140kg Al-backstop, 140kg Cu-backstop).

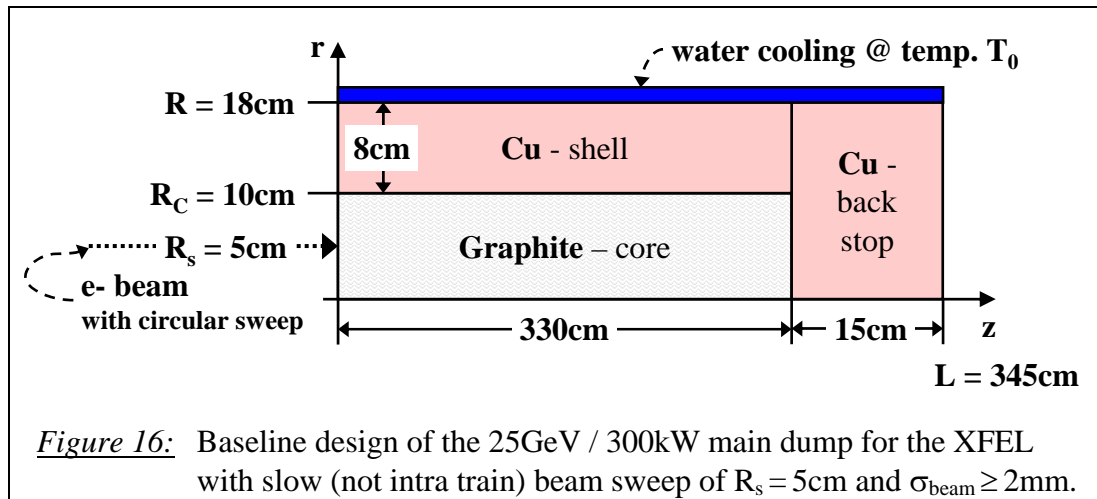
Nevertheless as mentioned at the beginning of this section, the introduction of a third material might cause additional trouble, which has to be compared with the advantage of the reduced length. When using the aluminium section, an additional boundary at the outer radius  $R$  is necessary to connect the aluminium surface with the copper pipes of the cooling water.



Alternatively the cooling water channels could be drilled directly into the aluminium, but then this water can not be used in direct contact with copper surfaces for electrochemical reasons. Therefore the problem is not solved but only shifted to the surface of the copper shell and copper backstop, where an additional boundary is required instead. In order to avoid these kind of problems, the longitudinal C / Cu-Al-Cu design is regarded as an option if length is really an issue, but the C / Cu-Cu geometry is taken as the baseline layout and described in further detail in the following chapter 3.

### 3 Baseline Design of the 25GeV / 300kW Dump with slow Sweeping

As a result of the basic layout considerations being made in the previous chapter 2, the desired cylindrical geometry is sketched in Figure 16. The 330cm long main part is composed of a graphite core ( $13.1 \cdot X_0$  of C with  $\rho = 1.71 \text{g/cm}^3$ ) with 20cm in diameter, which is embedded in a copper shell of 8cm ( $5 \cdot R_M$ ) radial thickness. A copper cylinder with a length of at least 15cm ( $10.4 \cdot X_0$  of Cu) and the same outer diameter as the preceding C / Cu compound acts as a backstop for the longitudinal shower tail. The average beam power has to be diluted in this dump by active deflection (sweeping) of the successive bunch trains on a  $R_s = 5\text{cm}$  sweep radius in order to keep the average temperature level in the graphite core below its



oxidation limit of around  $500^\circ\text{C}$ . A spot size of the incoming beam of  $\sigma_{\text{beam}} \geq 2\text{mm}$  ensures a long term cyclic operation as required by the instantaneous temperature and mechanical stress load, which is induced by each bunch train.

The energy capture capability of this baseline layout is given in Table 5. In absolute and relative numbers, it shows how much of the impinging beam power is deposited in the different dump sections for a beam of 7.5GeV or 25GeV at the same power of 300kW. The overall leaking fraction is worst for the 25GeV beam, but does not exceed 0.33%, which corresponds to 1kW at full energy and power. According to the MARS calculations, where a

	C-core	Cu-shell	Cu-backstop	cooling water	total leakage
<b>7.5 GeV</b>	275kW / 91.7%	20.8kW / 6.9%	4kW / 1.3%	20W / 67ppm	400W / 0.13%
<b>25 GeV</b>	280kW / 93.3%	19.2kW / 6.4%	10kW / 3.3%	25W / 83ppm	1000W / 0.33%

*Table 5:* Absolute and relative value of power, which is deposited by a 300kW beam in the various sections of the baseline dump geometry as shown in Figure 16.

water layer of 2cm thickness was put radially around the copper shell, the cooling circuit will receive less than 0.1 per mille and accordingly not more than 25W in the worst case. Hence problems like radiolysis are not an issue.

On page 22 the most relevant longitudinal and radial profiles of the baseline design are summarized. Figure 17 compares the profiles of longitudinal power density for a 300kW beam with the spatial energy density generated by one bunch train on the shower axis, at both energies of 7.5GeV and 25GeV respectively. This graph illustrates quite nicely the different position in depth ( $z = t_{\max}$  and  $z = t_E$ ), where these parameters, which determine average and instantaneous heating, have their maximum.

Figure 18 a) shows the equilibrium radial temperature profile in the C / Cu section near the shower maximum at  $z = t_{\max}$  and in the Cu-backstop taking the power density of about 1.6kW/cm near the beginning of the backstop at  $z = 330$ cm. We notice, that this leads to a flat temperature profile with a maximum level at about 200°C, which is still tolerable and a very conservative estimate. The power dissipation per unit of length decreases very rapidly with depth in the backstop as can be seen in Figure 17. Assuming pure radial heat flux is really conservative here, since the radius of the backstop is by far not small compared to the gradient of the longitudinal power profile there. As a consequence longitudinal heat flow will contribute to a considerable amount and reduce the average temperature.

Another more important information, that should be drawn from this graph, is the temperature at the boundary to water. Due to the quite high forward and return water temperatures and the temperature drop at the copper to water boundary, almost 100°C are achieved there at the worst case longitudinal slice. At the design mass flow of about 1.8kg/s the average power of 300kW will heat the cooling water from 33°C to 73°C only. But in between on its way from the forward water inlet to the return water outlet, there will be surfaces, which are hotter than that. In order to avoid boiling, the cooling circuit has to be pressurized as it would be done anyway. Only 0.3MPa (3bar) above atmosphere is necessary to push the boiling point of water up to a safe value of about 150°C. Even with un-pressurized water, its flow would prevent dangerous boiling processes as far as the critical heat flux densities are not exceeded.

Finally Figure 18 b) shows how the instantaneous energy density, deposited by one fully populated bunch train with a transverse size of  $\sigma_{\text{beam}} = 2$ mm, is radially distributed around the shower axis at the depth  $z = t_E$ , where  $dE/dm$  peaks longitudinally.

Nevertheless these results are based on simplified heating and stress calculations. Equilibrium temperature calculations for the swept beam assumed an ideal uniform distribution of beam power amongst the sweep circle, without taking into account that successive bunch trains are impinging there. Static stresses due to average temperature gradients in the dump have not been considered at all up to this point. Both topics are subject to the following sections of this chapter.

In addition the critical question of heat transfer at the radial C / Cu boundary will be addressed in more detail theoretically as well as practically in terms of first thoughts on its technical realization.

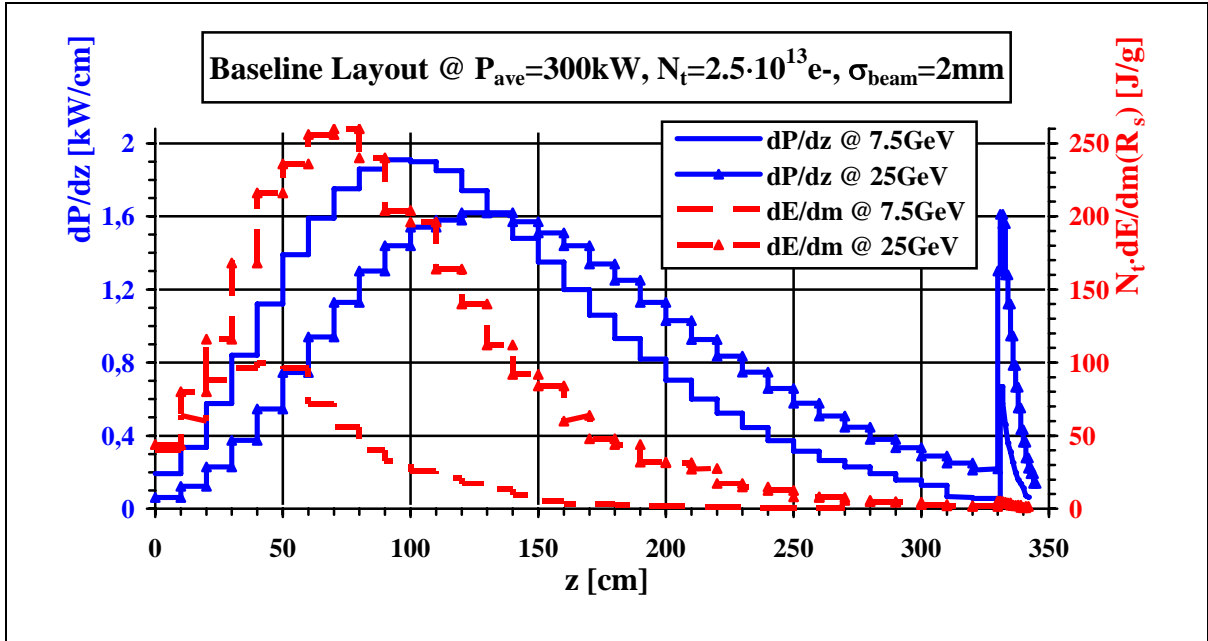


**Figure 17:** Longitudinal profiles of dissipated power density  $dP/dz$  at 300kW and energy density  $N_t \cdot dE/dm$  created by one bunch train with  $N_t = 2.5 \cdot 10^{13} e^-$  and a size of  $\sigma_{beam} = 2mm$  along the shower axis ( $r = R_s$ ) of the baseline C/Cu-Cu dump geometry as shown in Figure 16.

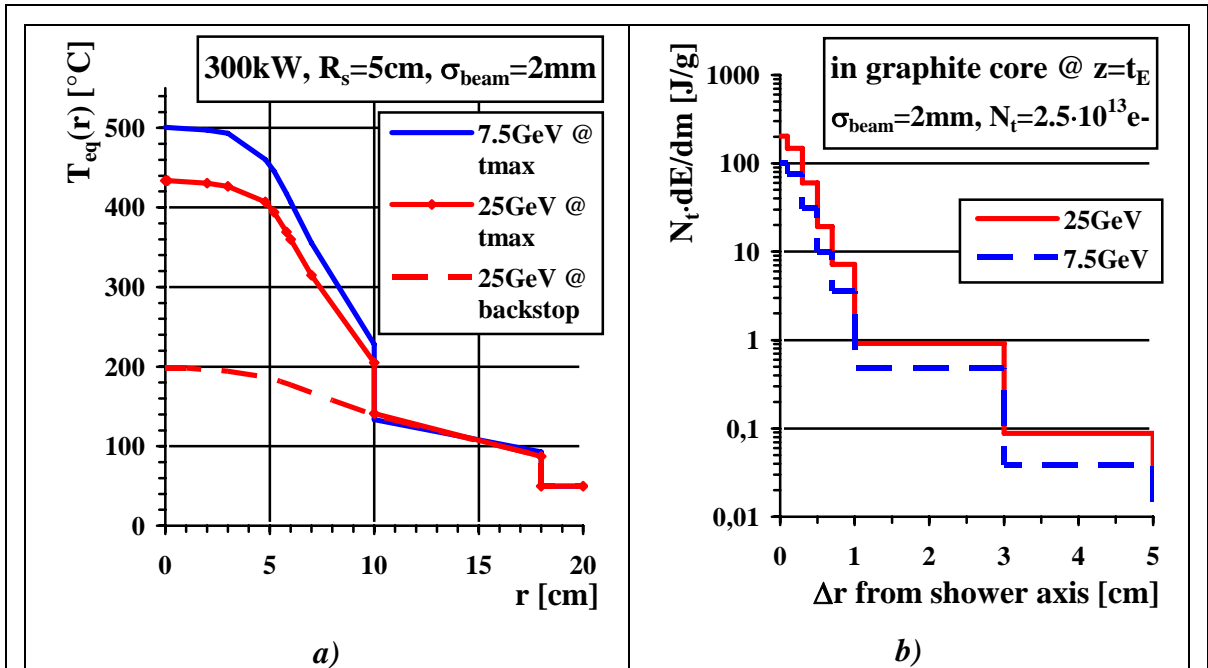


**Figure 18:** Radial profiles of the baseline C/Cu-Cu dump geometry as shown in Figure 16.  
 The 300kW beam has a size of  $\sigma_{beam} = 2mm$  and is swept on 5cm radius.  
 a) Equilibrium temperature profile at shower maximum and in Cu-backstop.  
 b) Energy density as a function of the radial distance from the shower axis, generated by one bunch train at  $z = t_E$ , where  $dE/dm$  has its maximum.

### 3.1 Consequences of slow Sweeping a pulsed Beam

From the point of view of the technical realisation a sweeping system should work at the lowest possible frequency, because it gets harder and harder to create high frequent deflection fields with significant amplitudes. At lower frequencies the required voltages and induced losses decrease. Thus one can think about resonant non-pulsed systems, for which survey of their proper functioning is easier to carry out.

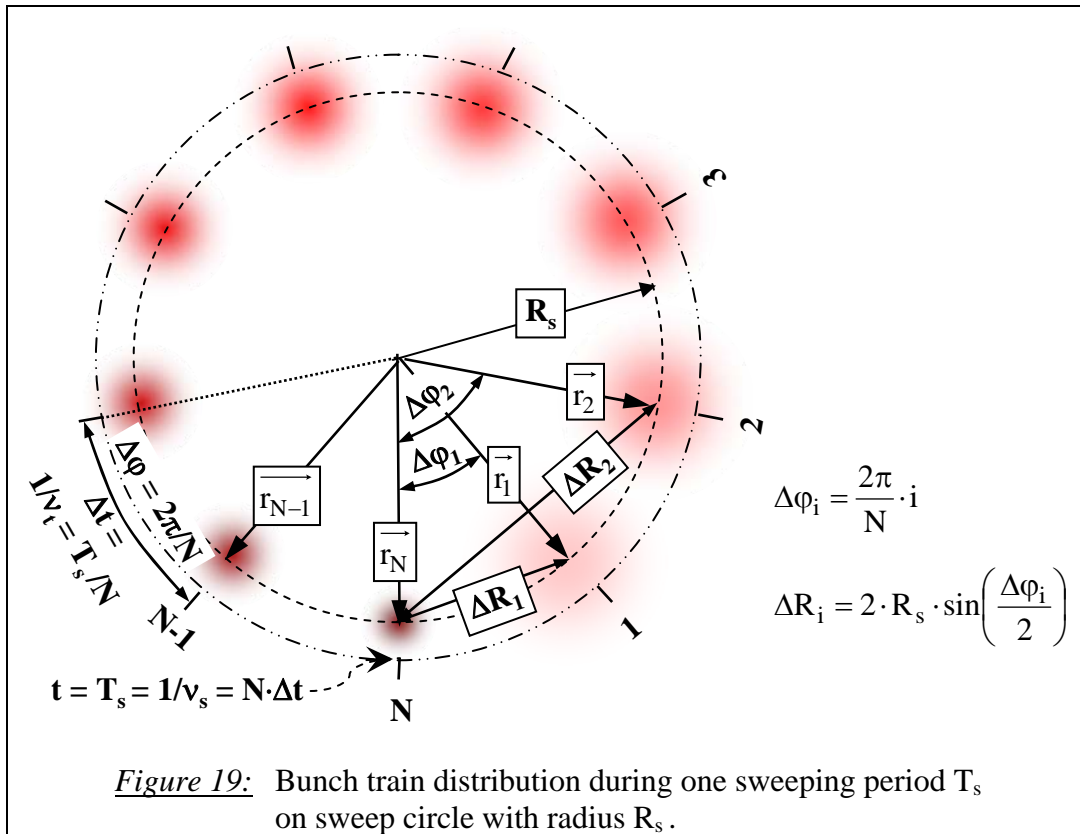
The ideal case of course would be to distribute the incoming electrons absolutely uniform on the sweep circle. If this was done that fast, that even the electrons within one bunch are swept, instantaneous effects would be smallest. But due to the short ( $\leq$  ps) bunches, more than THz sweeping frequencies would be required.

The next regime is the  $\approx 0.8$ ms intra bunch train time scale. Beam sweeping frequencies larger than  $\approx$  kHz would reduce instantaneous heating as induced by the total bunch train charge, but not the temperature jump caused by single bunches.

Due to the required beam size of  $\sigma_{\text{beam}} \geq 2$ mm the baseline design can accept the instantaneous load coming from each full bunch train. In this case beam sweeping only has to act on the most coarse time structure of the beam, namely the sequence of bunch trains spaced in time by  $1/v_t = \Delta t$ , as sketched in Figure 19. It shows the  $r$ - $\phi$  plane at a certain depth  $z$  in the graphite core of the dump. During one sweep period time  $T_s$ ,  $N$  bunch trains arriving with a repetition rate  $v_t$  are distributed in anti-clockwise direction on the sweep circle with radius  $R_s$  such that:

$$N \cdot \Delta t = T_s \Leftrightarrow N = T_s \cdot v_t \text{ respectively } N \cdot \Delta\phi = 2\pi \Leftrightarrow \Delta\phi = 2\pi / (T_s \cdot v_t) \quad \text{Equation 6}$$

The bunch trains are numbered from  $i=1$  to  $i=N$ . The position of the shower axis generated by the  $i$ -th bunch train is expressed by a two dimensional vector  $\vec{r}_i$  in the  $r$ - $\phi$  plane, i.e.  $|\vec{r}_i| = R_s$ . After  $N$  bunch trains have passed, the next  $N$  trains would hit the same positions



$\vec{r}_1$  to  $\vec{r}_N$  again under this condition. With respect to average heating this represents the worst case, since the average power is distributed into N thermal centers of gravity instead of being diluted over the whole sweep circle. In practice one would of course choose the sweeping period slightly deviating from that, in order to avoid an integer product  $T_s \cdot v_t$ , but for the following consideration we maintain it as a conservative assumption.

Within this frame the lowest sweeping period is  $T_s = \Delta t = 1/v_t$  and gives  $N = 1$ , which is identical to the non-swept case. A given bunch train distribution pattern characterized by the number N, can either be achieved by a sweep period  $T_{1s} = N/v_t$  or by a smaller sweep period  $T_{2s} = 1/(N \cdot v_t)$ . In both cases N bunch trains are distributed equidistant over the sweep circle within the time  $T_{1s}$ . In case 2 the sweeping system has a higher frequency without impact, since it performs an unnecessary number of cycles in between the arrival of two subsequent bunch trains. Thus case 2 has been excluded in the following considerations.

After quasi steady state has established, the temperature profile  $T(R_s, \varphi)$  at a certain time and depth z varies most with  $\varphi$ , if N is small and if the total dissipated longitudinal power density is high. Therefore at a given sweeping period the worst case in terms of absolute average temperature level and inhomogeneity along  $\varphi$  happens at 25GeV / 12 $\mu$ A conditions. Here still the maximum power of 300kW is achieved with fully populated bunch trains, but at a repetition rate of  $v_t = 3$ Hz only.

Looking at one of the positions  $\vec{r}_i$  in time, the temperature will oscillate there with the sweeping period of  $T_s$  around the average temperature level. The amplitude of this oscillation determines the cyclic load and is analytically calculated as a function of the sweeping period in section 3.1.1 in order to derive reasonable sweeping frequency limits. Profiles on absolute temperature and stress levels are calculated in section 3.1.2 fully numerically in 3d for the 25GeV / 12 $\mu$ A / 3Hz and the 7.5GeV / 40 $\mu$ A / 10Hz case with or without sweeping.

### 3.1.1 Reasonable Choice of Sweeping Frequency

Looking at Figure 19, the slower beam sweeping gets, the closer the axes of subsequent bunch trains are separated transversely. At a given time and position on the sweep circle, the spatial energy density will be influenced by neighbouring bunch trains more, the closer they are spaced. Looking at this position in time, its energy density and thus temperature will undergo oscillations with a repetition rate of the sweeping frequency  $v_s = 1/T_s$ . The amplitude of this oscillation determines the cyclic stress exposure of the material and should differ only negligible from the amount caused by one bunch train. In that case the simplified assumptions of chapter 2, from which the baseline layout was derived are still justified.

The highest temperature oscillation amplitude performs at one of the positions  $\vec{r}_i$ , and here we take  $\vec{r}_N$ . That is why one has to calculate the spatial energy density, which has been accumulated at position  $\vec{r}_N$  at the time  $t_N$ , when the N-th bunch train just enters there and from all N-1 preceding bunch trains, which arrived earlier at the other positions  $\vec{r}_1$  to  $\vec{r}_{n-1}$ . With respect to bunch train number N, the i-th train comes earlier by:

$$\Delta t_i = (N - i) \cdot \Delta t = (N - i)/v_t \quad \text{Equation 7}$$

As known from annex A.1.2 the radial profile of spatial energy density can be described by the sum of two Gauss functions. For peak spatial energy density considerations as we are interested in here, only the narrow core is relevant and thus only one simple Gauss distribution with a characteristic width  $\sigma_0(z)$  will be used in the following.

If heat flow from a point on the sweep circle  $r = R_s$  towards the graphite/copper boundary at  $r = R_s + 5\text{cm}$  is slow compared to the sweeping period  $T_s$ , the temporal development of the initial energy density profile during the sweep period can be treated fully by thermal diffusion in graphite. Therefore the following investigations are valid for sweeping periods  $T_s \ll (5\text{cm})^2 \cdot \rho \cdot c / \lambda \approx 60\text{s}$ . From explanations in annex B.2 it is known that a gaussian profile with the initial width  $\sigma_0(z)$  develops due to heat diffusion like:

$$\sigma^2(z, \Delta t_i) = \sigma_0^2(z) + 2 \cdot a \cdot \Delta t_i \quad \text{with : } a = \frac{\lambda}{\rho \cdot c} \quad \underline{\text{Equation 8}}$$

Thus the contribution of energy density  $\varepsilon_i(\vec{r}_N, z, \Delta t_i)$  at position  $\vec{r}_N$ , which comes from the  $i$ -th bunch train, which had entered the dump at position  $\vec{r}_i$  at a time  $t_N - \Delta t_i$  before, can be written as:

$$\varepsilon_i(\vec{r}_N, z, \Delta t_i) = \frac{dE}{dz}(z) \cdot \frac{1}{2\pi \cdot \sigma^2(z, \Delta t_i)} \cdot \exp\left[-\frac{(\vec{r}_N - \vec{r}_i)^2}{2 \cdot \sigma^2(z, \Delta t_i)}\right] \quad \underline{\text{Equation 9}}$$

Here  $(\vec{r}_N - \vec{r}_i)^2 = (\Delta R_i)^2$  is the closest radial distance between the position  $\vec{r}_N$ , where the energy density is summed up, and the position  $\vec{r}_i$ , where bunch train number  $i$  enters. From cosine theorem, summing rules of the trigonometric functions and using  $\Delta\varphi_i = i \cdot 2\pi/N$  one gets:

$$\Delta R_i = 2 \cdot R_s \cdot \sin\left(\frac{\Delta\varphi_i}{2}\right) = 2 \cdot R_s \cdot \sin\left(i \cdot \frac{\pi}{N}\right) \quad \underline{\text{Equation 10}}$$

Therefore the contribution from all  $N$  bunch trains is:

$$\varepsilon_\Sigma(\vec{r}_N, z, t_N) = \frac{dE}{dz}(z) \cdot \frac{1}{2\pi} \cdot \sum_{i=1}^N \frac{1}{\sigma_0^2(z) + 2 \cdot a \cdot \Delta t_i} \cdot \exp\left[-\frac{2 \cdot R_s^2 \cdot \sin^2(i \cdot \pi/N)}{\sigma_0^2(z) + 2 \cdot a \cdot \Delta t_i}\right] \quad \underline{\text{Equation 11}}$$

In order to see, how much the  $N-1$  preceding bunch trains contribute, one can normalize this figure to the energy density  $\varepsilon_N(\vec{r}_N, z, \Delta t_N)$  induced by the last bunch train  $i=N$ , which hits at  $\vec{r}_N$  at a time  $\Delta t_N=0$ :

$$\varepsilon_N(\vec{r}_N, z, t_N) = \frac{dE}{dz}(z) \cdot \frac{1}{2\pi \cdot \sigma_0^2(z)} \quad \underline{\text{Equation 12}}$$

The ratio  $\varepsilon_\Sigma / \varepsilon_N = \Psi$  gives the factor by which the cyclic load is increased compared to the simplified picture, in which all power is ideally uniformly distributed on the sweep circle and instantaneous cyclic load was calculated by the impact of one bunch train only, neglecting the diffusive contribution of preceding bunch trains, which impinge at a different lateral position. Replacing  $\Delta t_i = (N-i) / \nu_t$  this ratio looks like:

$$\Psi(R_s, T_s, \nu_t, \sigma_0(z)) = \sigma_0^2(z) \cdot \sum_{i=1}^{N=T_s \cdot \nu_t} \frac{1}{\sigma_0^2(z) + 2a \cdot \frac{(N-i)}{\nu_t}} \cdot \exp \left[ -\frac{2 \cdot R_s^2 \cdot \sin^2 \left( i \cdot \frac{\pi}{N} \right)}{\sigma_0^2(z) + 2a \cdot \frac{(N-i)}{\nu_t}} \right] \quad \text{Equation 13}$$

The simplified picture, which was assumed in chapter 2 to develop the baseline layout of the dump, is still justified if the ratio  $\Psi(R_s, T_s, \nu_t, \sigma_0(z))$  is close to 1.

In Figure 20 this ratio is plotted as a function of the initial width  $\sigma_0(z)$  of the radial energy density deposition profile for different sweeping periods  $T_s$  and two different specific bunch train repetition rates of 3Hz and 10Hz respectively. The qualitative behaviour of these curves is quite easy to understand. The influence of neighbouring bunch trains grows if the shower profile is wider or if the shower axes of neighbouring bunch trains are closer in time as well as in space. That is why the function  $\Psi$  increases with larger transverse shower size  $\sigma_0$ , with larger sweeping period  $T_s$  and larger bunch train repetition rate  $\nu_t$ . Both of the two latter conditions decrease the transversal separation of subsequent bunch trains, i.e. the number  $N$  increases. For a constant pattern with  $N$  bunch trains but a different bunch train repetition rate,  $\Psi$  differs only due to the effect of thermal diffusion because the temporal spacing of subsequent bunch trains  $\Delta t$  changes. That is why the curve for 1s/10Hz  $\Leftrightarrow N=10$  and 3s/3Hz  $\Leftrightarrow N=9$  are close together.

Since instantaneous heating goes with  $N_t \cdot \max(dE/dm)$ , the worst case will appear for a 25GeV beam and fully populated bunch trains. Restricted by the average power limit, the maximum bunch train repetition rate is not allowed to exceed a value of  $\nu_t=3\text{Hz}$ . During continuous operation at 10Hz, the bunch trains can only keep up their full charge if the energy does not reach beyond 7.5GeV, otherwise the power limit would be violated again. From Figure 17 one can see, that  $N_t \cdot dE/dm$  at  $z = t_E$  is a factor of 2.5 higher for a 25GeV incoming beam with a size of  $\sigma_{\text{beam}}=2\text{mm}$  than in the 7.5GeV case (250J/g instead of 100J/g). As explained in section 2.2.1 on page 10 the width  $\sigma_0(z)$  is about 2.8mm at  $z = t_E$  and about 4mm

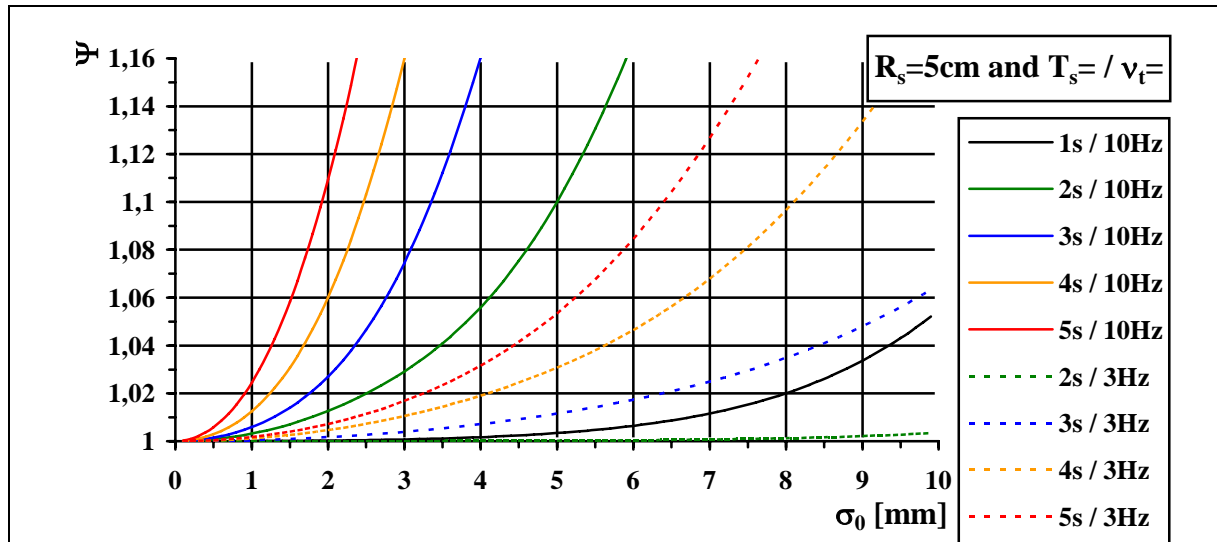


**Figure 20:** Ratio between amplitude of cyclic temperature change at a worst case position on the sweep circle of radius  $R_s = 5\text{cm}$ , if  $N$  bunch trains are distributed there within one sweep period ( $T_s \cdot \nu_t = N$ ), and the instantaneous temperature jump as induced by one bunch train.

at  $z = t_{\max}$  for an incoming beam (7.5GeV or 25GeV) with a 2mm size. That is why we have to concentrate on  $\sigma_0$  in the range 3mm to 4mm, when discussing the plots of the function  $\Psi$  for our situation.

The graphite based layout has a cyclic load limit of about 250J/g. This will be reached for a maximum populated bunch train ( $2.5 \cdot 10^{13} e^-$ ) entering with a size of  $\sigma_{\text{beam}} = 2\text{mm}$  and an energy of 25GeV. In continuous mode such an operation is possible at 3Hz only. If such a beam is circularly swept on a radius  $R_s = 5\text{cm}$ , Figure 20 indicates that the cyclic load increases by less than 1% if the sweeping period is restricted to  $T_s \leq 3\text{s}$ .

Under the same sweeping conditions this factor is already 1.16 at 10Hz bunch train repetition. Although not negligible in relative growth, in absolute numbers it means a cyclic load amplitude of 116J/g instead of 100J/g energy deposition generated by one bunch train. This is a consequence of the 300kW power limit, for which a continuous 10Hz operation with fully charged bunch trains can not be carried out at 25GeV but only up to 7.5GeV, where  $\max(dE/dm)$  is a factor of 2.5 smaller. In principle the ratio  $\Psi$  could show a value of 2.5 for the 7.5GeV / 10Hz case before exceeding the 250J/g limit and thus a sweeping period even up to  $T_s = 8\text{s}$  would do no harm in terms of cyclic load amplitude.

A simple sweeping system layout would use a fixed frequency, which has to cover the worst case operation scenario. Therefore under the aspect of cyclic load a sweeping period of  $T_s \leq 3\text{s}$  is a reasonable choice. On the other hand if the sweeping period becomes smaller, the number of bunch trains  $N$  and therefore the number of heat load centers on the sweep circle is less. As a consequence the average temperature profile shows a significant azimuthal inhomogeneity and centers of heat load build up with a high temperature level.

It has to be pointed out, that the assumption of an initial gaussian temperature or energy density profile, which undergoes thermal diffusion is violated if the average temperature is not flat along the sweep circle due to a small  $N$ . Hence the next section discusses by means of numerical methods, how temperature and stress will look like for a sweeping period of  $T_s = 1\text{s}$  and  $T_s = 2\text{s}$ , which gives  $N = 3$  and  $N = 6$  respectively for  $\nu_t = 3\text{Hz}$ , in order to see whether this is a dangerous point of operation. For that purpose of course the full radial layout with copper-shell, water cooling and assumptions on the heat transfer have to be included, otherwise the calculation of the absolute temperature level is not possible.

Again one has to remember, that here always the conservative constraint of an integer product  $T_s \cdot \nu_t = N$  is assumed. In practice a sweeping frequency, which differs slightly from that condition would be chosen and generated unsynchronized with respect to the bunch train repetition rate by an independent free running oscillator.

### 3.1.2 Analysis of Stresses and Temperatures in the Dump

The ANSYS code version 4.4 [4] has been applied to calculate temperature and mechanical stress distributions in the C/Cu-Al-Cu geometry as discussed in section 2.3.1. Compared to the baseline layout of Figure 16, a 50cm long Al-section is inserted between the 15cm long Cu-backstop and the leading C/Cu part, which here has a length of only 210cm instead of 330cm in the normal baseline design. The radial geometry does not differ between both layouts. That is why both geometries are completely identical within the first 210cm, which is far beyond the shower maximum, up to which the maximum temperatures and stresses in the C/Cu section will occur. In terms of the situation in the leading C/Cu section, all results within  $0 \leq z \leq 210\text{cm}$  from the calculated C/Cu-Al-Cu geometry are thus valid for the baseline layout as well. In addition to the information on the thermal and mechanical status of the C/Cu front part, a more correct answer on the maximum temperatures in the downstream Al and Cu regions is obtained from this calculation and discussed in section 3.1.2.1.

The results of the stress calculations in the leading C/Cu part can be compared with the mechanical stress limits of the material by means of a certain failure criterion expressed by the equivalent stress value  $\sigma_{eq}$ , which can be defined as:

$$\sigma_{eq} = \frac{1}{\sqrt{2}} \cdot \sqrt{(\sigma_1 - \sigma_2)^2 + (\sigma_2 - \sigma_3)^2 + (\sigma_3 - \sigma_1)^2} \quad \text{Equation 14}$$

At a given position  $\sigma_1$ ,  $\sigma_2$  and  $\sigma_3$  with  $\sigma_1 > \sigma_2 > \sigma_3$  are the stress components in the three main directions of the given coordinate system, here r, z and  $\varphi$ . Since  $\sigma_{eq}$  is always a positive value, it can be judged by the sign of the contributing stress components, whether the material has to withstand a compressive or tensile load. Compression (tension) forces correspond to a negative (positive) sign in ANSYS results. Comparing the equivalent stress and the amplitude of its cyclic change with the static and cyclic load limits of the material tells us, whether the operation is mechanically critical or not. In Table 6 the mechanical limits of cyclic and static load are summarized for graphite and copper. Except for the static limits of graphite they were

	<b>Graphite</b>	<b>Copper</b>
cyclic stress limit: $\sigma_u$ [MPa]	60 <sup>1)</sup> / 30 <sup>2)</sup>	60 – 100
static stress limit: [MPa]	100 – 250 <sup>3)</sup> for compression ≥ 40 <sup>3)</sup> for tension	$\sigma_{0.2} \approx 150 – 400$ <sup>3)</sup>

<sup>1)</sup> at compression / <sup>2)</sup> at tension, <sup>3)</sup> depending on specific material

**Table 6:** Relevant mechanical strength limits for graphite and copper.

already given in Table 2.

The boundary conditions for the following considerations are:

1.) Dump Geometry

A longitudinal segment of a certain length  $\Delta z$  of the main radial C / Cu section of the dump layout as discussed in section 2.3.1 is subject to the calculations. Thus a graphite core of radius  $R_C = 10\text{cm}$  is embedded in a  $\Delta R_{Cu} = 8\text{cm}$  copper shell, which is water cooled at its outer surface at  $r = R = 18\text{cm}$ .

2.) Boundary Conditions during Calculation

- a. The temperature of the cooling water is set to  $T_0 = 20^\circ\text{C}$  (attention: the results of chapter 2 are based on  $T_0 = 50^\circ\text{C}$  !).
- b. Heat transfer at the radial C / Cu boundary is regarded to be perfect, i.e. there is no temperature drop across this contact. Under real conditions the graphite core will be hotter and expands more than calculated. As a consequence the difference in elongation and thus stress at the C / Cu boundary due to the different thermal expansion of graphite and copper will diminish. Concerning stress at this boundary the given assumption on heat transfer is conservative.
- c. Heat transfer at the Cu / water respectively Al / water boundary is specified by a coefficient of  $K_{\rightarrow w} = 0.4\text{W/m}^2/\text{K}$  and uses the full surface area of  $\Delta A = 2\pi R \cdot \Delta z = 113\text{cm}^2 \cdot \Delta z/\text{cm}$ .
- d. Thermal diffusion is included in the calculations. Nevertheless due to the rather large beam size of  $\sigma_{beam} = 2\text{mm}$  the influence of thermal diffusion is negligible.
- e. The C / Cu boundary stays gap-free and is mechanically rigid. Thus a relative displacement, i.e. slippage of graphite against copper is not possible here.

- f. At the beginning of the calculations, before the beam enters, the geometry has no initial stresses and everywhere the same uniform temperature of  $T_0 = 20^\circ\text{C}$ . The results are shown at a time large enough, such that quasi steady state has established, i.e. average temperature distribution has reached its maximum and does not vary with time anymore.

### 3.) Beam Parameters

Two cases of beam operation are considered. In both cases the bunch trains are fully populated with  $N_t = 2.5 \cdot 10^{13} e^-$ , the average beam power is  $P_{\text{ave}} = 300\text{kW}$  and the beam enters the dump with a size of  $\sigma_{\text{beam}} = 2\text{mm}$ .

- $E_0 = 25\text{GeV}$ ,  $\nu_t = 3\text{Hz}$
- $E_0 = 7.5\text{GeV}$ ,  $\nu_t = 10\text{Hz}$

### 4.) Sweeping Parameters

Calculations are done without or with a swept beam.

If beam sweeping is applied, the following parameters are chosen:

- The sweep radius is set to  $R_s = 5\text{cm}$ .
- A sweep period of  $T_s = 1\text{s}$  is used in the  $7.5\text{GeV} / 10\text{Hz}$  and  $T_s = 2\text{s}$  in the  $25\text{GeV} / 3\text{Hz}$  case.
- The effect of a faster sweeping with  $T_s = 1\text{s}$  is studied for the  $25\text{GeV} / 3\text{Hz}$  situation as well. This situation gives a very inhomogeneous bunch train distribution pattern with  $N = 3$  only and serves as a worst case investigation.

#### 3.1.2.1 *Without Beam Sweep*

Of course the maximum stresses and temperatures are obtained if the beam is not swept and the graphite core is not segmented longitudinally. In that case the longitudinal segment has a length of  $\Delta z = 210\text{cm}$ . The resulting longitudinal temperature profile on the dump axis ( $=$  shower axis) at  $r = 0$  is plotted in Figure 21 for the  $7.5\text{GeV} / 10\text{Hz}$  case just before and just after the arrival of a bunch train. Let us introduce the longitudinal position of maximum

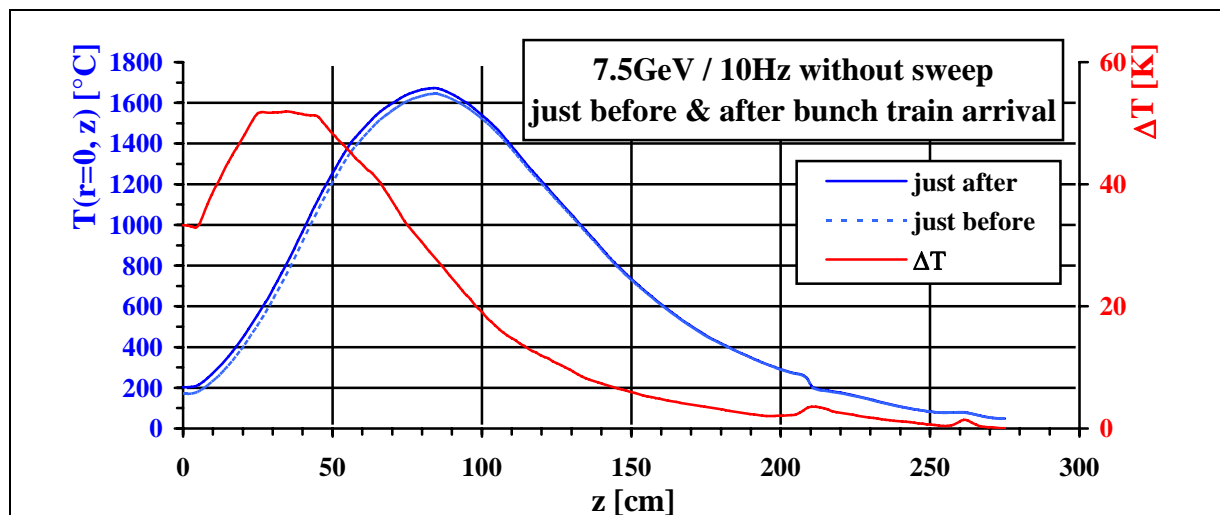


**Figure 21:** Longitudinal steady state temperature profile on the axis ( $r = 0$ ) of the C/Cu-Al-Cu dump geometry (210cm C/Cu + 50cm Al + 15cm Cu), as discussed in section 2.3.1, just before and just after the arrival of a fully charged bunch train. The bunch trains ( $N_t = 2.5 \cdot 10^{13} e^-$ ) are not swept and enter on the dump axis with  $E_0 = 7.5\text{GeV}$ ,  $\nu_t = 10\text{Hz}$  and a size of  $\sigma_{\text{beam}} = 2\text{mm}$ .

temperature  $z = t_T$ , which is at  $t_T \approx 83\text{cm}$  for this 7.5GeV beam. It is somehow in between the depth of maximum spatial energy density  $t_E = 45\text{cm}$  and the shower maximum at  $t_{\max} = 95\text{cm}$ , because instantaneous and equilibrium temperatures add. For a 25GeV beam this position shifts a little deeper into the dump towards  $t_T \approx 90 - 100\text{cm}$ .

The maximum temperature at  $z = t_T$  is about  $1670^\circ\text{C}$  just after a 7.5GeV bunch train passage. The cyclic amplitude  $\Delta T$ , between the temperatures just before and just after a bunch train arrival, is plotted on the secondary scale in Figure 21 too. Its maximum value is only  $\Delta T = 50\text{K}$  due to the increased heat capacity of graphite, which is already near to  $2\text{J/g/K}$  according to Equation 1 at such a high temperature.

Also clearly visible, by tiny peaks in the temperature curves of Figure 21, are the beginning of the 50cm long Al-section at  $z = 210\text{cm}$  and the beginning of the 15cm long Cu-backstop at  $z = 260\text{cm}$ . The upstream end of the Al part operates at a maximum temperature level of around  $200^\circ\text{C}$  and each bunch train generates a jump of less than  $4\text{K}$  there. The Cu-backstop runs only at a moderate operation temperature of about  $80^\circ\text{C}$  and the cyclic contribution by each bunch train is around  $1.5\text{K}$ . Maximum quasi steady state temperature and cyclic instantaneous temperature rise in Al and Cu regions are safely within the limits as given by Table 2 and Table 3.

The peak stresses in graphite at  $r = 0$  for this non-swept case have been calculated as:

$$\sigma_{\text{eq}} = 153\text{MPa}, \sigma_1 = -163\text{MPa} \text{ and } \sigma_3 = -313\text{MPa}$$

Due to the negative sign the graphite experiences pure compression forces on the axis, which are beyond the tolerable limits. Cutting the 330cm long dump into shorter disks introduces longitudinal decoupling of forces and reduces the stress situation. If the disks are 30cm or 10cm long, the maximum equivalent stress is decreased to  $\sigma_{\text{eq}} = 103\text{MPa}$  or even  $\sigma_{\text{eq}} = 71\text{MPa}$ . The latter value is already close to the compressive endurance limit of graphite. That is why 10cm long disks of the radial C / Cu structure are considered in the following stress calculations under the conditions of a swept beam.

Nevertheless without beam sweeping temperature and stress in graphite exceed the tolerable limits.

### 3.1.2.2 With Beam Sweep

In this section the beam will be swept circularly on a radius of  $R_s = 5\text{cm}$ . The geometry of the dump remains unchanged with respect to the previous section, where the beam was not swept. Longitudinally the dump is segmented into disks with a length of  $\Delta z = 10\text{cm}$ . Temperature and stress distribution as derived by ANSYS calculations are shown for such a disk being located at a depth of most relevance, namely near the shower maximum  $z = t_{\max}$  and at  $z = t_T$ , where the maximum amplitude of temperature oscillations is observed.

In total 3 different combinations of beam and sweep parameters were investigated as mentioned in section 3.1.2 on page 29. In all cases the bunch trains have their maximum charge of  $N_t = 2.5 \cdot 10^{13}e^-$  and a beam size of  $\sigma_{\text{beam}} = 2\text{mm}$ . The average power is  $P_{\text{ave}} = 300\text{kW}$  and the sweep radius is  $R_s = 5\text{cm}$ . The first two cases cover the 25GeV beam operation with a bunch train repetition rate of  $\nu_t = 3\text{Hz}$ . In Case 1 the sweeping period  $T_s = 1\text{s}$  and thus the bunch trains are distributed into  $N = 3$  positions on the sweep circle. Case 1 can be regarded as a worst case scenario, since it combines the highest spatial energy density  $dE/dm$  with a very non uniform distribution of maximum average power. Concerning this uniformity case 2 is a little relaxed, since the sweeping period is  $T_s = 2\text{s}$  and the power is diluted into  $N = 6$  heat load centers. Case 3 finally deals with a 7.5GeV beam and a  $\nu_t = 10\text{Hz}$  bunch train repetition. Under these conditions the density of longitudinal power dissipation  $dP/dz$  is at its maximum.

The sweep period is chosen to be  $T_s = 1\text{s}$  in case 3, which gives a distribution pattern with  $N = 10$  bunch trains on the sweep circle. In that sense these 3 cases cover the worst case operation conditions for the dump.

Table 7 summarizes the ANSYS results in terms of maximum temperatures and stresses as well as their maximum variation with time (before / after bunch train passage), which is relevant for the cyclic load impact on the material. The maximum temperature of  $522^\circ\text{C}$  just after a bunch train passage arises from case 1, as can be seen in Figure 22 a). Just before entering of this bunch train, the same position has cooled down to  $380^\circ\text{C}$ . The temporal temperature cycle on the sweep circle of  $\Delta T = 142\text{K}$  results in an equivalent stress oscillation between the limits of  $3.4\text{MPa}$  and  $8.2\text{MPa}$ , as shown in Figure 22 b). In other words the equivalent stress  $\sigma_{\text{eq}}$  cycles with an amplitude of  $\Delta\sigma_{\text{eq}} = \pm 2.4\text{MPa}$  around a mean value of  $5.8\text{MPa}$ . In terms of cyclic variation case 2 performs a similar temperature amplitude of  $\Delta T = 144\text{K}$  at a slightly lower temperature level. The equivalent stress situation here is worse than in case 1, since it cycles with an amplitude of  $\Delta\sigma_{\text{eq}} = \pm 4.1\text{MPa}$  around a mean value of  $7.2\text{MPa}$ . As expected case 3 is most relaxed due to a quite homogeneous distribution of  $N = 10$  bunch trains along the sweep circle.

All cyclic load in graphite is mainly of a compressive type. Therefore the maximum amplitude of  $\pm 4.1\text{MPa}$  is a safe situation, when comparing it with the compressive endurance strength of  $\sigma_u = 60\text{MPa}$ , but would even be safe for the tensile limit of  $30\text{MPa}$ .

From Figure 23 it is obvious, that temporal temperature and thus stress variations rapidly fall off within a radial seam of  $\Delta r = \pm 1\text{cm}$  around the sweep circle and are negligible compared to the average value around which they oscillate. Mean temperature levels do not exceed the  $500^\circ\text{C}$  oxidation limit of graphite and decrease the more uniform the bunch trains are distributed on the sweep circle.

Except for the  $\pm 1\text{cm}$  region around the sweep circle, graphite is mainly loaded statically. Maximum static stress levels are found in the center at  $r = 0$ , where an equivalent compression pressure of up to  $23\text{MPa}$  is generated due to the temperature profile in the graphite core. As a result of different thermal expansion between graphite and copper, high stress is expected also at the radial C / Cu boundary at  $r = 10\text{cm}$ . In Figure 24 a) equivalent stresses of up to  $25\text{MPa}$  are indicated there, especially at the longitudinal edges, where the difference in expansion has most influence. In this region tension and shear contribute significantly to the equivalent stress. But fortunately a value of  $25\text{MPa}$  is still much less than graphite's tensile strength of at least  $40\text{MPa}$ .

Not shown in the plots of Figure 22 through Figure 25 are the stresses in the copper shell. Quite far away from the sweep circle, the copper shell is not affected cyclically. The maximum of static load in copper in terms of equivalent stress does not exceed  $40\text{--}50\text{MPa}$ , which is well below the yield strength even of soft annealed copper materials.

From these results it can be concluded, that a dump with the baseline radial C / Cu geometry as shown in Figure 16 should provide the required lifetime of  $\approx 10$  years respectively  $\approx 10^9$  bunch train passages.

In order to indicate the influence of the pulsed beam structure, the bottom of Table 7 lists the temperature and stress levels for a beam, which has no time structure. The temperature in the dump for such a non pulsed pure dc-beam has already been shown in Figure 18 a). Before putting them in Table 7 these values have been corrected by subtracting the temperature drop across the C / Cu boundary and a constant amount of  $30\text{K}$ , because the ANSYS calculations

assumed an ideal heat transfer at the C / Cu boundary and took a cooling water temperature of  $T_0 = 20^\circ\text{C}$  instead of  $T_0 = 50^\circ\text{C}$  as assumed in Figure 18 a).

The equivalent stress of about 10–14MPa in the center of the graphite core under dc-beam operation was calculated by using the radial temperature profile  $T(r)$  of Figure 18 a). The main stress components can be estimated as:

$$\begin{aligned}\sigma_r &= \alpha \cdot E \cdot (\xi(R) - \xi(r)) / (1 - \nu) \\ \sigma_\phi &= \alpha \cdot E \cdot (\xi(R) + \xi(r) - T(r)) / (1 - \nu) \quad \text{with: } \xi(r) = \frac{1}{r^2} \cdot \int_{x=0}^r T(x) \cdot x \, dx \quad \text{Equation 15} \\ \sigma_z &= \alpha \cdot E \cdot (2 \cdot \xi(R) - T(r)) / (1 - \nu)\end{aligned}$$

Where  $\alpha$ ,  $\nu$  and  $E$  are the thermal expansion coefficient, the Poisson ratio and the elastic modulus of graphite as given in Table 2. The radial temperature profile  $T(r)$  was numerically integrated to calculate  $\sigma_r$ ,  $\sigma_\phi$  and  $\sigma_z$  from which the equivalent stress is derived similar to Equation 14 like:

$$\sigma_{\text{eq}} = \frac{1}{\sqrt{2}} \cdot \sqrt{(\sigma_\phi - \sigma_r)^2 + (\sigma_\phi - \sigma_z)^2 + (\sigma_z - \sigma_r)^2} \quad \text{Equation 16}$$

In longitudinal symmetry plane of 10cm disk							
		Temperature @ r = , (T <sub>0</sub> =20°C)		Equivalent Stress, $\sigma_{eq}$ @ r =			
Case #: E <sub>0</sub> v <sub>t</sub> /T <sub>s</sub> /N	disk position [cm]	center r = 0cm	sweep circle r = 5cm	center r = 0cm	r = 4cm	sweep circle r = 5cm	C / Cu contact r = 10cm
		mean value [°C]	before / after [°C] — $\Delta T$ [K]	mean value [MPa]	after / before — $\Delta\sigma$ [MPa]	after / before — $\Delta\sigma$ [MPa]	mean value [MPa]
Case 1: 25GeV 3Hz / 1s / 3	near z = t <sub>T</sub> 90-100	330 <sup>*)</sup>	380 / 522 — 142	20.1 <sup>*)</sup>		3.4 / 8.2 — 4.8	21.6 <sup>*)</sup>
	near z = t <sub>T</sub> 90-100	342 <sup>*)</sup>	308 / 452 — 144	19.7 <sup>*)</sup>	14.4 / 15.5 — 1.1	3.1 / 11.2 — 8.1	20.6 <sup>*)</sup>
Case 2: 25GeV 3Hz / 2s / 6	near z = t <sub>max</sub> 120-130	382 <sup>*)</sup>	340 / 436 — 96	22 <sup>*)</sup>	15.9 / 16.5 — 0.6	6.7 / 12.8 — 6.1	21 <sup>*)</sup>
	near z = t <sub>max</sub> 90-100	416 <sup>*)</sup>	375 / 409 — 34	23 <sup>*)</sup>	17.7 / 18 — 0.3	12.7 / 15.2 — 2.5	24 <sup>*)</sup>
dc-beam 300kW	25GeV	z = t <sub>max</sub> 120-130	339	300	10-14		
	7.5GeV	z = t <sub>max</sub> 90-100	375	320			

<sup>\*)</sup> amplitude of thermal and stress oscillation is less than 0.5% of the mean value

*Table 7:* Comparison of temperature and stress status in the graphite core of the baseline dump geometry being impinged by a swept beam.

**Temperature and Stress distributions in Case 1 at  $z = t_T = 90-100\text{cm}$ :**

$E_0 = 25\text{GeV}$ ,  $v_t = 3\text{Hz}$ ,  $T_s = 1\text{s}$ ,  $N = 3$ ,  $T_0 = 20^\circ\text{C}$

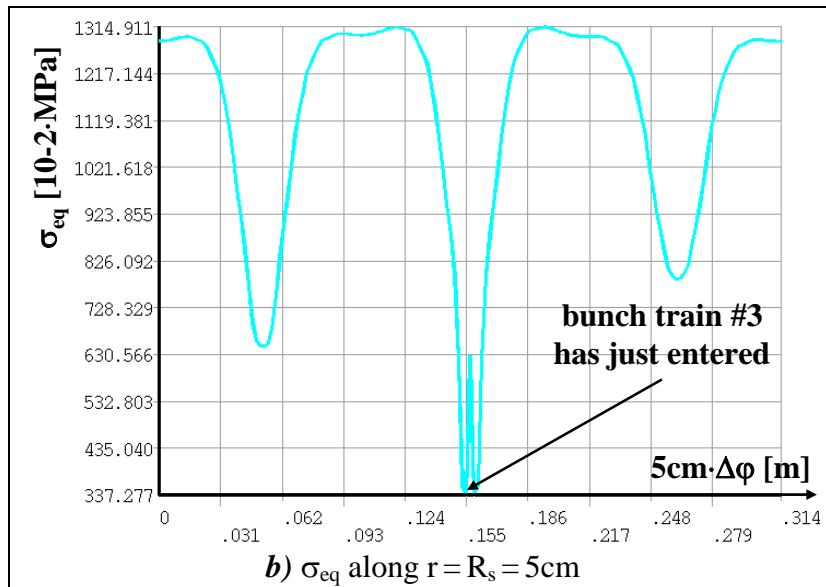
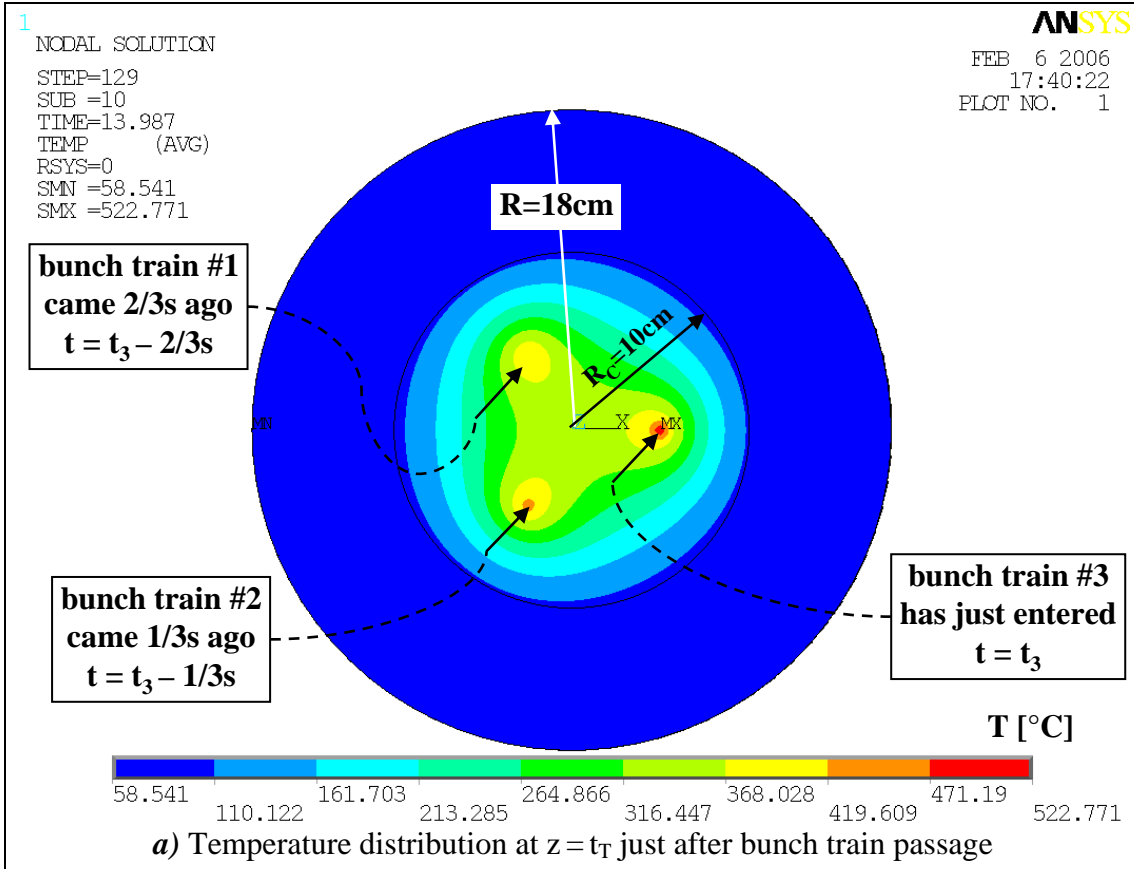


**Figure 22:** a) 2-d temperature profile and b) azimuthal stress distribution along sweep circle in case 1, i.e. for 25GeV / 3Hz beam parameters with 1s sweeping period, just after a bunch train passage and at the depth  $z = t_T$ , where temperature oscillations have their maximum.

**Temperature distributions in Case 2:**  
 $E_0 = 25\text{GeV}$ ,  $\nu_t = 3\text{Hz}$ ,  $T_s = 2\text{s}$ ,  $N = 6$ ,  $T_0 = 20^\circ\text{C}$

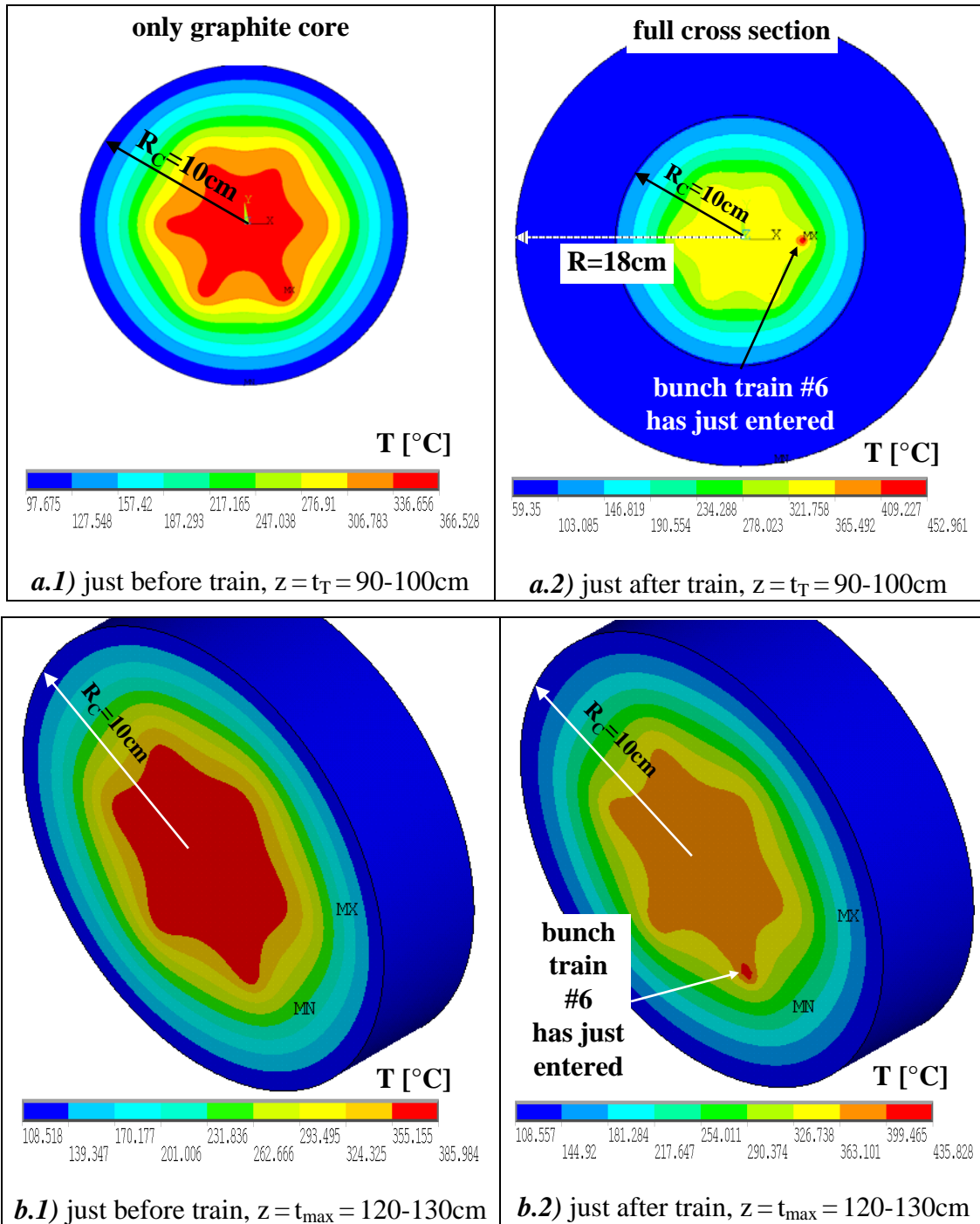


**Figure 23:** Temperature distribution in case 2, i.e. for 25GeV / 3Hz beam parameters with 2s sweep period, just before (.1) and after (.2) a bunch train passage. a) at the depth  $z = t_T$ , where temperature oscillations have their maximum b) near the shower maximum  $z = t_{\text{max}}$  (position of just impinging, i.e. here 6<sup>th</sup> bunch train is indicated)

**Stress distributions in Case 2 just after bunch train passage at  $z = t_{\max} = 120-130\text{cm}$**   
 $E_0 = 25\text{GeV}$ ,  $\nu_t = 3\text{Hz}$ ,  $T_s = 2\text{s}$ ,  $N = 6$

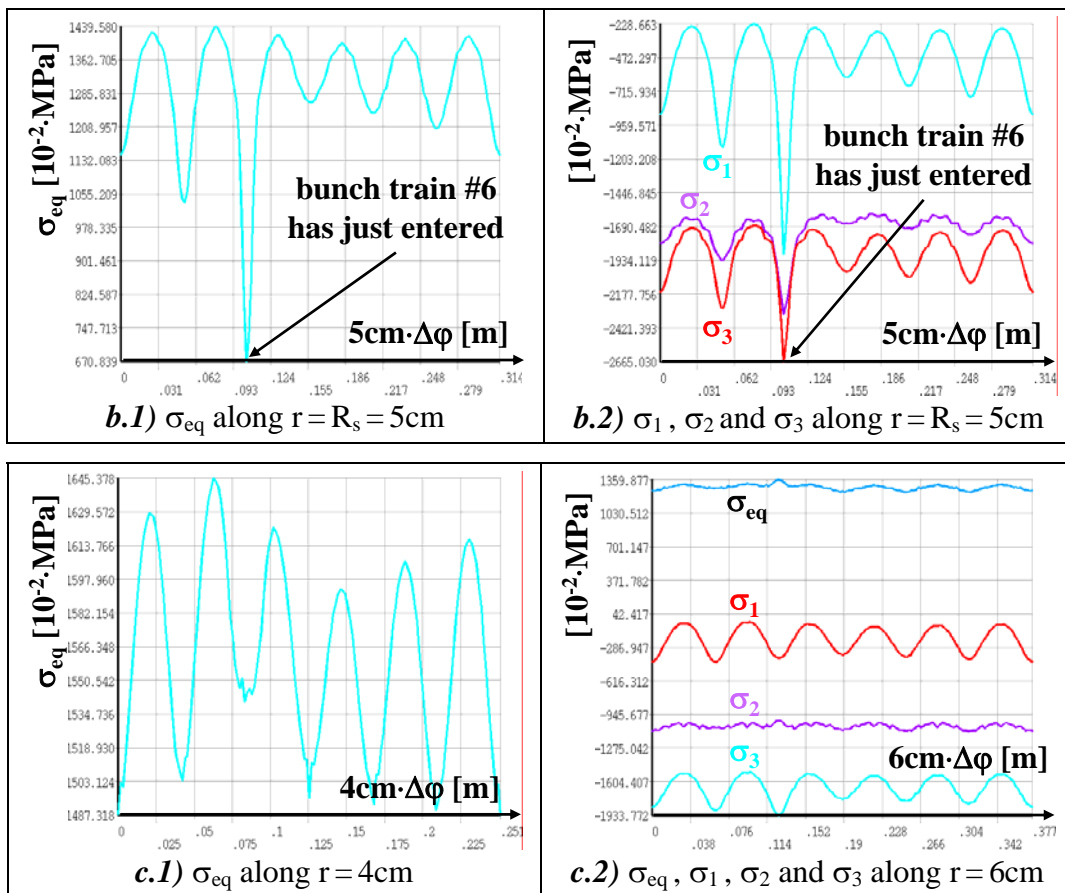
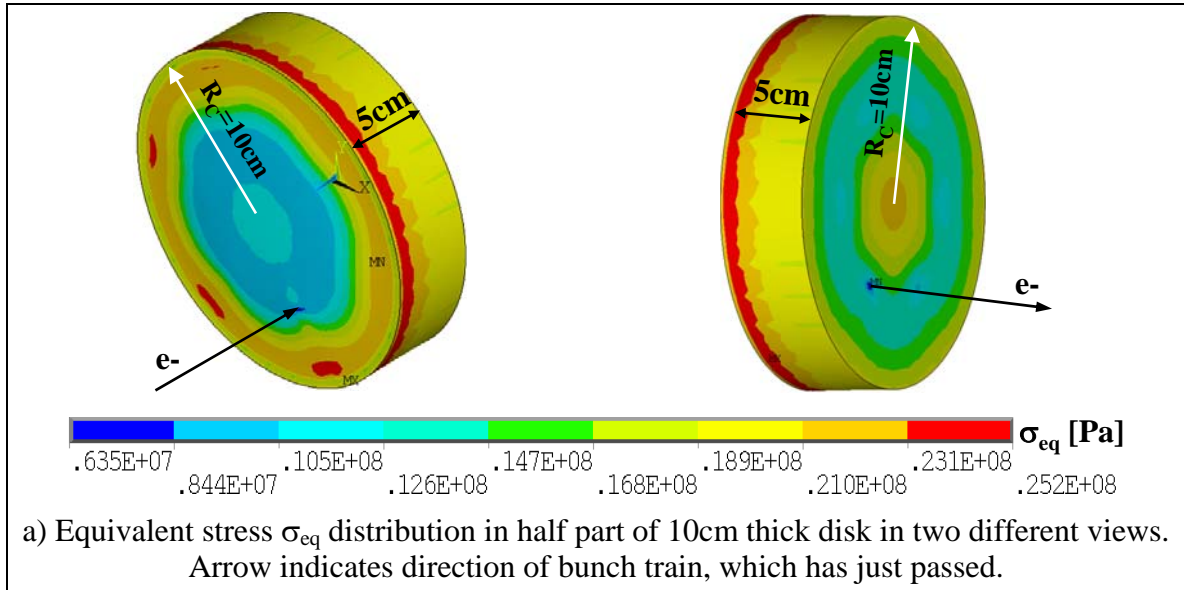


**Figure 24:** Stress status in case 2, i.e. for 25GeV / 3Hz beam parameters and a 2s sweep. a) 3d view and azimuthal distributions in the middle of the disk along a circle with radius b.1), b.2)  $r = R_s = 5\text{cm}$ , c.1)  $r = 4\text{cm}$  and c.2)  $r = 6\text{cm}$ . (position of just impinging, i.e. here 6<sup>th</sup> bunch train is indicated)

**Temperature and Stress distributions in Case 3 at  $z = t_{\max} = 90\text{-}100\text{cm}$**

$E_0 = 7.5\text{GeV}$ ,  $v_t = 10\text{Hz}$ ,  $T_s = 1\text{s}$ ,  $N = 10$ ,  $T_0 = 20^\circ\text{C}$

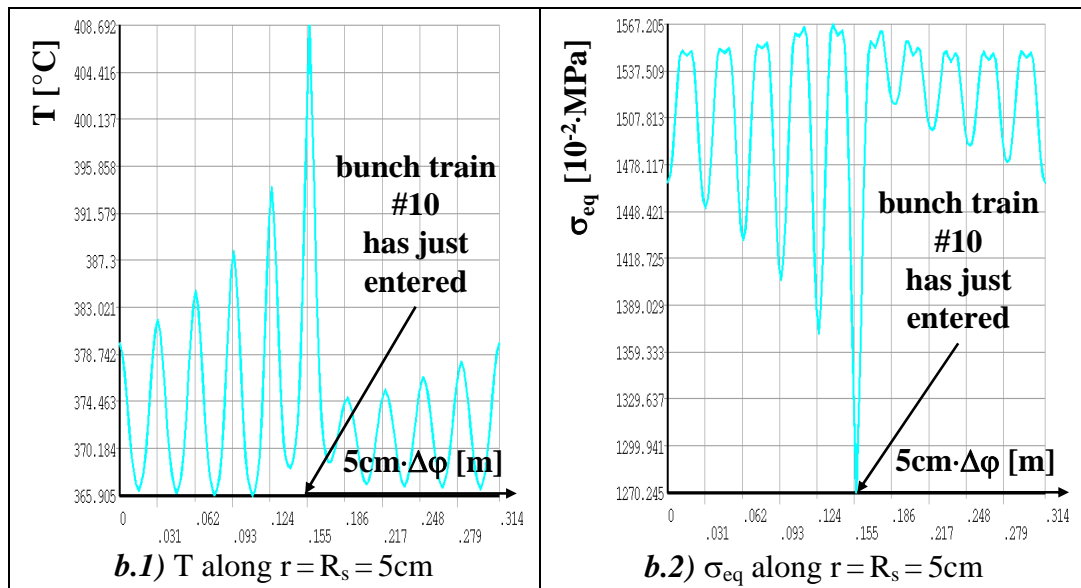
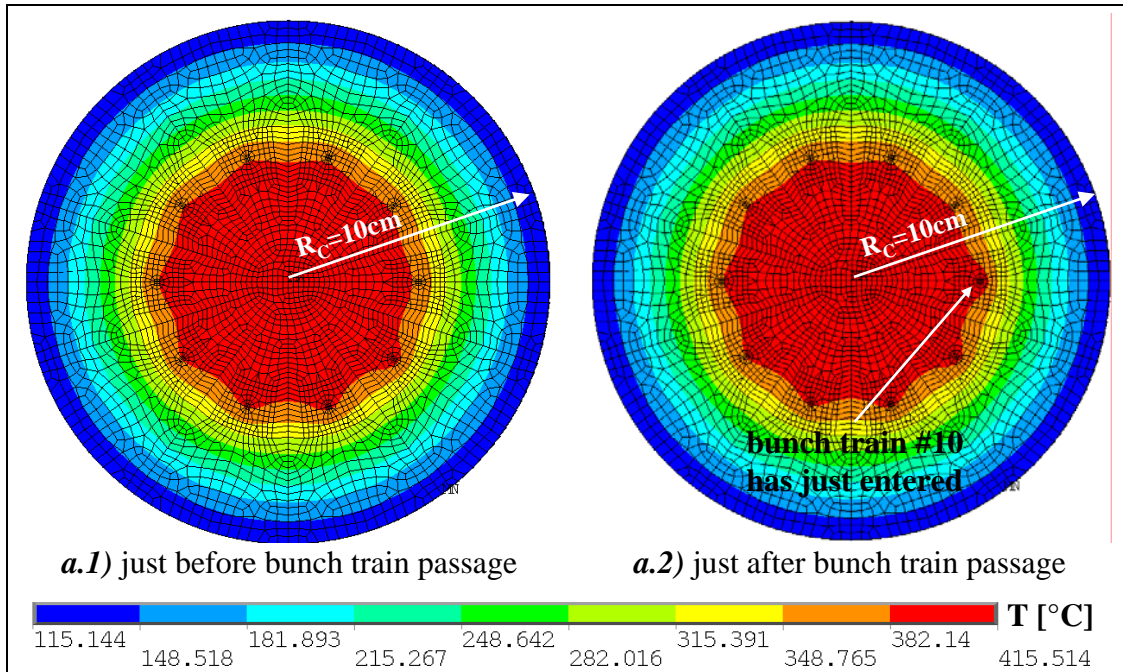


**Figure 25:** Distributions in case 3, i.e. for 7.5GeV / 10Hz beam parameters with 1s sweep period,  
*a)* 2-d views of temperatures near shower maximum  
*a.1)* just before and *a.2)* just after bunch train passage.  
*b)* Azimuthal distributions in the middle of the disk along the sweep circle.  
*b.1)* Temperatures just after bunch train passage  
*b.2)* Equivalent stress just after bunch train passage (position of just impinging, i.e. here 10<sup>th</sup> bunch train is indicated)

### 3.2 Heat Transfer at the Graphite-Copper Boundary

As intensively pointed out in section 2.2 heat extraction is the key issue of a solid based beam dump, which is operated at high longitudinal power densities. Hence in addition to the thermal conductivity of the participating materials, every material boundary will add to the temperature of the dump core, according to the temperature drop across it. Two boundaries contribute in the baseline dump layout, namely the contact between the graphite core and the copper shell at  $r=R_C=10\text{cm}$  as well as the one from the copper shell to the cooling water at  $r=R=18\text{cm}$ .

In the worst case a heat flux density of  $1840 \frac{\text{kW}}{\text{cm}} \cdot \frac{1}{2\pi \cdot R_C} \approx 30 \text{ W/cm}^2$  has to be handled at the C / Cu boundary near the shower maximum at  $z=t_{\text{max}} \approx 95\text{cm}$  with a  $7.5\text{GeV} / 300\text{kW}$  beam. Due to the larger surface the heat transfer towards the cooling water is less critical with a maximum heat flux density of about  $1840 \frac{\text{kW}}{\text{cm}} \cdot \frac{1}{2\pi \cdot R} \approx 16 \text{ W/cm}^2$ . These values assume that the total cylindrical surface area at the radius of the boundary serves as a transition cross section for the heat. Heat transfer coefficients on water cooled metal surfaces are quite well known as a function of temperature, pressure and flow properties of the cooling water. That is why the assumed coefficient of about  $0.4\text{W/cm}^2/\text{K}$  is a realistic value and adds a temperature drop of about  $40\text{K}$  to the average temperature profile at the shower maximum.

Under the same assumptions the contribution from the C / Cu boundary is about  $75\text{K}$ . This is already a non negligible 16% fraction of the total difference between the graphite core temperature of  $\approx 500^\circ\text{C}$  and the water temperature of  $T_0=50^\circ\text{C}$ . Therefore the following sections 3.2.1 and 3.2.2 investigate in more detail, under which conditions the assumed heat transfer coefficient of  $K_{\rightarrow\text{Cu}} \geq 0.4\text{W/cm}^2/\text{K}$  can be achieved.

#### 3.2.1 Pressed Contact

Looking at the contact of two materials a little closer, there are two surfaces of a certain roughness pressed together with a pressure  $p$ . In general the interstices between the rough surfaces are filled with a gas. The overall heat transfer coefficient  $K$  of such a contact can be expressed as the sum of these two contributions:

$$K = K_{\text{direct}} + K_{\text{gas}} \quad \text{Equation 17}$$

The heat, which flows from one material (1) to the other (2) via points, where they have direct contact is described by  $K_{\text{direct}}$ . Heat, which is transported through the contact by using the thermal conductivity of the gas in the interstices, is covered by  $K_{\text{gas}}$ .

According to measured data [5] an empirical formula expresses the direct heat transfer coefficient  $K_{\text{direct}}$  as:

$$K_{\text{direct}} = 212 \cdot \frac{\lambda_m}{\text{cm}} \cdot \left( \frac{p}{E_m} \cdot B_s \right)^{0.8} \quad \text{with:} \quad \begin{aligned} \lambda_m &= 2 \cdot \frac{\lambda_1 \cdot \lambda_2}{\lambda_1 + \lambda_2} \\ E_m &= 2 \cdot \frac{E_1 \cdot E_2}{E_1 + E_2} \end{aligned} \quad \text{Equation 18}$$

Here  $p$  is the pressure by which the two adjacent material surfaces are kept together. The thermal conductivity and the elastic modulus of both participating partners are named  $\lambda_1$ ,  $E_1$  and  $\lambda_2$ ,  $E_2$  respectively. The empirical formula of Equation 18 is based on experimental results from materials with a surface finish in the range from N3 to N10. In this nomenclature N1 corresponds to an arithmetic mean value of surface roughness  $R_a=0.025\mu\text{m}$ . Every

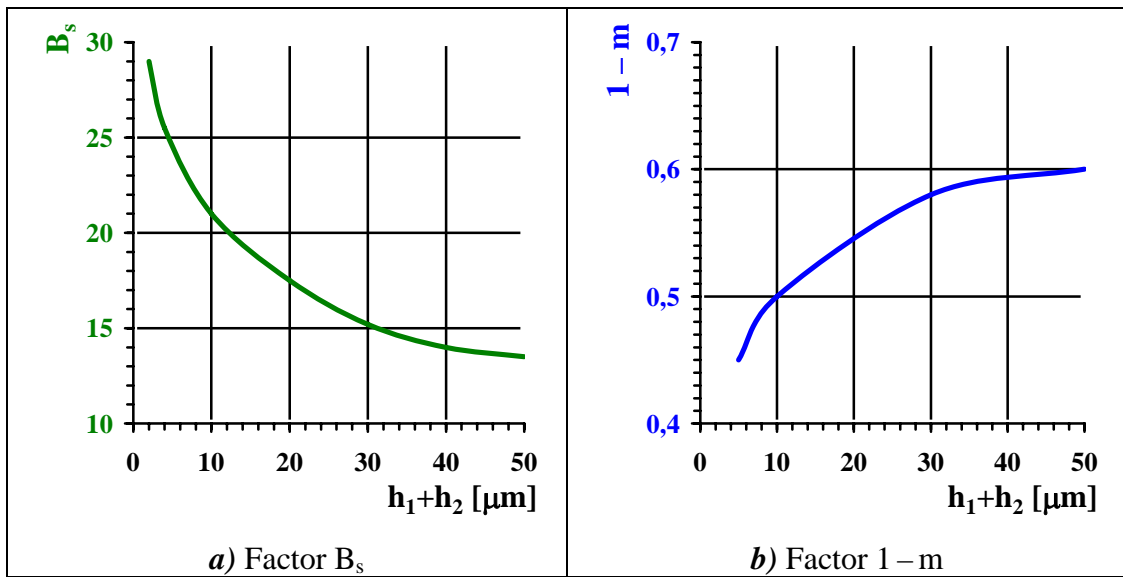


**Figure 26:** Influence of the surface roughness  $h_1$  and  $h_2$  of the contacting materials on:  
 a) the factor  $B_s$ , which is used in the empirical Equation 18 to determine the direct heat transfer coefficient  $K_{\text{direct}}$ .  
 b) the factor  $1 - m$ , which is used in Equation 19 to determine the heat transfer coefficient  $K_{\text{gas}}$  of the residing gas between the contacting materials.

increment by 1 doubles  $R_a$ , thus N3 corresponds to  $R_a=0.1\mu\text{m}$  and N10 is equivalent to  $R_a=12.5\mu\text{m}$ . The dependence of  $K_{\text{direct}}$  on the surface roughness is expressed by the non dimensional factor  $B_s$ , which was experimentally determined [5] and is plotted in Figure 26 a) as a function of the sum  $h_1 + h_2$ , where  $h_1$  and  $h_2$  is the surface roughness of material 1 and material 2 expressed in terms of the depth of the surface micro profile.

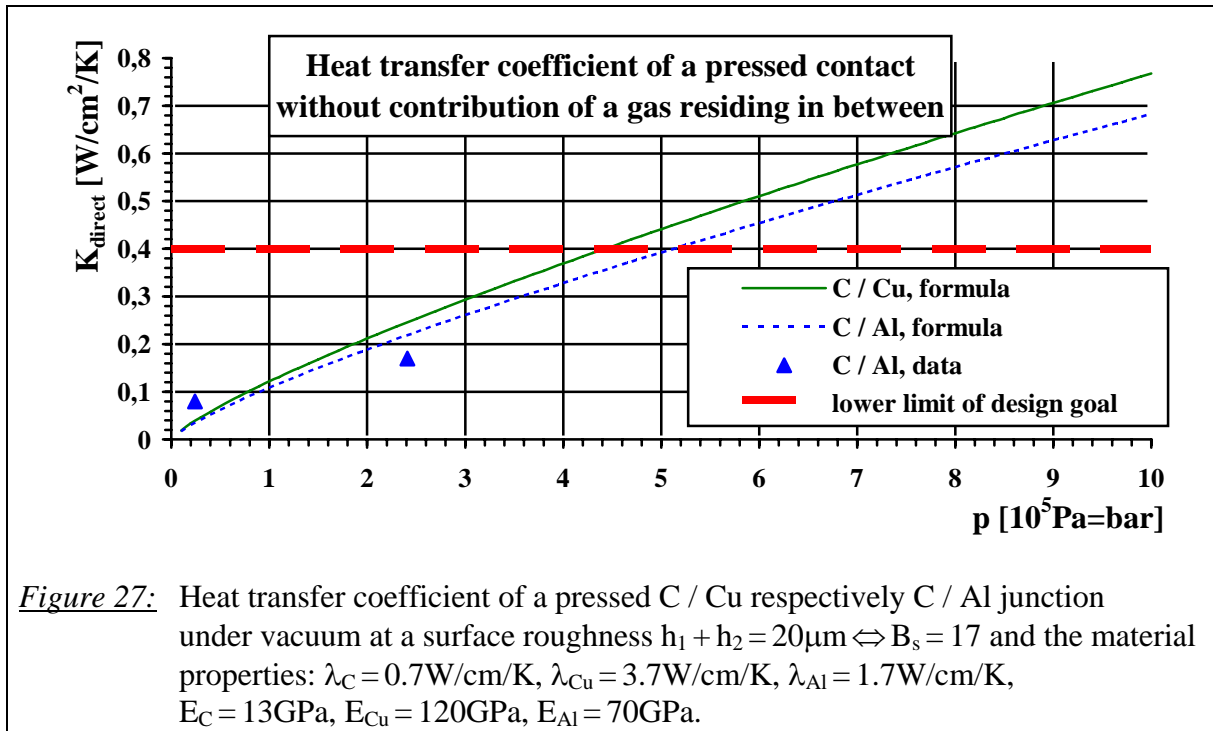
It is obvious, that the heat transfer coefficient  $K_{\text{direct}}$  is improved when using very smooth surfaces, materials with low E and a high contact pressure. Every of these conditions helps to increase the effective contact area. In addition good thermal conductors should be selected, but they are required for our application anyhow.

The second summand in Equation 17 is determined by:

$$K_{\text{gas}} = \frac{\lambda_{\text{gas}}}{(h_1 + h_2) \cdot (1 - m)} \quad \text{Equation 19}$$

Again  $h_1$  and  $h_2$  describe the amplitude of the micro surface profile of the contacting surfaces and  $\lambda_{\text{gas}}$  is the thermal conductivity of the gas, which resides in the interstices of the boundary. Besides the sum  $h_1 + h_2$ , the influence of the surface is hidden in the non dimensional function  $(1 - m)$  in the denominator of Equation 19. It somehow characterizes the effective thickness of the gas layer as a function of  $h_1 + h_2$  and is shown in Figure 26 b). Both factors in the denominator of  $K_{\text{gas}}$  increase with roughness and thus the heat transfer contribution via the gas layer qualitatively behaves similar as  $K_{\text{direct}}$ , since it improves with smoother surfaces.

By means of these empirical equations, the heat transfer coefficient at the graphite to copper contact can be estimated. In a conservative approach we assume, that the graphite core is kept under vacuum. In that case only  $K_{\text{direct}}$  contributes to the heat transfer across the boundary from core to shell. Figure 27 shows the heat transfer coefficient  $K_{\text{direct}}$  as a function of the contact pressure  $p$  between the graphite core and the copper shell. For comparison the



situation for a graphite / aluminium junction is plotted too. The roughness of the surfaces was characterized by  $h_1 + h_2 = 20\mu\text{m}$ , which according to Figure 26 a) results in  $B_s = 17$  and is technically easily to achieve. A temperature of around  $200^\circ\text{C}$  was presumed at the boundary. The corresponding material properties used for the graphs in Figure 27 are listed in the caption there and were taken from Table 2, Figure 2 b) and Figure 3.

In order to achieve a thermal contact with a transfer coefficient of better than  $0.4\text{W/cm}^2/\text{K}$  as was assumed in the baseline layout, a contact pressure of  $p \geq 0.5\text{MPa}$  ( $= 5\text{bar}$ ) is required. The validity of the empirical formula is indicated by two data points. At  $35\text{psi} = 2.413\text{bar}$  the C / Al curve ( $0.22\text{W/cm}^2/\text{K}$ ) agrees within an accuracy of 20% - 30% with a measurement ( $\approx 0.17 \pm 0.01\text{W/cm}^2/\text{K}$ ) given by Popov [5]. At small pressure levels the relative accuracy is worse. For  $p = 3.5\text{psi} = 0.24\text{bar}$  the measured value was  $0.08\text{W/cm}^2/\text{K}$  while the empirical formula gives roughly half of that. As an additional result, this plot also slightly favours copper to be used as a shell material and thus agrees with the other constraints, which lead already to this material choice in section 2.2.2.

If the core / shell junction is operated in the presence of a gas, the second mechanism described by  $K_{\text{gas}}$  adds to the total heat transfer coefficient. The same surface roughness of  $h_1 + h_2 = 20\mu\text{m}$  is assumed as before. Nitrogen and helium are considered to fill the interstices of the contact. Table 8 shows the heat transfer coefficient  $K_{\text{gas}}$  as calculated by Equation 19 for a gas pressure of 1atm and at two different temperatures of  $0^\circ\text{C}$  and  $400^\circ\text{C}$  respectively. For a given surface roughness condition  $K_{\text{gas}}$  only depends on the thermal conductivity of the

	$K_{\text{gas}}$ [W/cm <sup>2</sup> /K]	
	@ T = 0°C	@ T = 400°C
Nitrogen	0.22	0.4
Helium	1.1	2

**Table 8:** Heat transfer contribution from a gas at 1atm, which fills the interstices of a contact between two materials with a surface roughness of  $h_1 + h_2 = 20\mu\text{m}$ .

applied gas. From that point of view, helium is outstanding by a factor of 5 compared to nitrogen ( $\lambda(\text{N}_2)=0.026\text{W/m/K}$ ), but normally being used only for leak detection purposes. Thus flooding the dump with helium would raise a lot of objections. Nevertheless nitrogen still contributes with  $0.2\text{W/cm}^2/\text{K}$  at  $0^\circ\text{C}$  and improves by a factor of 2 at  $400^\circ\text{C}$ .

From the preceding remarks one can conclude, that a heat transfer coefficient of a pressed C / Cu contact of better than  $0.4\text{W/cm}^2/\text{K}$  can be obtained, either if the surfaces are under vacuum and pressed together by more than  $p=5\text{bar}$  or if the dump is flooded with  $1\text{atm}$  nitrogen and a reduced contact pressure of about  $p=2\text{bar}$  is applied.

### 3.2.2 Brazed Contact

A graphite / copper junction technologically offers the possibility to be brazed. The heat transfer coefficient of such a connection is promising. Experimentally this has been measured to perform better than  $0.8\text{W/cm}^2/\text{K}$ . The drawback of this solution is related to the substantial difference in thermal expansion between copper ( $\approx 16\cdot 10^{-6}/\text{K}$ ) and graphite ( $\approx 7\cdot 10^{-6}/\text{K}$ ).

Starting from a form locked cylindrical graphite-core / copper-shell geometry at room temperature, a radial gap of  $0.88\text{mm}$  opens up after everything is heated up to the brazing temperature of about  $820^\circ\text{C}$  and would prevent the brazing process. Perhaps this problem can be solved by azimuthal sectioning of the copper shell and strong clamping in order to form fit the copper around the graphite core at high temperature, when copper gets quite weak. Provided that this works, quite a bit of mostly compressive stress is induced in graphite during cool down after materials are brazed together, since copper shrinks more than graphite. These problems have to be investigated and there might be a technical solution, since pure annealed copper is a soft material at temperatures above  $300^\circ\text{C}$ , and thus significant stresses can not build up in that temperature regime but are transformed into non elastic deformation of the copper.

The brazed junction is an attractive option. The contact is thermally reliable and the graphite core could be operated under vacuum. This avoids a gas system, which has to be permanently controlled and gives an additional redundancy in case of a window failure, since beam operation might be continued. The copper shell together with the backstop would serve as a vacuum vessel for the graphite core. By that means the water cooling is automatically separated from the vacuum volume and a water leak would not cause severe trouble. Therefore the brazed option is the preferred solution for which a technical solution is under investigation.

## 4 Alternative Dump Designs without slow Sweeping

The considerations in chapter 2 and chapter 3 result in the baseline dump design, which uses a graphite core in order to deal with the instantaneous heating of each bunch train and introduces a slow circular beam sweeping in order to handle the extraction of the average beam power out of the dump. From the technical point of view a slow sweeping deflection device with a sweep frequency of around  $1\text{Hz}$ , as aimed for in our case, and monitoring its correct functioning will not be a big challenge. Nevertheless it is an active system and thus this chapter concentrates on alternative passive options, which can handle the average beam power while fulfilling the  $500^\circ\text{C}$  operation temperature limit of the graphite core.

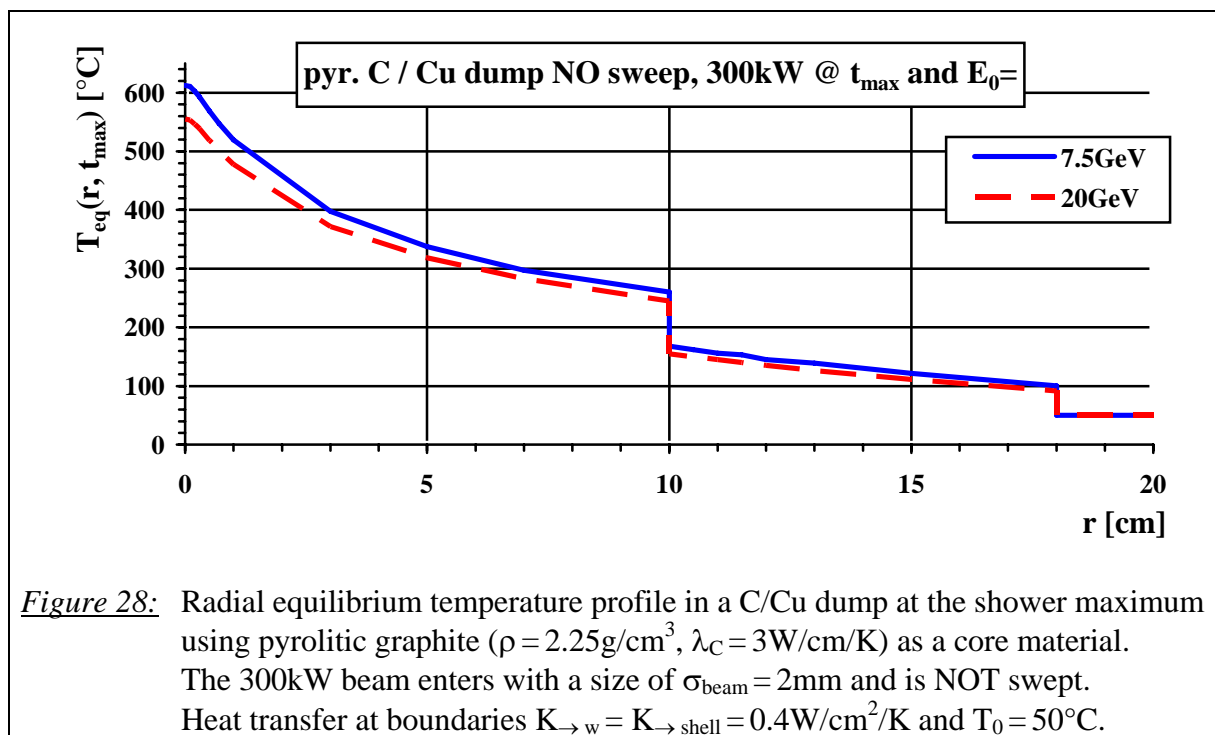
The following proposals will not change the requirement on the incoming beam spot size of  $\sigma_{\text{beam}} \geq 2\text{mm}$ , because it is difficult to find a suitable core material other than graphite. That is why the following options still use a graphite core, but instead of beam sweeping heat extraction is managed by an improved thermal conductivity in the next section 4.1 or by dilution of the power source. The latter can be done passively by means of upstream spoilers as described in section 4.2 or with a segmented dump core. This last option, as presented in

section 4.3, combines elongation and radial widening of the shower with a geometrical enhancement of heat conductivity.

In principle each of these 3 passive options are possible, but as discussed in the specific section they also involve at least one drawback, which is rated more severe than the advantage of getting rid of an active sweeping system. Thus none of these passive solutions can really compete with the baseline design, but have to be mentioned here for completeness.

#### 4.1 Pyrolytic Graphite Dump Core

If the baseline dump layout with a graphite core radius of  $R_C = 10\text{cm}$  is being hit by a non swept beam, the average temperature level on the axis near the shower maximum is around  $1610^\circ\text{C}$ . Figure 12 c) indicates, that the major fraction of the temperature drop is created due to heat conduction in graphite along the path from  $r=0$  to  $r=R_C=10\text{cm}$ , namely almost  $1390\text{K}$ . The remainder of  $170\text{K}$  towards the  $50^\circ\text{C}$  cooling water is subdivided into  $75\text{K}$  across the graphite to copper boundary,  $55\text{K}$  of conduction in copper and  $40\text{K}$  due to the heat transfer into the cooling water. At both boundaries a heat transfer coefficient of  $0.4\text{W}/\text{cm}^2/\text{K}$



was assumed.

Hence one solution to decrease the temperature level is obtained by a significant improvement of the thermal conductivity in the graphite core. In fact this can be achieved with pyrolytic graphite. This is also a pure carbon material, but compared to standard graphite the hexagonal matrix widely extends and results in a macroscopic layer structure. The material is produced by sublimation from the gas phase under high temperatures. Compared to the standard type pyrolytic graphite has a larger density of about  $\rho = 2.25\text{g}/\text{cm}^3$  and a high anisotropic behaviour depending on the degree of physical structuring. Within the plane of layers the thermal conductivity can be very high. Up to several  $10\text{W}/\text{cm}/\text{K}$  can be achieved there, while only a quite small value of around  $0.01\text{W}/\text{cm}/\text{K}$  can be expected in a direction perpendicular to the planes.

If the standard isomorphous graphite in the core of the baseline dump geometry is replaced by the pyrolytic type, one can profit from its higher thermal conductivity. The radial equilibrium temperature profile for this case without beam sweep is shown in Figure 28. The

cooling water temperature is set to  $T_0 = 50^\circ\text{C}$  and the heat transfer from pyrolytic graphite to copper and from copper to water is specified by a coefficient of  $0.4\text{W}/\text{cm}^2/\text{K}$ . In terms of longitudinal power density the worst case is given at the shower maximum for a  $7.5\text{GeV} / 300\text{kW}$  beam. Due to the higher density of pyrolytic graphite a peak power of about  $2400\text{kW}/\text{cm}$  is dissipated there instead of  $1840\text{W}/\text{cm}$  for standard graphite and the  $7.5\text{GeV}$  shower maximum is located around  $t_{\text{max}} \approx 70\text{cm}$  compared to  $95\text{cm}$  in standard graphite.

Taking only the 30% escalation in longitudinal power density into account a maximum equilibrium temperature level of  $1.3 \cdot 1610^\circ\text{C} \approx 2100^\circ\text{C}$  would be expected. Nevertheless due to the excellent thermal conductivity of pyrolytic graphite, which is assumed to be  $\lambda_C = 3\text{W}/\text{cm}/\text{K}$  in Figure 28, only a  $350\text{K}$  temperature drop is build up across the pyrolytic graphite core. Including the other contributions a maximum graphite temperature of around  $600^\circ\text{C}$  will occur at a cooling water temperature of  $50^\circ\text{C}$ . In  $20\text{GeV} / 300\text{kW}$  operation this level is reduced by about  $50\text{K}$ , since the longitudinal power density drops a little down to  $2200\text{W}/\text{cm}$ .

By means of a pyrolytic graphite core, average operation temperatures in the  $500^\circ\text{C}$  to  $600^\circ\text{C}$  range can be obtained even without a slow beam sweeping system. Up to now the same radial size as for the baseline layout was assumed, where the diameter of the graphite core is determined by the required sweep radius. Hence there is room for optimisation of this approach.

As explained in Figure 10 in section 2.2.2 a radial graphite thickness of  $\Delta R = 5\text{cm}$  should at least separate the shower axis from the inner radius of the copper shell. Since the beam is not swept, graphite core and outer radius of the dump can be diminished by  $5\text{cm}$  down to  $R_C = 5\text{cm}$  and  $R = 13\text{cm}$  respectively. According to Figure 28 the temperature drop in graphite lessens by about  $100\text{K}$ , but on the other hand the temperature drop across the graphite to copper boundary doubles, if the quality of the thermal contact remains constant. This is because the surface area is halved, when the graphite core radius is reduced from  $R_C = 10\text{cm}$  to  $5\text{cm}$ . Under the assumption of a heat transfer with  $K_{\rightarrow\text{shell}} = 0.4\text{W}/\text{cm}^2/\text{K}$  the temperature drop would scale up from  $95\text{K}$  to  $190\text{K}$ . Therefore the benefit of a shorter heat path in graphite cancels completely and the temperature level in the graphite core will stay unchanged at the  $500^\circ\text{C}$  to  $600^\circ\text{C}$  level, unless the quality of the thermal contact between graphite and copper is not changed. Generally speaking: the smaller the graphite core, the more emphasis is put on its thermal contact to the copper shell.

In addition to the radial reduction in size also a longitudinal optimisation is possible. Due to the higher density of pyrolytic graphite, the shower is shorter and the Cu-backstop can be placed after a graphite core length  $L_C$ , which is shorter than  $330\text{cm}$  as in the baseline layout. For a  $20\text{GeV} / 300\text{kW}$  operation (i.e.  $I_{\text{ave}} = 15\mu\text{A}$ ) Table 9 lists the maximum longitudinal power density at the beginning of the Cu-backstop as a function of the pyrolytic graphite core length  $L_C$  in front of it. For the case  $L_C = 240\text{cm}$  the longitudinal profile of the power density  $dP/dz$  is plotted in Figure 29 for a  $300\text{kW}$  beam at  $20\text{GeV}$  and  $7.5\text{GeV}$  respectively.

Under the simplification of pure radial heat flow, this power density in combination with the radial profile of deposited energy, which is not shown, results in a temperature drop  $\Delta T_{\text{Cu}}$  between the axis ( $r=0$ ) of the backstop and its outer radius  $R$ , which is still assumed to be  $R = 18\text{cm}$ . Adding the temperature drop  $\Delta T_{\rightarrow w}$  across the boundary to water, which is described by  $K_{\rightarrow w} = 0.4\text{W}/\text{cm}^2/\text{K}$  and the cooling water temperature of  $T_0 = 50^\circ\text{C}$  results in the maximum equilibrium temperature  $T_{\text{eq}}(r)$  on the axis of the Cu-backstop, which is also listed in Table 9. This temperature can be kept below a safe value of  $150^\circ\text{C}$ , if the length of the graphite core is not shorter than  $L_C = 280\text{cm}$

	$dP/dz$	$\Delta T_{Cu}$	$\Delta T_{\rightarrow w}$	$T_{eq}(r=0) = \Delta T_{Cu} + \Delta T_{\rightarrow w} + T_0$
$L_C$	[W/cm]	[K]	[K]	[°C]
<b>240 cm</b>	1650	190	36	<b>280</b>
<b>260 cm</b>	975	110	22	<b>180</b>
<b>280 cm</b>	630	70	14	<b>135</b>
<b>300 cm</b>	390	45	9	<b>105</b>

**Table 9:** Longitudinal power density  $dP/dz$  and equilibrium temperature  $T_{eq}(r=0)$  at the beginning of a Cu-backstop, which is placed behind a pyrolytic graphite ( $\rho = 2.25\text{g/cm}^3$ ) core of length  $L_C$ . The outer radius of the backstop is  $R = 18\text{cm}$ . A 20GeV / 300kW beam enters with a size of  $\sigma_{beam} = 2\text{mm}$  and is NOT swept. The cooling water has a temperature of  $T_0 = 50^\circ\text{C}$  and the thermal contact between copper and water is described by  $K_{\rightarrow w} = 0.4\text{W/cm}^2/\text{K}$ .

As a result of radial and longitudinal optimisation the pyrolytic graphite based dump design could have a size as sketched in Figure 30. Compared to the baseline layout, as shown in Figure 16, it is 50cm shorter, 10cm smaller in diameter and nearly about half in weight, namely about 1.3 tons (1150kg Cu-shell, 50kg C-core, 70kg Cu-backstop). Furthermore the diameter of the incoming beam pipe and the beam window can be reduced as well, since a non swept beam requires less aperture.

In spite all of these advantages, which make this option a very attractive one, a quite severe unknown risk is associated with this solution. The success of the layout strictly depends on the high thermal conductivity of the graphite core. This property is achieved by a highly structured and oriented graphite material. In a beam dump application the material has to operate in an environment of high radiation fields. Especially neutrons can damage the structured graphite lattice and therefore degradation of its thermal conductivity may happen with time. It is difficult to predict the extent of this effect and thus the pyrolytic graphite dump option is regarded as a non reliable and risky solution.

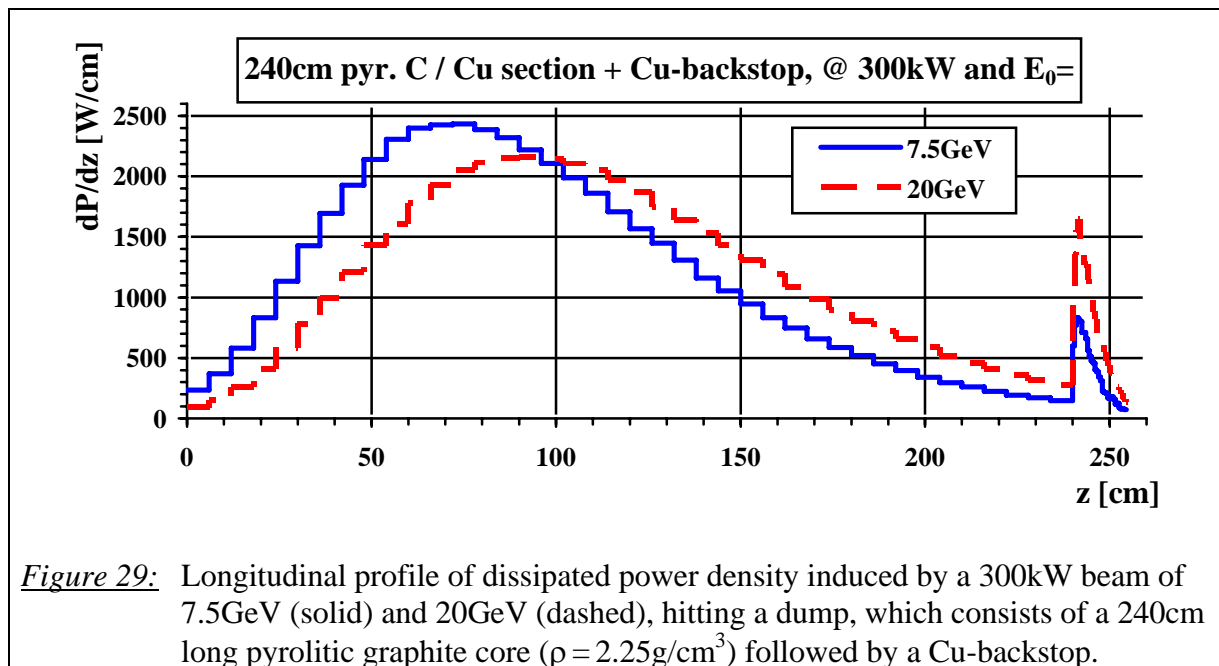
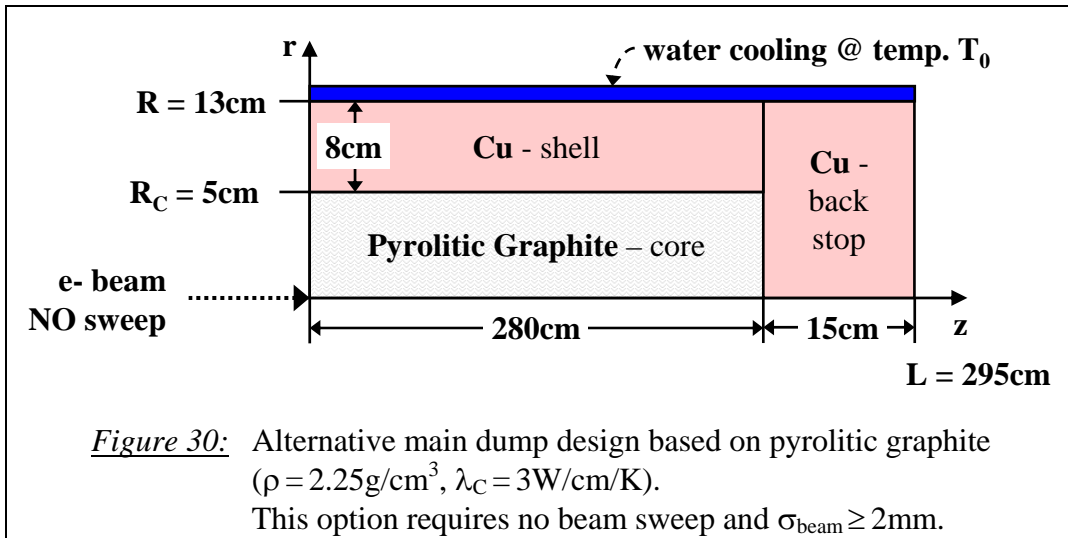


**Figure 29:** Longitudinal profile of dissipated power density induced by a 300kW beam of 7.5GeV (solid) and 20GeV (dashed), hitting a dump, which consists of a 240cm long pyrolytic graphite core ( $\rho = 2.25\text{g/cm}^3$ ) followed by a Cu-backstop.



Aside from this major drawback other disadvantages of this concept should be mentioned as well. As a consequence of the production process, pyrolytic graphite disks are available up to a thickness of around 10mm only. The 280cm long graphite core would have to be build up by 280 of these thin disks. It is difficult to imagine how such a compound is technically realised, especially from the point of view that every of these disks has to have the same perfect thermal contact with the surrounding copper shell. As already mentioned, this junction is yet more vital here as in the baseline design, because of the smaller heat transfer surface. But even with a radial size as in the baseline geometry, the maximum longitudinal power density is 30% higher as for standard graphite and leads to increased temperature drops at both material boundaries, if their quality is not improved.

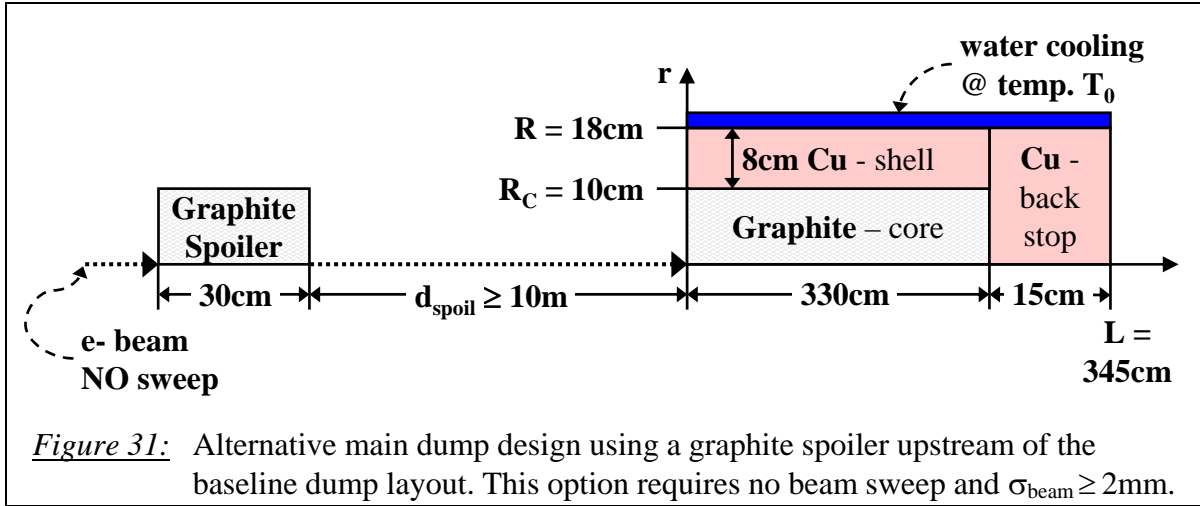
All in all a beam dump layout based on pyrolytic graphite is not considered to be a long term reliable alternative.

## 4.2 Upstream Spoilers

Instead of introducing a material of high thermal conductivity as in the previous section 4.1, a reduction of equilibrium heating can be obtained when the heat source has a wide radial profile. Thus a big spot size of the beam at the entrance of the baseline dump layout would solve the problem. In order to have a similar effect on average heating as with slow sweeping, the required beam size should be in the order of the sweep radius, namely 50mm.

Passively a transverse blow up of the beam profile is possible by means of a spoiler, which is located in a distance  $d_{\text{spoil}}$  upstream of the baseline beam dump. A sketch of this layout is shown in Figure 31. For the same reasons why standard graphite ( $\rho = 1.71\text{g/cm}^3$ ) is used as a core material in the dump, it is also the best candidate for the spoiler. The influence of a  $1.2 \cdot X_0 = 30\text{cm}$  long graphite spoiler, which is located in a distance of  $d_{\text{spoil}} = 5\text{m}$  respectively  $d_{\text{spoil}} = 10\text{m}$  in front of the baseline dump, is given in Figure 32 in comparison to the situation without any spoiler.

A 7.5GeV beam with a size of  $\sigma_{\text{beam}} = 2\text{mm}$  enters the spoiler and Figure 32 a) shows the radial profile of the spatial energy density  $dE/dm$  at the shower maximum in the graphite core of the baseline dump downstream of the spoiler. As expected the profile broadens and its peak value on the axis ( $r=0$ ) diminishes with increasing distance  $d_{\text{spoil}}$  between spoiler and dump. In the presence of a spoiler the radial width of the spatial energy density profile at the shower maximum in the dump is dominated by the width of the spoiled beam profile, which enters the dump. Therefore the position of maximum spatial energy density is close to the shower maximum, i.e.  $t_E \approx t_{\text{max}}$ . As known from Figure 17 one fully charged bunch train with



$N_t = 2.5 \cdot 10^{13}$  electrons of 7.5GeV deposits about 100J/g on the axis at  $z = t_E$ . Normalized to one electron this corresponds to 0.025GeV/g. According to the results of the spoiler calculations in Figure 32 a) this value is reduced to 0.002GeV/g or even 0.0008GeV/g if a 30cm long graphite spoiler is placed 5m or 10m in front of the dump. Thus instantaneous heating effects in the dump are reduced by a factor of 10 respectively 30.

However the main purpose of the spoiler is to broaden the radial profile of spatial energy density, which is evidently visible in Figure 32 a). Combining this 7.5GeV profile with an average beam current of  $I_{\text{ave}} = 40\mu\text{A}$  and solving Equation 63 for steady state heat flow in the baseline dump geometry results in the radial equilibrium temperature profiles as plotted in Figure 32 b). The assumptions on the heat transfer coefficients and the cooling water temperature are identical to those as were made previously for the baseline design with slow beam sweep, namely  $K_{\rightarrow\text{shell}} = K_{\rightarrow\text{w}} = 0.4\text{W/cm}^2/\text{K}$  and  $T_0 = 50^\circ\text{C}$ . Without a spoiler a non-swept 7.5GeV / 300kW beam with 2mm spot size would heat the graphite core up to 1610°C on its axis at the shower maximum. With a 30cm long graphite spoiler this temperature is significantly lowered to about 800°C if the spoiler is sitting 5m upstream. For a  $d_{\text{spoil}} = 10\text{m}$  distance between spoiler and dump a maximum temperature level of 600°C will build up, which is just at the upper edge of the 500°C to 600°C design goal.

By means of an upstream located spoiler the baseline dump can be operated at tolerable temperature levels without requiring a slow beam sweeping system and in addition the instantaneous effects are reduced by more than one order of magnitude.

Nevertheless the relaxation of the situation in the dump is achieved on the account of the situation at the spoiler. In terms of energy deposition it is given by the results in the first 30cm of the baseline dump without sweep and can be looked up in Figure 17. For an incoming beam with size  $\sigma_{\text{beam}} = 2\text{mm}$  a maximum spatial energy density of around 170J/g is deposited by one fully populated bunch train of  $N_t = 2.5 \cdot 10^{13}$  electrons at 25GeV near the end of the spoiler at  $z = 30\text{cm}$ . Hence there is still a 50% margin towards the tolerable limit of 240J/g for cyclic operation as given in Table 3.

The dissipated power per unit of length at 7.5GeV / 300kW operation varies between 190W/cm at the beginning of the spoiler to 700W/cm at its rear end. The radial size of the spoiler should not be less than the beam pipe aperture. Thus a radius not bigger than  $R_{\text{spoil}} = 5\text{cm}$  is fully sufficient. At its circumference the spoiler would be embedded in a thin copper tube, which is cooled with water. The maximum average temperature level in the spoiler can be estimated by means of Equation 65. In a conservative manner we assume, that the radial profile of spatial energy density at the end of the spoiler has not broadened up due to shower processes, but is still the same as given by the beam size at the entrance of the

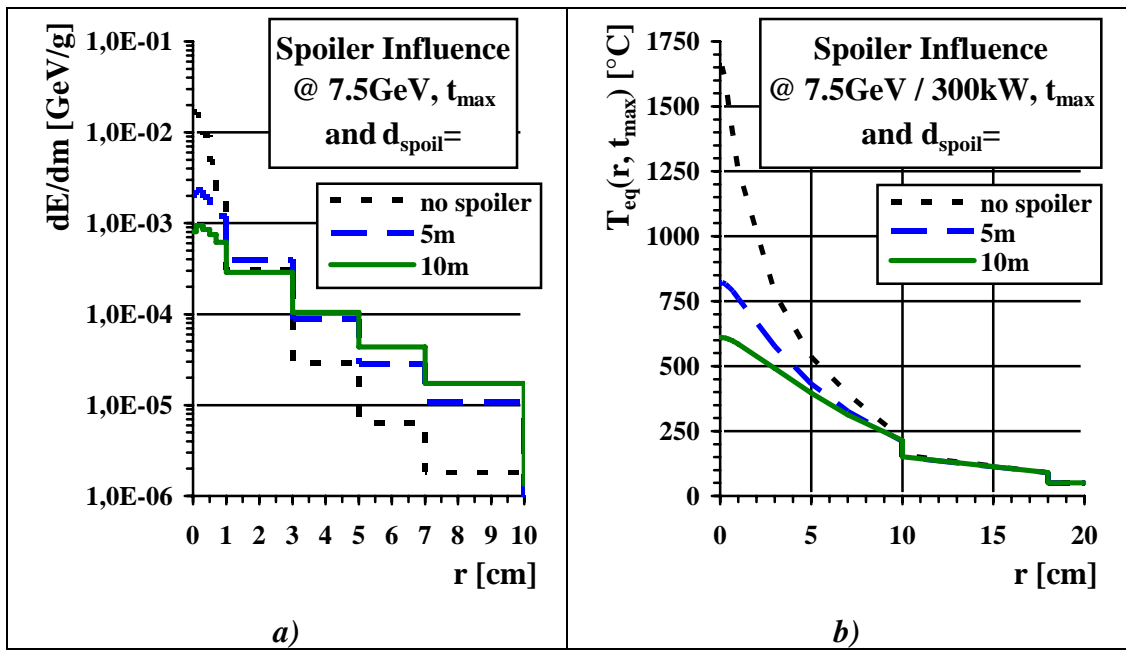


**Figure 32:** Radial profiles at the shower maximum  $z = t_{\max}$  of the baseline dump with and without a 30cm long graphite spoiler placed in a distance  $d_{\text{spoil}}$  upstream of it. *a)* Spatial energy density  $dE/dm$  as created by one primary 7.5GeV electron. *b)* Resulting equilibrium temperature  $T_{\text{eq}}$  at 7.5GeV / 300kW operation. The beam size at the spoiler is  $\sigma_{\text{beam}} = 2\text{mm}$ . Heat transfer coefficient at all boundaries  $0.4\text{W}/\text{cm}^2/\text{K}$  and  $T_0 = 50^\circ\text{C}$ .

spoiler. Thus  $\sigma(t_{\max}) = \sigma_{\text{beam}} = 2\text{mm}$  is used in the equation. The outer radius is set to  $R = R_{\text{spoil}} = 5\text{cm}$ , the power dissipation is given by  $700\text{W}/\text{cm}$  and the thermal conductivity of graphite is safely assumed as  $0.7\text{W}/\text{cm}/\text{K}$ . With these numbers a temperature drop of about  $460\text{K}$  is estimated across the graphite. In addition two heat transfer boundaries at  $R = 5\text{cm}$  specified by  $K = 0.4\text{W}/\text{cm}^2/\text{K}$  contribute with about  $55\text{K}$  each and the cooling water temperature of  $T_0 = 50^\circ\text{C}$  has to be added. All in all, this conservative estimate gives a maximum temperature of  $620^\circ\text{C}$  in the graphite spoiler.

In terms of heating the spoiler is technically feasible, but for two major reasons the spoiler option is not an adequate alternative. One reason is the overall power dissipation in the spoiler. At  $7.5\text{GeV} / 300\text{kW}$  it varies from front to end between  $190\text{W}/\text{cm}$  to  $700\text{W}/\text{cm}$  and gives a total dissipation of about  $450\text{W}/\text{cm} \cdot 30\text{cm} \geq 13\text{kW}$  in the spoiler. Although a little relaxed the equivalent numbers at  $25\text{GeV} / 300\text{kW}$  operation are  $60\text{W}/\text{cm}$  at the beginning of the spoiler and  $300\text{W}/\text{cm}$  at its end. Thus the total power dissipation will be around the  $180\text{W}/\text{cm} \cdot 30\text{cm} \geq 5\text{kW}$  level.

Several few kilowatts of dissipated power represent a strong additional source of radiation, which is not located in close vicinity of the dump. The spoiler has to be shielded separately especially in order to suppress air activation. But nevertheless the whole beam line downstream of the spoiler will become a long region of activated components, which is not aimed for.

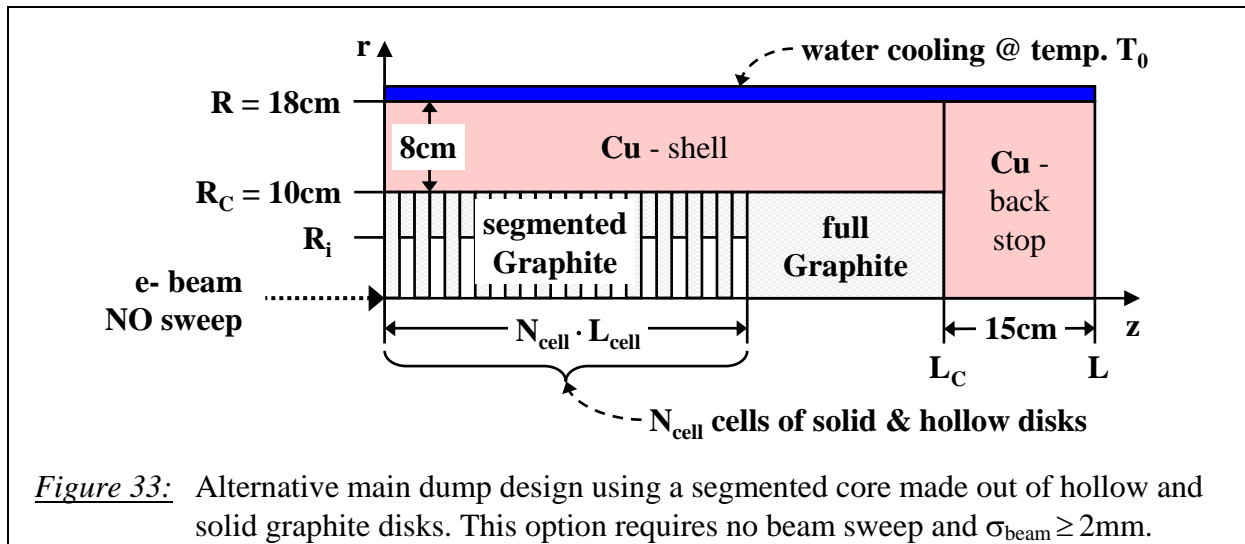
A second drawback of the spoiler option maybe the fact, that the beam size of  $2\text{mm}$  has to be generated already  $10\text{m}$  upstream of the dump, i.e. at the spoiler. In the present baseline dump design the defocusing quadrupoles are located downstream of the dipoles, which separate the electrons from the FEL-photons and direct them vertically down into the dump. These quads can neither be shifted  $10\text{m}$  further upstream due to the limited length of the beam line downstream of the dipoles nor can beam defocusing start upstream of these dipoles,

because in between of them an energy spread measurement device requires dedicated beam optics, which can not be mixed with the needs of the dump system.

### 4.3 Segmented Graphite Dump Core

As a third solution, which does not require any active beam sweeping, the graphite core could consist of a periodic structure of solid and hollow graphite disks as shown in Figure 33. Compared to the baseline dump geometry the radial size and the 15cm long Cu-backstop remains untouched. Even the graphite material of the dump stays the same, but only its geometry is modified. Instead of having a fully solid graphite core, the front part consists of solid and hollow graphite disks in an alternating sequence.

The outer radius of these disks is the graphite core radius, namely  $R_C = 10\text{cm}$ . Both disk types have an individual thickness, named  $L_S$  for the solid one and  $L_H$  for the hollow disk respectively. The hollow disk has a borehole with a radius of  $R_i$ . Putting the hollow disk behind the solid one, results in one cell of the periodic segmented dump core. The geometry of such a cell is sketched in Figure 34. The total length of one cell is given by  $L_S + L_H = L_{\text{cell}}$ . If the segmented front part of the dump is built up by a total number of  $N_{\text{cell}}$  cells, it has a length of  $N_{\text{cell}} \cdot L_{\text{cell}}$ .

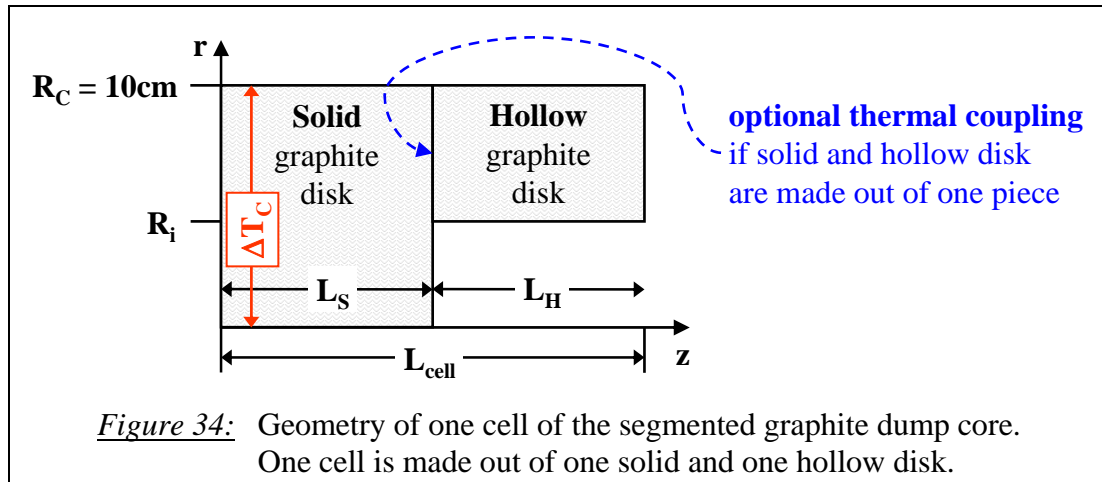


Compared to the baseline geometry a reduction of temperatures is expected by the segmented layout due to the following effects.

First of all a periodic structure of solid and hollow graphite disks necessarily stretches the shower longitudinally and thus the maximum power density per unit of length must decrease. This effect linearly affects all equilibrium temperature drops along the path of heat flow.

In addition such a segmented structure can be regarded as a system of distributed spoilers inside of the dump, which will lead to broaden up the radial profile of deposited energy. As a result of a wider radial heat source profile, not only the equilibrium temperature drop  $\Delta T_C$  (see Figure 34) due to radial heat conduction across the graphite disks from  $r = 0$  to  $r = R_C$  will diminish, but also the amount of instantaneous heating is reduced.

As indicated in Figure 34 the solid and the hollow are not necessarily thermally coupled at their adjacent longitudinal face. But if so, heat extraction from the solid disks is enhanced just because of a geometrical effect. The heat, which is dissipated in the core of these disks and flows towards the circumference of the dump, profits from an enlarged radial cross section beyond  $r \geq R_i$ . A quantitative analysis of this geometrical effect is done in section 4.3.2.



The following section 4.3.1 discusses the results of electromagnetic shower simulations for the segmented graphite core. From the radial and longitudinal energy density profiles as given there, equilibrium and instantaneous heating in the solid / hollow structured graphite dump core are derived in section 4.3.3.

As a conclusion it can be stated, that tolerable graphite temperatures below the 500°C limit are possible without beam sweep with the segmented dump core approach. Unfortunately quite a long core of around  $L_C \approx 600\text{cm}$  is necessary. As a consequence the whole dump module including the 2m concrete filled front extension exceeds the 6m limit, beyond which transportation, installation and exchange can not be carried out any more. Therefore this option is out of discussion.

More over the usage of hollow graphite disks holds an additional risk. If they break, thermally uncoupled material falls in the empty region of the dump core and is probably heated up to evaporation.

#### 4.3.1 Energy Deposition in the segmented Dump Core

By means of MARS simulations the spatial distributions of deposited energy in a segmented graphite dump core are presented in this section. For all considerations here the disks, which are used in the segmented core have an outer radius of  $R_C = 10\text{cm}$ , which is the size as used in the baseline dump design. As a result of mechanical stress evaluation in section 3.1.2, the length of the solid disks is set to  $L_S = 10\text{cm}$  and not subject to variation. Merely the length  $L_H$  of the hollow disk, its bore radius  $R_i$  and the total number of cells  $N_{\text{cell}}$  is varied. The beam enters with a size of  $\sigma_{\text{beam}} = 2\text{mm}$  on the axis of the segmented core. For reference the results are compared to the situation of a fully solid core as it is used in the baseline design.

The longitudinal profile of dissipated power density at 300kW beam operation is shown in Figure 35 a) through d) for different cases with respect to the beam energy, the number of cells  $N_{\text{cell}}$  and the shape of the hollow disk, which is defined by  $L_H$  and  $R_i$ . Comparing the results with the situation in the unstructured core of the baseline dump, which is implemented in the graphs of Figure 35 a) and b), shows a reduction of the peak power density and a downstream shift of its position.

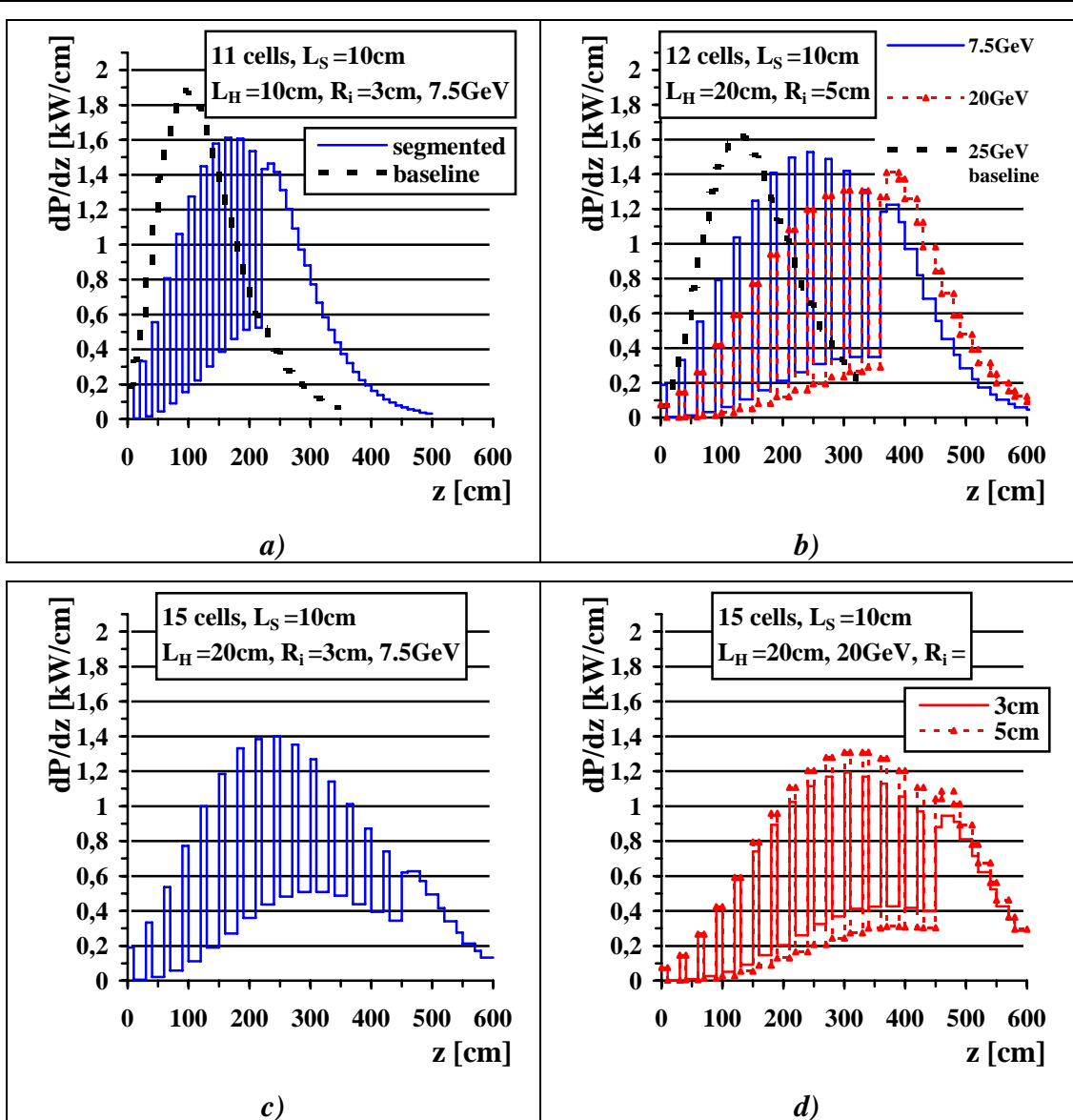


**Figure 35:** Longitudinal profile of dissipated power density  $dP/dz$  at 300kW operation for a segmented graphite core with an outer radius of  $R_C=10\text{cm}$  and:

- a)  $N_{\text{cell}} = 11$ ,  $L_S = 10\text{cm}$ ,  $L_H = 10\text{cm}$ ,  $R_i = 3\text{cm}$  at 7.5GeV.
- b)  $N_{\text{cell}} = 12$ ,  $L_S = 10\text{cm}$ ,  $L_H = 20\text{cm}$ ,  $R_i = 5\text{cm}$  at 7.5GeV and 20GeV.
- c)  $N_{\text{cell}} = 15$ ,  $L_S = 10\text{cm}$ ,  $L_H = 20\text{cm}$ ,  $R_i = 3\text{cm}$  at 7.5GeV.
- d)  $N_{\text{cell}} = 15$ ,  $L_S = 10\text{cm}$ ,  $L_H = 20\text{cm}$ ,  $R_i = 3\text{cm}$  at 20GeV.

For reference the 7.5GeV and 25GeV profiles as induced in the baseline design are plotted in a) and b) too.

The number of cells  $N_{\text{max}}$ , after which the shower maximum appears in a segmented core, is roughly given by  $N_{\text{max}} \cdot L_C = t_{\text{max}}^{\text{ns}}$ , where  $t_{\text{max}}^{\text{ns}}$  is the longitudinal position of the shower maximum in a non-segmented core. For a 7.5GeV beam this number is  $t_{\text{max}}^{\text{ns}} \approx 95\text{cm}$ , as we know from Table 4. Thus the power density in the solid disks of a segmented core will peak around cell number 9 to 10, if the solid disks have a length of  $L_S=10\text{cm}$ . This is nicely confirmed in the graphs of Figure 35 a), b) and c). The larger the ratio  $L_H/L_S$  between the length of the hollow and the solid disk is, the more reduces the absolute value of the peak power density.

<b>max(dP/dz) [kW/cm] in a segmented graphite dump core</b> being axially hit by a 300kW beam with a size of $\sigma_{\text{beam}} = 2\text{mm}$				
<b>E<sub>0</sub></b>	<b>R<sub>i</sub> = 3cm</b>	<b>R<sub>i</sub> = 5cm</b>	<b>R<sub>i</sub> = 7cm</b>	<b>baseline <math>\leftrightarrow</math> R<sub>i</sub> = 0cm</b>
<b>7.5 GeV</b>	1.4	1.53	1.64	1.84
<b>20 GeV</b>	1.19	1.31	1.42	1.68

*Table 10:* Longitudinal power density  $dP/dz$  at the shower maximum  $z = t_{\text{max}}$  of a segmented dump, which consists of 30cm long cells and is hit by a non-swept 300kW beam.

The solid disk is  $L_S = 10\text{cm}$  long and the hollow one is  $L_H = 20\text{cm}$  long, while its borehole radius  $R_i$  is varied.

The size of the borehole in the hollow disk determines the balance between the power dissipation in the hollow and the solid disk. In the limit of a large hollow disk aperture near  $R_i \approx R_C$ , power dissipation in the solid disks will finally reach the level, which occurs in the non-structured core. With a decreasing bore radius  $R_i$ , more and more power is dissipated in the hollow disk to the benefit of the solid one as listed in Table 10 starting from  $R_i = 7\text{cm}$  down to  $R_i = 3\text{cm}$ . A further reduction of the hole in the hollow disk equalizes the difference between the solid and the hollow disk in terms of power dissipation, which at the same time increases again and finally ends at the level of the non-segmented core of the baseline layout if  $R_i \approx 0\text{cm}$ . Taking into account a relaxed alignment procedure within  $\pm 1\text{cm}$  around the design axis and a beam steering margin of similar amount, a hollow disk aperture in the range  $3\text{cm} \leq R_i \leq 5\text{cm}$  seems a reasonable choice.

As derived from Figure 35 a) only a negligible 10% reduction of power density is achieved if the hollow disks have a length of  $L_H = 10\text{cm}$ . As will be seen in section 4.3.3  $L_H = 20\text{cm}$  long graphite disks of the hollow type are required to stay below the  $500^\circ\text{C}$  goal. Such a length of  $L_H = 20\text{cm}$  has a noticeable effect on the power density, which is reduced by about 25% in this case and helps significantly to widen the radial energy profile as will be discussed later in this section.

In order to make use of the reduced power density, the segmented part of the core must extend that far, such that the power density in the solid graphite part behind it does not exceed the level in the solid disks. With  $L_H = 20\text{cm}$  a number of 12 cells is not sufficient to fulfil this requirement for a 20GeV beam, as can be seen in Figure 35 b) and Figure 35 d) shows, that this problem is solved for  $N_{\text{cell}} = 15$ .

The total length of the graphite core should give the same accumulated graphite material path length on the axis as in the baseline design, where the Cu-backstop is placed behind a 330cm long solid graphite core. A segmented part with 15 cells of 10cm long solid and 20cm long hollow disks is 450cm long, but results in a graphite path length on the axis at  $r=0$  of only 150cm. Hence the solid graphite part must add about 180cm to obtain a total graphite path of 330cm on the axis. The overall length of the graphite core thus amounts to  $L_C = (450+180)\text{cm} = 630\text{cm}$ , after which a 15cm long Cu-backstop can be placed at the end. The total weight of this approach is almost twice of that of the baseline layout, namely 4.4 tons. The Cu-shell mainly contributes with almost 4 tons. The whole graphite core adds 300kg (80kg solid disks, 120kg hollow disks, 100kg solid part of the C-core) and the Cu-backstop weights 140kg.

In order to calculate the average heating in a slice of the segmented core, the radial profile of the heat source is required in addition to the dissipated power. Figure 36 shows the radial profile of the deposited energy density at the shower maximum of a segmented dump, which

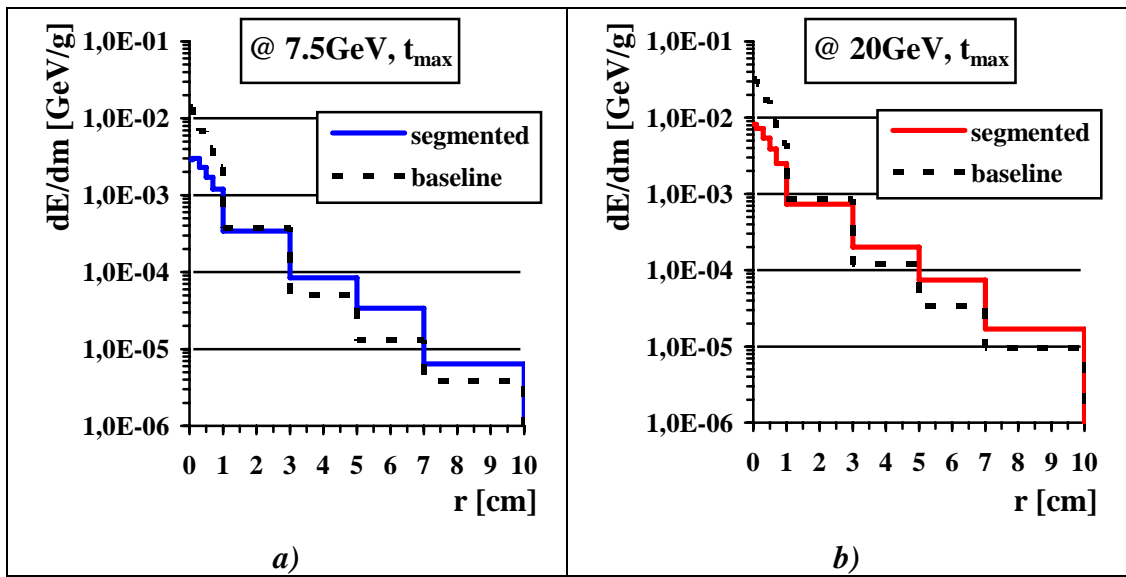


**Figure 36:** Radial profiles of the spatial energy density  $dE/dm$  at the shower maximum  $z = t_{\max}$  in the solid disk of a segmented dump, with  $L_S = 10\text{cm}$ ,  $L_H = 20\text{cm}$  and  $R_i = 5\text{cm}$ , in comparison with a fully solid core of the baseline dump. The incoming beam has a size of  $\sigma_{\text{beam}} = 2\text{mm}$  and an energy of *a)*  $7.5\text{GeV}$  and *b)*  $20\text{GeV}$  respectively. The results are normalized to one primary electron.

is build up by  $10\text{cm}$  long solid and  $20\text{cm}$  long hollow disks with a bore radius of  $R_i = 5\text{cm}$ . The  $7.5\text{GeV}$  and  $20\text{GeV}$  profiles are compared with those of the baseline dump. The narrow core of this distribution is increased by a factor of more than 2. As a result the energy density is reduced by more than a factor of  $2^2 = 4$ , which is confirmed in Table 11 when comparing the numbers of  $L_H = 20\text{cm}$  with the baseline case  $L_H = 0\text{cm}$  at  $z = t_{\max}$ . The equivalent factor at  $z = t_E$  lies between 1.7 and 1.9, which directly almost halves all instantaneous heating effects with respect to the baseline design.

Table 11 also justifies the choice of  $L_H = 20\text{cm}$ . While the increment from  $L_H = 10\text{cm}$  to  $L_H = 20\text{cm}$  has still a considerable impact, especially for a  $20\text{GeV}$  beam, the next step towards

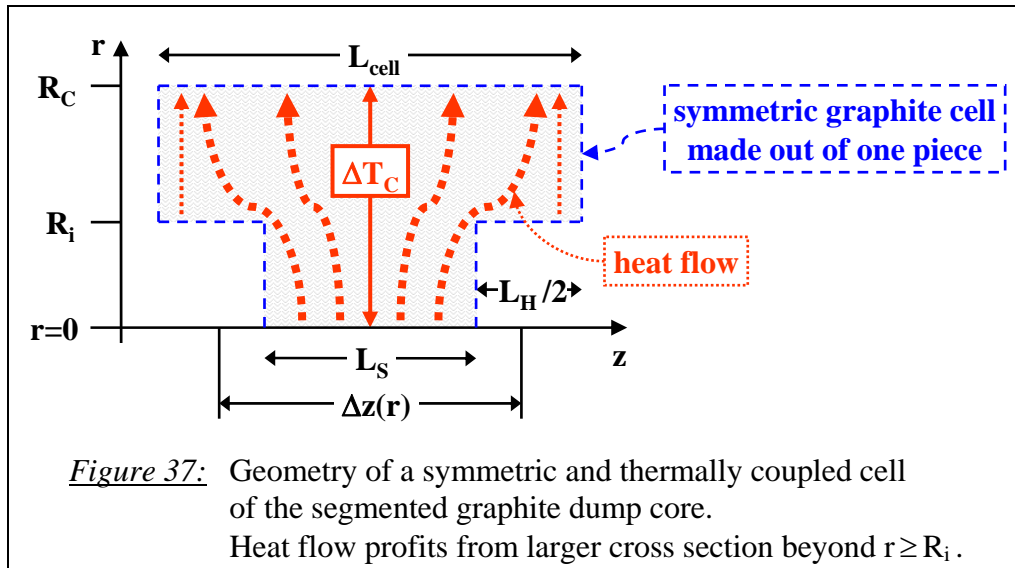
		<b><math>dE/dm</math> [GeV/g] in a segmented graphite dump core being axially hit by a beam with a size of <math>\sigma_{\text{beam}} = 2\text{mm}</math></b>			
<b><math>E_0</math></b>		<b>baseline <math>\leftrightarrow L_H = 0\text{cm}</math></b>	<b><math>L_H = 10\text{cm}</math></b>	<b><math>L_H = 20\text{cm}</math></b>	<b><math>L_H = 30\text{cm}</math></b>
<b>@ <math>z = t_E</math></b>	<b>7.5 GeV</b>	0.025	0.018	0.015	0.013
	<b>20 GeV</b>	0.051	0.034	0.027	0.022
	<b>25 GeV</b>	0.062	–	–	–
<b>@ <math>z = t_{\max}</math></b>	<b>7.5 GeV</b>	0.014	0.0049	0.0029	0.0026
	<b>20 GeV</b>	0.032	0.013	0.0073	0.0052

**Table 11:** Spatial energy density  $dE/dm$  as induced by one primary electron on the axis of a solid disk of a segmented dump at  $z = t_E$ , where  $dE/dm$  peaks and at the shower maximum  $z = t_{\max}$ . The solid disks are  $L_S = 10\text{cm}$  long while the length  $L_H$  of the hollow ones is varied. The borehole of the hollow disks is large compared to the incoming beam size, i.e.  $R_i \gg \sigma_{\text{beam}}$ .

$L_H=30\text{cm}$  is not that efficient anymore, but would make the dump 150cm longer and 1 ton heavier. Thus  $L_H=20\text{cm}$  is a reasonable choice and sufficient to reach tolerable graphite temperatures as will be seen in section 4.3.3.

#### 4.3.2 Heat Extraction in the segmented Dump Core

The segmented geometry widens the energy density in the radial as well as in the longitudinal direction and by that means lowers instantaneous and average heating levels in the graphite core. Average heating can be further reduced, if the solid and hollow disks are thermally coupled. In that case a symmetric cell as shown in Figure 37 has to be manufactured out of one graphite block. During its flow towards the circumference of such a cell at  $r=R_C$ , the heat, which is dissipated within the length  $L_S$  at  $r \leq R_i$ , profits from an increased radial surface beyond  $R_i$ . As a result of this geometrical effect the heat extraction is improved and the corresponding temperature drop  $\Delta T_C$  between the axis ( $r=0$ ) and the



circumference ( $r=R_C$ ) of such a cell is reduced.

By means of analytical methods the quantitative amount of this pure geometrical effect is studied. For that purpose the temperature drop  $\Delta T_C$  is calculated for a cell like sketched in Figure 37, whose length  $\Delta z(r)$  varies as a function of the radius  $r$  like:

$$\Delta z(r) = \begin{cases} L_S & \text{for: } r \leq R_i \\ L_{\text{cell}} & \text{for: } R_i \leq r \leq R_C \end{cases} \quad \text{Equation 20}$$

The result from such a geometry is compared with the temperature drop  $\Delta T_C^{\text{ns}}$  of a non-segmented fully cylindrical cell, i.e.  $R_i=0$ .

In order to enable an analytical solution of the stationary heat equation for this geometry, the following assumptions are required. The spatial distribution of the heat source  $dP/dV$  in the cell will be radially described by the Grindhammer profile, i.e.:

$$\frac{dP}{dV}(r,z) = \frac{dP}{dz}(z) \cdot \frac{2 \cdot \sigma^2(z)}{\pi \cdot (r^2 + 2 \cdot \sigma^2(z))^2} \quad \text{Equation 21}$$

The longitudinal power density  $dP/dz$  is regarded to be constant over the length  $L_{\text{cell}}$  of the cell. The last assumption simplifies the situation of heat flow at  $r=R_i$ , where the length of the

cell increases from  $L_S$  to  $L_{\text{cell}}$ . The heat, which crosses the radial surface  $2\pi \cdot R_i \cdot L_S$  at  $r = R_i$  is assumed to spread out longitudinally and makes immediate use of the larger surface  $2\pi \cdot R_i \cdot L_{\text{cell}}$  for  $r \geq R_i$ . This assumption overestimates the geometrical effect, but it is nearly fulfilled if  $L_H/2 \ll (R_C - R_i)$ . In that case the heat can sufficiently spread out in longitudinal direction before reaching the circumference of the cell.

For the given geometry and under the previously explained conditions, the stationary heat equation (see Equation 63) has to be modified a little and  $\Delta T_C$  can be written as:

$$\Delta T_C(r=0, z) = \frac{1}{\lambda} \cdot \frac{dP}{dz}(z) \cdot \int_{s=0}^R \frac{1}{\Delta z(s)} \cdot \frac{ds}{s} \int_{u=0}^s \Delta z(u) \cdot \frac{2 \cdot \sigma^2(z)}{\pi \cdot (u^2 + 2 \cdot \sigma^2(z))^2} \cdot u \cdot du \quad \text{Equation 22}$$

The result of this integration for the non-segmented geometry, which has a constant length independent of  $r$ , i.e.  $\Delta z(r) = \text{const}$ , is already presented in Equation 64. Thus  $\Delta T_C^{\text{ns}}$  is given by:

$$\Delta T_C^{\text{ns}}(r=0, z) = \frac{1}{4\pi \cdot \lambda} \cdot \frac{dP}{dz}(z) \cdot \ln \left( 1 + \frac{R_C^2}{2 \cdot \sigma^2(z)} \right) \quad \text{Equation 23}$$

In a similar way  $\Delta T_C$  can be calculated and normalized to  $\Delta T_C^{\text{ns}}$ , which gives the following result:

$$\Theta_{\text{rel}} = \frac{\Delta T_C(r=0)}{\Delta T_C^{\text{ns}}(r=0)} = 1 - \frac{2 \cdot \left[ 1 - \frac{2 \cdot \sigma^2}{2 \cdot \sigma^2 + R_i^2} \right] \cdot \left[ 1 - \frac{L_S}{L_{\text{cell}}} \right] \cdot \ln \left( \frac{R_C}{R_i} \right)}{\ln \left( 1 + \frac{R_C^2}{2 \cdot \sigma^2} \right)} \quad \text{Equation 24}$$

For the favoured situation of  $R_C = 10\text{cm}$ ,  $L_{\text{cell}} = 30\text{cm}$  and  $L_S = 10\text{cm}$  the ratio  $\Theta_{\text{rel}}$  is plotted in Figure 38 as a function of  $R_i$ . The four curves in that plot differ in the characteristic width  $\sigma$  of the radial energy density profile. As known from section 2.2.1 a realistic value of the width  $\sigma_2$  of the radial energy density profile, which describes the broad energy carrying fraction, has a size near to 10mm at the shower maximum in a graphite core. Thus the curve for  $\sigma = 2\text{mm}$  describes the situation at the beginning of the dump while  $\sigma = 10\text{mm}$  represents the shower maximum. The two remaining curves of  $\sigma = 5\text{mm}$  and  $\sigma = 30\text{mm}$  are added to get an impression of the sensitivity of  $\Theta_{\text{rel}}$  with respect to  $\sigma$ .

The behaviour of the plotted ratio  $\Theta_{\text{rel}}$  is easy to understand. In the limits  $R_i = 0$  and  $R_i = R_C$  a purely cylindrical disk without a hollow volume exists. This situation is identical to the fully solid reference geometry and the ratio hence is  $\Theta_{\text{rel}} = 1$ . In between these limits  $\Theta_{\text{rel}}$  drops down to a minimum, whose position concerning  $R_i$  and whose level depends on the width  $\sigma$ . If  $R_i \ll \sigma$  a lot of power is still dissipated in the long sector of the cell at  $r \geq R_i$ . Therefore the heat flux density is not decreased there significantly. If  $R_i \gg \sigma$  nearly 100% of the power is dissipated in the short sector and has to flow there a while before it can benefit from the enlarged radial cross section of the long sector. The optimum geometrical enhancement of heat conduction, i.e. the minimum of  $\Theta_{\text{rel}}$  occurs, when  $R_i$  is chosen such that the short sector just captures most of the dissipated power, while the long sector primarily serves as a large area heat conductor.

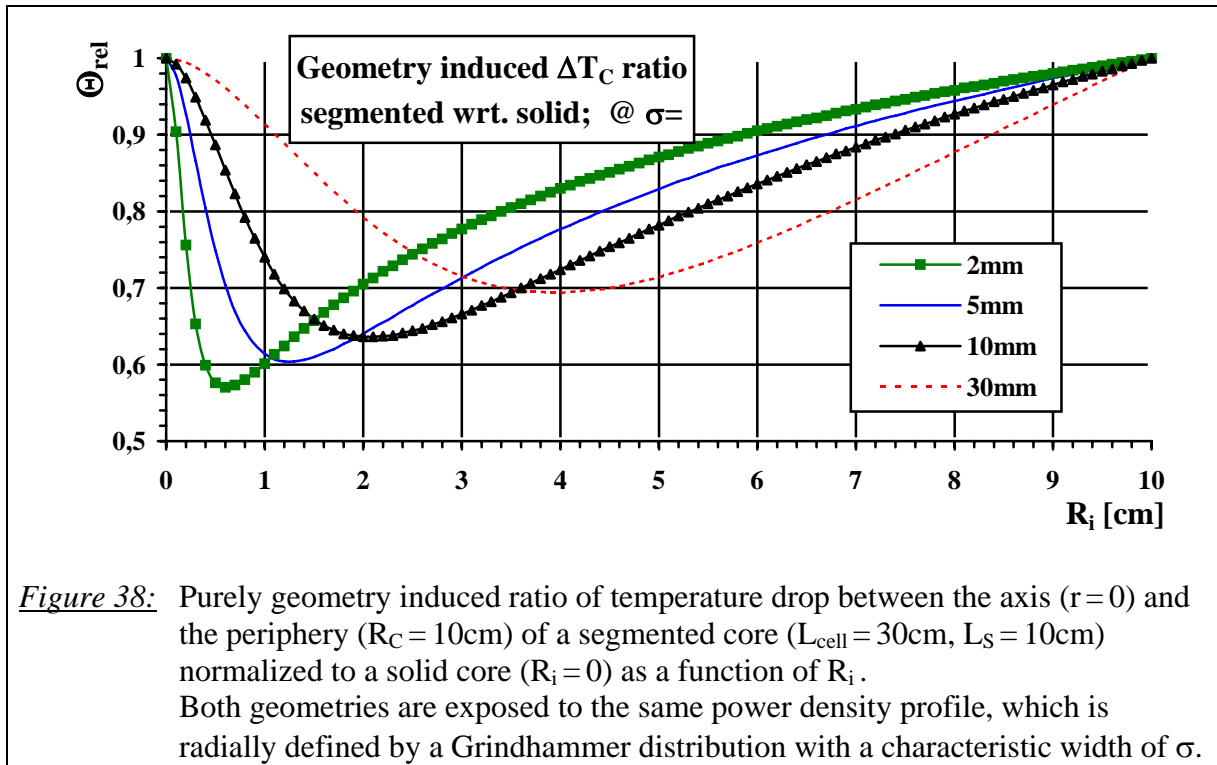


**Figure 38:** Purely geometry induced ratio of temperature drop between the axis ( $r=0$ ) and the periphery ( $R_C=10\text{cm}$ ) of a segmented core ( $L_{\text{cell}}=30\text{cm}$ ,  $L_S=10\text{cm}$ ) normalized to a solid core ( $R_i=0$ ) as a function of  $R_i$ . Both geometries are exposed to the same power density profile, which is radially defined by a Grindhammer distribution with a characteristic width of  $\sigma$ .

The temperature drop across the segmented graphite core at the shower maximum, where we assume  $\sigma = 10\text{mm}$ , is reduced to the level of about 67% or 78% if  $R_i$  is chosen to be 3cm or 5cm respectively. The optimum reduction lowers the temperature drop to the level of 64% and is achieved for a bore radius of  $R_i=2\text{cm}$ , which is too small if beam steering and alignment tolerances should be taken into account.

Average heating is a combined effect to which both, the magnitude of the heat source and the quality of the heat extraction contribute. On top of the temperature reduction, which is achieved by a reduction of the heat source term due to widening the shower profile in a segmented dump, a geometrical enhancement of heat extraction lowers the radial temperature drop between the axis ( $r=0$ ) and the periphery ( $r=R_C$ ) of a segmented core to a level in the order of 90% to 70% if the disks are thermally coupled.

### 4.3.3 Longitudinal Temperature Profiles of the segmented Dump Layout

After having discussed the energy deposition distribution in section 4.3.1 and the positive geometrical impact on heat extraction in section 4.3.2, this section finally informs about the derived temperatures in a dump with a segmented graphite core. The results are based on the dump geometry as shown in Figure 33, where the graphite core with a radius of  $R_C=10\text{cm}$  is embedded in a radial Cu-shell of 8cm thickness, which is water cooled at its circumference. The leading part of the graphite core is built up by a total number of  $N_{\text{cell}}$  cells, in which each cell consists of one solid and one hollow disk. Downstream of this segmented part of the graphite core a non-segmented full graphite section follows, before the Cu-backstop terminates the dump longitudinally. The total length of segmented and full graphite core together is  $L_C$ .

A 7.5GeV or 20GeV beam with an average power of 300kW and a size of  $\sigma_{\text{beam}}=2\text{mm}$  enters such a dump axially and the resulting longitudinal profile of the equilibrium temperature along the axis  $T_{\text{eq}}(r=0,z)$  is plotted in Figure 39 a) and b). Both radial heat transfer boundaries (graphite to Cu-shell and Cu-shell to cooling water) are included with a coefficient of  $0.4\text{W}/\text{cm}^2/\text{K}$  and the cooling water has a temperature of  $T_0=50^\circ\text{C}$ . While the shape of the solid disk is fixed with a length of  $L_S=10\text{cm}$ , the hollow disk has a length of

$L_H = 10\text{cm}$  with a bore radius of  $R_i = 3\text{cm}$  in case a) and a length of  $L_H = 20\text{cm}$  with a bore radius of  $R_i = 5\text{cm}$  in case b).

The geometrical enhancement effect of heat extraction, as described in the previous section 4.3.2, is taken into account in all plots as well, i.e. solid and hollow disk of each cell are ideally thermally coupled in longitudinal direction. For comparison the uncoupled situation is shown in case a) in addition. Here thermal coupling lowers the temperature level in the center of the solid disks to around 70% of the uncoupled situation. Nevertheless maximum temperatures around  $700^\circ\text{C}$ , which are beyond the design goal, can not be avoided.

However if the length of the hollow disk is doubled to  $L_H = 20\text{cm}$  and its bore radius is

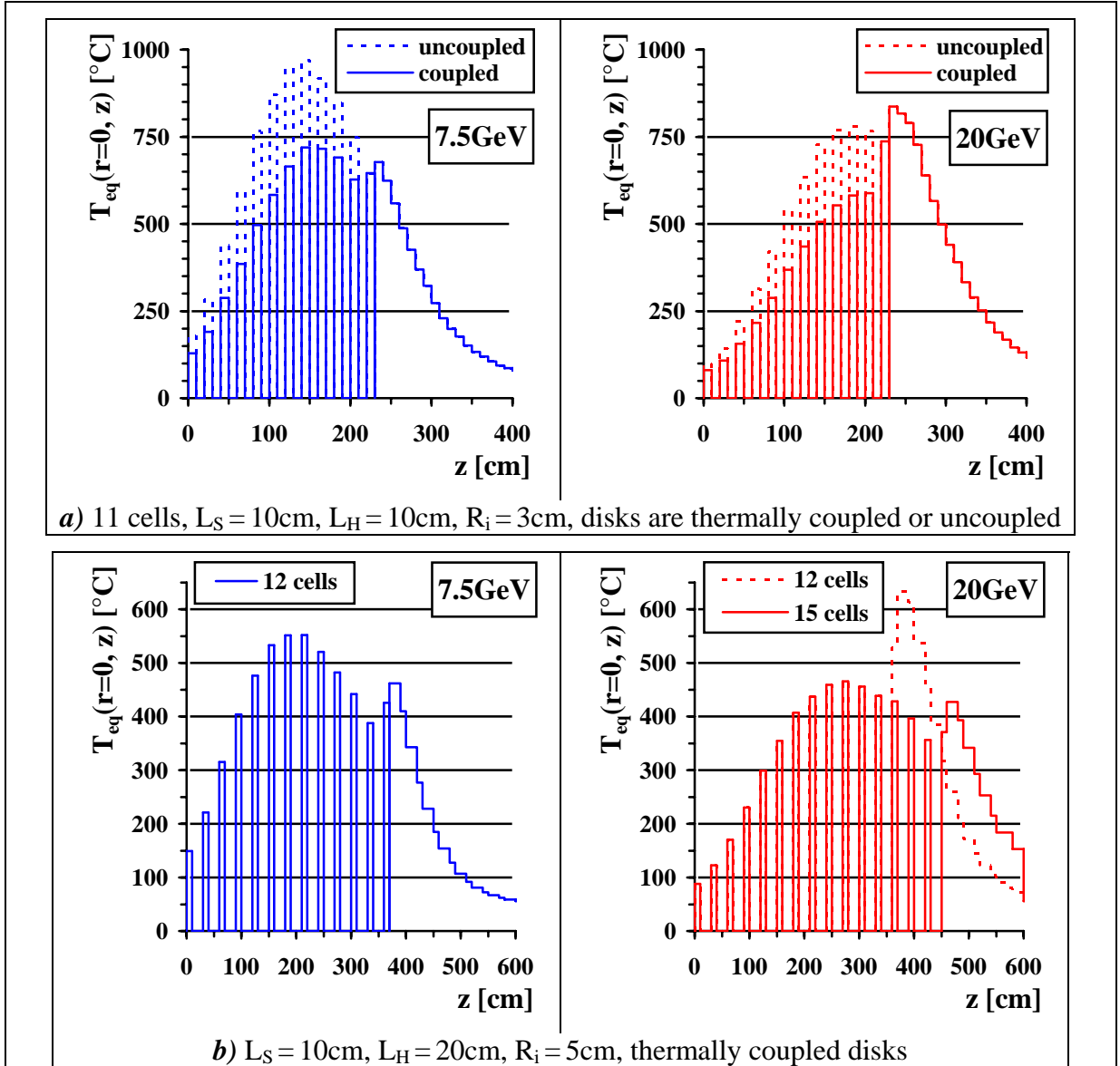


**Figure 39:** Longitudinal profile of equilibrium temperature  $T_{\text{eq}}$  along the axis ( $r=0$ ) of a segmented beam dump as shown in Figure 33, which is axially hit by  $300\text{kW}$  average power coming from a  $7.5\text{GeV}$  respectively  $20\text{GeV}$  non-swept beam with a size of  $\sigma_{\text{beam}} = 2\text{mm}$ .

A cell consists of a solid disk with a length of  $L_S = 10\text{cm}$  and a hollow one with:  
a)  $L_H = 10\text{cm}$ ,  $R_i = 3\text{cm}$ , or b)  $L_H = 20\text{cm}$ ,  $R_i = 5\text{cm}$ .

Thermally coupled disks are compared with the uncoupled case and the number of cells is varied. Heat transfer is specified by  $K_{\rightarrow w} = K_{\rightarrow \text{shell}} = 0.4\text{W/cm}^2/\text{K}$  and the cooling water temperature is  $T_0 = 50^\circ\text{C}$ .

increased to  $R_i = 5\text{cm}$  as in case b), the maximum equilibrium temperature can be kept close to  $500^\circ\text{C}$ . The total length of the segmented part must not fall below 15 cells, i.e.  $450\text{cm}$ . Otherwise the temperatures in the full graphite part exceed those in the segmented section, especially for a long shower at high energy, which is illustrated in Figure 39 b) for the  $20\text{GeV}$  beam, when comparing the 12 cell situation with 15 cells.

Although not finally optimized in shape, the segmented dump of case b) can already handle a non-swept  $300\text{kW}$  beam with a spot size of  $\sigma_{\text{beam}} \geq 2\text{mm}$ , without exceeding the desired temperature limits. Hitting the non-segmented dump of the baseline layout, such a beam creates maximum equilibrium temperatures around  $1600^\circ\text{C}$  (see Figure 12 c)). The reduction down to the  $500^\circ\text{C}$  level is obtained by a combination of the following contributions:

- 1.) The longitudinal power density  $dP/dz$  at the shower maximum  $z = t_{\text{max}}$  is decreased by  $\approx 25\%$ .
- 2.) The width of the radial profile of deposited energy  $dE/dm$  at the shower maximum  $z = t_{\text{max}}$  is increased by a factor of  $\approx 2$ .
- 3.) The heat extraction from the core to the periphery is improved by a geometrical effect of about  $10\%$  to  $30\%$ , when solid and hollow disk are thermally coupled.

Widening of the shower cross section as indicated by item 2) is the mechanism, which contributes most.

In addition this effect is also responsible for the reduction of instantaneous heating. The instantaneous temperature rise  $\Delta T_{\text{inst}}(r=0, z)$ , which is induced during the passage of a fully populated bunch train ( $N_t = 2 \cdot 10^{13} \text{e}$ ,  $\sigma_{\text{beam}} = 2\text{mm}$ ) on the axis of a segmented dump, is shown in Figure 40 for  $7.5\text{GeV}$  and  $20\text{GeV}$  electrons. The graph assumes an initial graphite temperature of  $T_i = 220^\circ\text{C}$ . As known from Table 4 the non-segmented graphite core experiences a maximum instantaneous temperature jump of  $\max(\Delta T_{\text{inst}}) = 150\text{K}$  at  $z = t_E$  for a  $20\text{GeV}$  bunch train. In the segmented core almost half of this value is generated only.

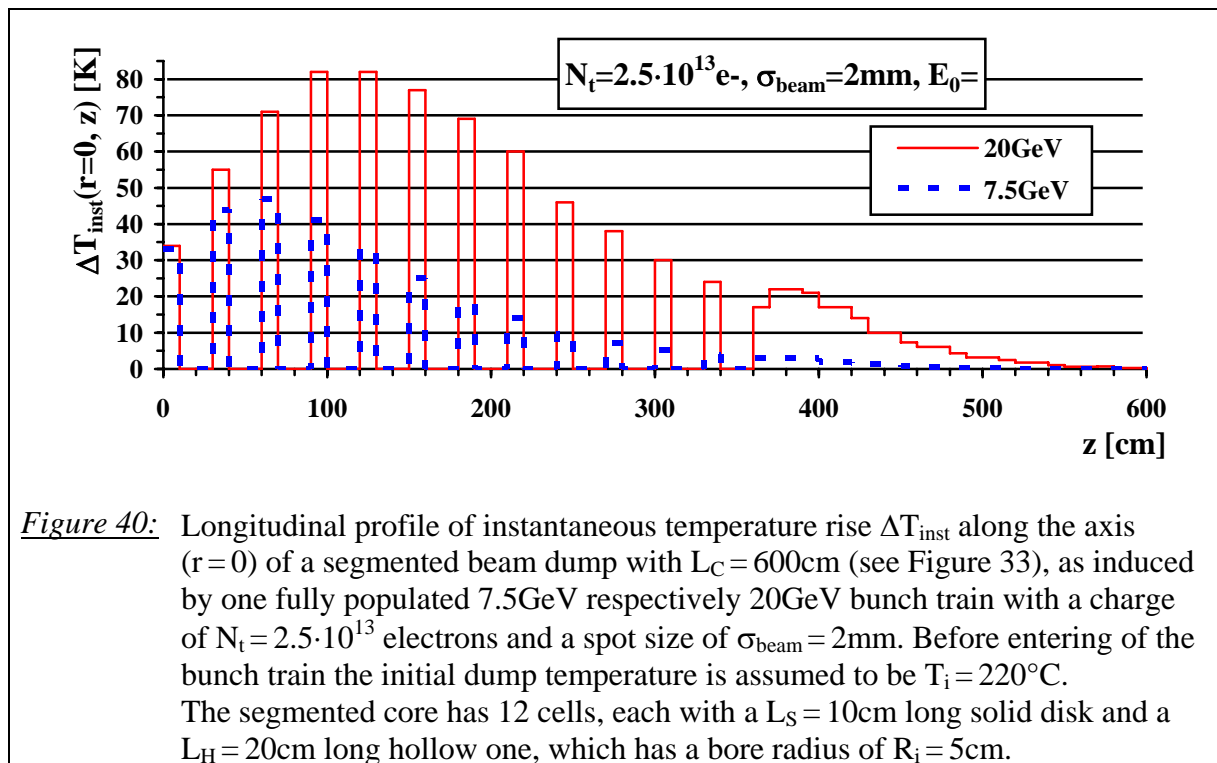


**Figure 40:** Longitudinal profile of instantaneous temperature rise  $\Delta T_{\text{inst}}$  along the axis ( $r=0$ ) of a segmented beam dump with  $L_C = 600\text{cm}$  (see Figure 33), as induced by one fully populated  $7.5\text{GeV}$  respectively  $20\text{GeV}$  bunch train with a charge of  $N_t = 2.5 \cdot 10^{13}$  electrons and a spot size of  $\sigma_{\text{beam}} = 2\text{mm}$ . Before entering of the bunch train the initial dump temperature is assumed to be  $T_i = 220^\circ\text{C}$ . The segmented core has 12 cells, each with a  $L_S = 10\text{cm}$  long solid disk and a  $L_H = 20\text{cm}$  long hollow one, which has a bore radius of  $R_i = 5\text{cm}$ .

The segmented dump core approach looks quite attractive amongst all presented passive options. Nevertheless due to its length, weight and the risk of breaking the graphite ring of the hollow part, it can not compete seriously with the baseline design.

## 5 Comparative Summary

The dump considerations up to chapter 3 culminated into the baseline layout, which requires the use of a slow beam sweeping system. This system should provide a circular sweep with radius of  $R_s = 5\text{cm}$  in order to enable heat extraction at tolerable graphite temperatures below  $500^\circ\text{C}$  to  $600^\circ\text{C}$ . To be exact, this sweep circle has to be created at the shower maximum, where the maximum of power is dissipated. If the deflecting magnet pair is located 10m upstream of the shower maximum ( $t_{\text{max}} \approx 1\text{m}$  @  $7.5\text{GeV}$ ), which is 7m upstream of the 2m long concrete front part of the dump module, a kick of 5mrad is necessary. Thus only a moderate field amplitude of  $|\text{Bdl}| \leq 0.5\text{Tm}$  is required at 25GeV for this system, which harmonically oscillates at a frequency of around 1kHz.

Indeed it is desired to design the beam dump with a minimum of active subsystems, but the quite simple slow sweeping system would not limit the whole system in terms of reliability. Its proper functioning can be surveyed easily and actions to inhibit beam operation in a failure case have to be taken only on the time scale of the bunch train repetition, but not within a bunch train.

Nevertheless 3 alternative solutions, which avoid such an active beam sweep have been studied in chapter 4. The main characteristics of all layouts are listed in Table 12 for comparison. The requirement on the incoming beam spot size of  $\sigma_{\text{beam}} \geq 2\text{mm}$  has to be fulfilled in each of the layouts, because of the instantaneous heating limit in graphite, from which the core respectively the spoiler are made of in all cases.

In the spoiler option the baseline geometry would remain untouched, but the sweeping system is replaced by a graphite spoiler of about 1 radiation length. Unfortunately an additional huge source of radiation is introduced by the spoiler, which is located about 10m upstream of the dump face, i.e. outside of the concrete shielding in which the dump is buried in. The whole beam line from spoiler to dump and the vicinity of the spoiler, in which an average power on the 10kW level is dissipated, will suffer from activation of the components and the ambient air.

The most compact approach in size and weight is achieved with a pyrolytic graphite dump core. It relies upon the outstanding thermal conductivity of this material, which may degrade with time under the influence of neutron irradiation.

The last alternative implements the function of a spoiler into the dump, by means of segmenting its core into solid and hollow graphite disks. Hence the problem of an external radiation source is avoided, but the absorbing part of the segmented dump module (without the 2m long concrete front section) will almost double in length and weight compared to the baseline design.

When evaluating all solutions, the baseline approach with a slow sweeping system is still the preferred one. The passive (without sweeping system) options can not compete, because they introduce disadvantages and unknown risks, which are much more severe.

	WITH Slow Sweep $R_s = 5\text{cm}$		Alternative Options WITHOUT Slow Sweep		
	Baseline normal C/Cu-Cu	Baseline short C/Cu-Al-Cu	Pyrolitic C - Core PyC/Cu-Cu	C - Spoiler Option 1·X <sub>0</sub> C-spoiler 10m upstream baseline dump	Segmented C - Core 10cm solid + 20cm hollow $R_i = 3\text{cm to } 5\text{cm}$
<b>Dump Core</b>					
Material	standard graphite $\rho = 1.71\text{g/cm}^3$		pyrolitic graphite $\rho = 2.25\text{g/cm}^3$ $\lambda \geq 3\text{W/cm/K}$	standard graphite $\rho = 1.71\text{g/cm}^3$	
Length, L <sub>c</sub>	330 cm	210 cm	280 cm	330 cm	≈ 630 cm 450cm (15 cells) + 180cm solid part
Radius, R <sub>c</sub>	10 cm		5 cm	10 cm	
<b>Cu-shell</b>					
Thickness, $\Delta R_{\text{shell}}$	8 cm				
<b>Backstop</b>					
Length and Material	15 cm Cu	50 cm Al + 15 cm Cu	15 cm Cu		
<b>Overall Size (without 2m concrete front part)</b>					
Radius, R	18 cm		13 cm	18 cm	
Length, L	345 cm	275 cm	295 cm	345 cm	645 cm
<b>Weight (without 2m concrete front part, beam pipe and cooling water tubing)</b>					
<b>total</b>	≥ 2.4 tons	≥ 1.8 tons	≥ 1.3 tons	≥ 2.4 tons	≥ 4.4 tons
C-Core	180 kg	110 kg	50 kg	180 kg	300 kg
Cu-Shell	2100 kg	1400 kg	1150 kg	2100 kg	4000 kg
Backstop	140 kg Cu	140 kg Al 140 kg Cu	70 kg Cu	140 kg Cu	140 kg Cu
<b>max(T<sub>eq</sub>) in Core</b> <b>0.4W/cm<sup>2</sup>/K, T<sub>0</sub>=50°C</b>	500 °C		600 °C		550 °C
<b>max(ΔT<sub>inst</sub>) in Core</b> <b>for</b> <b>N<sub>i</sub>=2.5·10<sup>13</sup>, T<sub>i</sub>=220°C</b>	180 K @ 25 GeV 150 K @ 20 GeV 80 K @ 7.5 GeV			≤ 20 K	90 K @ 25 GeV 80 K @ 20 GeV 50 K @ 7.5 GeV
<b>Disadvantage</b>	active sweeping system, but no severe challenge in terms of reliability		questionable long term thermal conductivity	additional source of radiation → activation	length, weight

*Table 12:* Comparison of the baseline dump layout for the XFEL Main Dump with alternative options, which do not require active beam sweeping. Spot size of incoming beam must be  $\sigma_{\text{beam}} \geq 2\text{mm}$  at all dumps resp. spoiler.

## A Fundamentals on Energy Deposition in an Electron Dump

High energy electrons hitting an absorber initiate a particle shower, which causes a certain spatial distribution of dissipated energy in the material. This energy distribution serves as an essential basis for all dump layout considerations. Together with the time structure of the impinging electron beam it represents the heat source term of the heat equation, from which the temperature profiles can be derived as shown in the next annex B. The temperature distributions in the dump finally determine the corresponding mechanical stress in the materials involved.

In terms of energy deposition the central part of the cascade is dominated by the charged electromagnetic shower components, which dissipate their energy in the material by excitation and ionization of its atoms. Therefore this annex describes the development of an electromagnetic shower and gives useful analytical formulae for its characterization. By that means some simplified estimations on energy deposition can be done even without running a shower simulation code. In addition due to photonuclear reactions the cascade has a hadronic component as well. This is of important interest when investigating shielding, activation or far range energy deposition aspects, but is out of the focus of this report.

### A.1 Electromagnetic Shower (EMS) Development

In general electrons hitting matter can lose their energy by collisions with atoms and radiation of bremsstrahlung. The energy lost by collisions is mostly spent into excitation or ionization and is therefore dissipated in the material. Quantitatively the ionization loss per unit length  $dE/dz$  has a minimum at a relativistic  $\gamma$  of about 3. Normalized to the mass density this minimum is almost constant for all materials, namely:

$$\left( \frac{1}{\rho} \cdot \frac{dE}{dz} \right)_{\min} \approx (1.0 \dots 2.0) \frac{\text{MeV} \cdot \text{cm}^2}{\text{g}} \quad \text{Equation 25}$$

Since there is only a very weak rise at higher energies, this number can be used to approximate the energy, which is dissipated along the path of a high relativistic charged particle in matter.

The radiation process is based on the fact, that a charged particle loses energy in form of electromagnetic radiation when experiencing a transverse or decelerating force. In our case the electron travelling through matter is exposed to the coulomb forces of the nuclei and therefore radiates the so called bremsstrahlung. The characteristic length, after which the electron energy in average has fallen off to the level of  $1/e$ , is called radiation length  $X_0$ . It depends on both, the atomic number  $Z$  and the mass number  $A$  and is of course inversely proportional to the density  $\rho$  of the material. To an accuracy of better than 5% it can be calculated by the following approximation [6]:

$$X_0 = \frac{716 \frac{\text{g}}{\text{cm}^2} \cdot A}{Z \cdot (Z+1) \cdot \ln(287/\sqrt{Z})} \cdot \frac{1}{\rho} \quad \text{Equation 26}$$

The energy loss of highly relativistic ( $\gamma \gg 1$ ) electrons due to ionization is approximately constant, while the radiation process scales linear with energy. The energy, at which both mechanisms contribute equally to the energy loss of the particle, is called the critical energy  $E_c$ . This is a material parameter and can be approximated [6] as a function of its atomic number  $Z$ :

$$\text{solids and liquids: } E_c = \frac{610 \text{ MeV}}{Z+1.24} \quad ; \quad \text{gases: } E_c = \frac{710 \text{ MeV}}{Z+0.92} \quad \text{Equation 27}$$

Typically in our considerations the energy of the primary electron  $E_0$  is large compared to  $E_c$ . Therefore it mainly loses its energy by emitting bremsstrahlung photons along its way. These photons materialize into electron positron pairs, which again emit bremsstrahlung and so on. The result of the combined phenomena of bremsstrahlung and pair production is the occurrence of a cascade, called the electromagnetic shower, which mainly consists of electrons, positrons and photons. The number of particles increases exponentially, while their average energy decays exponentially with ongoing depth in the material. This process continues until the energy of the charged constituents falls below  $E_c$ , where radiation, the driving process of cascade development, becomes negligible and the shower will thus cease.

The shower multiplies one incident electron into electrons, positrons and photons, while dissipative processes like ionization along the path of each charged particle deposit a certain amount of energy  $dE(dV)$  in the volume  $dV(\vec{r})$  at the position  $\vec{r}$  in the absorbing medium. Hence the spatial energy density, which is the energy per unit of volume at the position  $\vec{r}$ , as deposited by one incident electron, can be defined by:

$$\varepsilon(\vec{r}) = \frac{dE(dV(\vec{r}))}{dV(\vec{r})} \quad \text{Equation 28}$$

Sometimes it might be more useful to express the energy density with respect to the unit of mass, i.e.:

$$\frac{dE}{dm}(\vec{r}) = \frac{1}{\rho} \cdot \varepsilon(\vec{r}) \quad \text{Equation 29}$$

Whether  $dE/dV$  or  $dE/dm$  should be referred to, might be motivated by the following examples. Firstly if energy deposition time period is short compared to thermal conduction processes, the corresponding temperature rise in a region can be simply derived by dividing  $dE/dm$  by the specific heat capacity of the material in that region. Secondly let us assume a given geometry, in which an EMS has developed. Now we assume a small volume being replaced by a material of different density. If the volume is small in a sense, that the overall development of the shower experiences only a negligible distortion, then  $dE/dm$  in the replaced volume will remain more or less the same as before, but  $dE/dV$  would of course show a discontinuity according to the change in density between the surrounding volume and the replaced one. Hence  $dE/dV$  should be used in plots to recognize regions of different materials and  $dE/dm$  is the figure which behaves continuously at density boundaries.

A full knowledge about the spatial distribution of the deposited energy density is only gained by a so called monte carlo shower simulation program, e.g. the MARS code [2], which was used in the context of this report. Nevertheless an EMS can be described to a certain extend by analytical expressions, which are subject of the following sections A.1.1 and A.1.2. Since the shower develops with rotational symmetry around the axis of the incoming beam, a cylindrical coordinate system with  $r$ ,  $z$  and  $\varphi$  to describe the position  $\vec{r}$  is the adequate choice. Due to azimuthal symmetry the spatial energy density function is independent of  $\varphi$  and reduces to  $\varepsilon(r,z)$ . In the following considerations it is assumed, that a homogeneous material extends infinitely wide around the positive  $z$ -axis, i.e. within the limits:  $0 \leq r \leq \infty$ ,  $0 \leq z \leq \infty$  and  $0 \leq \varphi \leq 2\pi$ . The incoming electron hits the surface of this material perpendicular at  $r = z = 0$ .

### A.1.1 Longitudinal Characterization

Imagine a transverse plane at the position  $z$  having an infinitesimal thickness  $dz$ . The amount of energy  $dE(z)$  deposited in this plane is calculated by integrating  $\varepsilon(r,z)$  over the volume of this slice. Therefore the longitudinal energy density, which is the energy per unit of length at the position  $z$  as deposited by one incident electron, can be written as:

$$\frac{dE}{dz}(z) = \int_{r=0}^{\infty} \varepsilon(r,z) \cdot 2\pi r \cdot dr \quad \text{Equation 30}$$

At the beginning for  $z \ll X_0$  when particle multiplication has not yet started, there is only the primary high energy electron, which deposits energy by ionization (see Equation 25) and the longitudinal energy density can be approximated as:

$$\frac{dE}{dz}(z \ll X_0) \approx \left( \frac{1}{\rho} \cdot \frac{dE}{dz} \right)_{\min} \cdot \rho \quad \text{Equation 31}$$

Going on in depth the  $dE/dz$  profile rises exponentially according to the shower development up to a broad peak, called the shower maximum, after which it declines gradually.

Evaluations of the longitudinal shower profile of a homogeneous and radially non limited absorber show, that 99% of the primary energy is absorbed within a length  $L_{99\%}$ , which can be expressed as:

$$L_{99\%} = \left( 1.52 \cdot \ln\left(\frac{E_0}{\text{MeV}}\right) - 4.1 \cdot \ln\left(\frac{E_c}{\text{MeV}}\right) + 17.6 \right) \cdot X_0$$

$$\text{gives: } \int_{r=0}^{\infty} \int_{z=0}^{L_{99\%}} \varepsilon(r,z) \cdot 2\pi r \, dr \, dz = \int_{z=0}^{L_{99\%}} \frac{dE}{dz}(z) \, dz = 99\% E_0 \quad \text{Equation 32}$$

The longitudinal position of the shower maximum  $t_{\max}$  has been estimated by Rossi [7]:

$$t_{\max} = 1.01 \cdot \left[ \ln\left(\frac{E_0}{E_c}\right) - 1 \right] \cdot X_0 \quad \text{Equation 33}$$

The number of charged particles, i.e. electrons and positrons, at a certain depth  $z$  in the shower generated by one primary electron is called multiplicity  $M(z)$ . Rossi [7] gives the following approximation for the multiplicity at the shower maximum:

$$M(t_{\max}) = \frac{0.31}{\sqrt{\ln\left(\frac{E_0}{E_c}\right) - 0.37}} \cdot \frac{E_0}{E_c} \quad \text{Equation 34}$$

In analogy to Equation 31 we approximate the dissipated energy of each of the charged particle at the shower maximum as minimum ionization loss. Thus one can estimate the longitudinal energy density generated by one primary electron at the shower maximum as:

$$\max\left(\frac{dE}{dz}\right) = \frac{dE}{dz}(z = t_{\max}) \approx \left( \frac{1}{\rho} \cdot \frac{dE}{dz} \right)_{\min} \cdot \rho \cdot M(t_{\max}) \quad \text{Equation 35}$$

In practice of course a beam of electrons rather than a single electron will hit the absorber. If  $I_{ave}$  denotes the time averaged current of the beam, the average longitudinal power density, which is the power dissipation per unit length, is obviously given by:

$$\frac{dP}{dz}(z) = \frac{dE}{dz}(z) \cdot \frac{I_{ave}}{e} \quad \underline{\text{Equation 36}}$$

Using Equation 31 and Equation 35 the longitudinal power density  $dP/dz$  can be quantitatively estimated at the beginning of the absorber or in a beam window and at the shower maximum by:

$$\frac{dP}{dz}(z) \approx \left( \frac{1}{\rho} \cdot \frac{dE}{dz} \right)_{min} \cdot \rho \cdot \frac{I_{ave}}{e} \cdot \begin{cases} 1 & \text{at } z \ll X_0 \\ \approx 30 \frac{W}{cm} \cdot \frac{\rho}{2 \frac{g}{cm^3}} \cdot \frac{I_{ave}}{10 \mu A} & \text{at } z \ll X_0 \\ M(t_{max}) & \text{at } z = t_{max} \end{cases} \quad \underline{\text{Equation 37}}$$

When we insert  $M(t_{max})$  from Equation 34 and introduce the average beam power  $P_{ave} = E_0 \cdot I_{ave}/e$  the longitudinal power density at the shower maximum can be rewritten as:

$$\max\left(\frac{dP}{dz}\right) = \frac{dP}{dz}(z = t_{max}) = \left( \frac{1}{\rho} \cdot \frac{dE}{dz} \right)_{min} \cdot \rho \cdot \frac{0.31}{E_c} \cdot \frac{P_{ave}}{\sqrt{\ln\left(\frac{E_0}{E_c}\right) - 0.37}} \quad \underline{\text{Equation 38}}$$

Since the dissipated power has to be extracted from the absorber, its peak value is one of the main criteria, which decides about the layout of a beam dump. It is important to point out that for a given material this figure does not only scale linearly with the average power of the incoming beam, but in addition also shows a weak decline with increasing beam energy. This can be easily understood, since the shower becomes longer with energy. Thus the longitudinal power density has to fall with energy if the average beam power remains constant. As a consequence a beam dump, which is designed for a certain beam energy and average beam power, is not automatically qualified to work at lower beam energy while still taking the same average beam power. In this respect one has to determine which point in the energy-power parameter space, for which the dump shall be designed for, will cause the highest longitudinal power density. This point will not necessarily be the one of highest energy and highest power. Maximum beam energy and maximum average beam power are therefore not sufficient to specify a dump in terms of average power dissipation.

### A.1.2 Radial Characterization

This section will inform about the radial dependence of the energy density function  $\varepsilon(r,z)$ . Even without knowing the radial distribution explicitly, the radial extension of an electromagnetic shower is characterized by the Molière radius  $R_M$  [6]:

$$R_M \approx \frac{21.2 \text{ MeV}}{E_c} \cdot X_0 \quad \underline{\text{Equation 39}}$$

In a similar way as  $L_{99\%}$  for the longitudinal shower content, now the radius  $R_{90\%}$  respectively  $R_{99\%}$  of an infinitely long homogeneous absorber, in which 90% respectively 99% of the primary energy is absorbed, can be expressed in terms of the Molière radius as:

$$R_{90\%} \approx R_M \quad \text{gives:} \quad \int_{r=0}^{R_{90\%}} \int_{z=0}^{\infty} \varepsilon(r, z) \cdot 2\pi r \, dr \, dz = 90\% E_0$$

and

Equation 40

$$R_{99\%} \approx 5 \cdot R_M \quad \text{gives:} \quad \int_{r=0}^{R_{99\%}} \int_{z=0}^{\infty} \varepsilon(r, z) \cdot 2\pi r \, dr \, dz = 99\% E_0$$

These values agree quite well with the results of MARS calculations for different materials as previously shown in Figure 6. Since  $R_M$  is independent of  $E_0$ , the radial layout of a beam dump to absorb a certain fraction of the primary energy is not affected by the incoming beam energy, provided there are no other constraints (e.g. energy density), that would exceed the limits of the given layout at another beam energy and therefore may require a change.

As discussed in the previous section A.1.1  $dE(z)/dz$  tells how much energy is totally deposited in a transverse plane of thickness  $dz$  in the absorber. Now we are asking for a normalized distribution function  $f$ , which describes the radial profile of the energy in such a plane. Mathematically this means:

$$\varepsilon(r, z) = \frac{dE}{dz}(z) \cdot f(r, z) \quad \text{with:} \quad \int_{r=0}^{\infty} f(r, z) \cdot 2\pi r \, dr = 1 \quad \text{Equation 41}$$

As a result of scattering and shower processes the transverse profile broadens up with depth in material. That is why  $f$  has a  $z$ -dependence as well.

The transverse shower profile is characterized by a narrow core in combination with a broad contribution. Hence one way of describing  $f$  is by using a sum of two Gaussians:

$$f_{\text{gs}}(r, z) = \frac{\eta_1(z)}{2\pi\sigma_1^2(z)} \cdot e^{-\frac{r^2}{2\sigma_1^2(z)}} + \frac{\eta_2(z)}{2\pi\sigma_2^2(z)} \cdot e^{-\frac{r^2}{2\sigma_2^2(z)}} \quad \text{with:} \quad \eta_1(z) + \eta_2(z) = 1 \quad \text{Equation 42}$$

Here  $\eta_1$  denotes the fraction of energy, which is found in the narrow core having the width  $\sigma_1$ , while  $\eta_2$  and  $\sigma_2$  describe the broad part of the distribution. Typically  $\eta_1 < \eta_2$  but  $\eta_1/\sigma_1^2 \gg \eta_2/\sigma_2^2$ , which means, that the broad part contains the major fraction of the deposited energy, while the narrow core is responsible for the energy density maximum at a certain position  $z$ . For analytical applications, especially when integration is required as for the solution of the heat equation (see annex B), the empirical distribution function  $f_{\text{gh}}$ , also known as Grindhammer parameterization [8], is more useful:

$$f_{\text{gh}}(r, z) = \frac{2 \cdot \sigma^2(z)}{\pi \cdot (r^2 + 2 \cdot \sigma^2(z))^2} \quad \text{Equation 43}$$

It should be mentioned, that the Grindhammer distribution function leads to the same value at  $r=0$  as a simple Gaussian of the same width  $\sigma$  namely:  $f(r=0, z) = 1/(2\pi\sigma^2(z))$ .

However which of the distribution functions is chosen their parameters  $\eta$  and  $\sigma$  have to be derived from fitting them to the results of an EMS simulation code. For a transversely extended primary beam the width  $\sigma(z)$  of the transverse energy profile results of course from a convolution of the pure shower distribution with a width  $\sigma_s(z)$  as coming from a single

primary electron or a point-like beam and the distribution of the incoming electrons having a width  $\sigma_{\text{beam}}$ , i.e.  $\sigma^2(z) = \sigma_s^2(z) + \sigma_{\text{beam}}^2$ .

With the approximation on dissipated energy as done in section A.1.1 the spatial energy density in the shower at least up to the shower maximum can be expressed as:

$$\varepsilon(r, z) = \left( \frac{1}{\rho} \cdot \frac{dE}{dz} \right)_{\min} \cdot \rho \cdot M(z) \cdot f(r, z) \quad \text{for: } 0 \leq z \leq t_{\max} \quad \text{Equation 44}$$

In annex B we will see, that  $\max(\varepsilon(r, z))$  defines the highest instantaneous temperature jump, while  $\max(dP/dz)$  which is located at the shower maximum (see Equation 38) determines the average temperature level in the dump. The maximum spatial energy density  $\max(\varepsilon)$  is of course located somewhere on the shower axis (i.e.  $r=0$ ) in a depth, which will be called  $z = t_E$ . Using the Grindhammer distribution  $f_{\text{gh}}(r=0, z = t_E)$  we can write:

$$\max(\varepsilon) = \varepsilon(r=0, z = t_E) = \left( \frac{1}{\rho} \cdot \frac{dE}{dz} \right)_{\min} \cdot \rho \cdot \frac{M(t_E)}{2\pi\sigma^2(t_E)} \propto \frac{M(t_E)}{\sigma_s^2(t_E) + \sigma_{\text{beam}}^2} \quad \text{Equation 45}$$

Obviously the maximum spatial energy density is longitudinally located at a depth  $t_E$ , where the ratio between the multiplicity and the square of the width of the radial energy distribution peaks. Therefore it depends on the incoming beam spot size. It will be located near the shower maximum if  $\sigma_{\text{beam}} > \sigma_s(t_{\max})$ , but moves more and more towards the dump entrance when the beam spot decreases. This is the reason why maximum longitudinal power density and maximum spatial energy density may well be located at different longitudinal positions  $t_{\max}$  and  $t_E$ , which have to be strictly distinguished. That means in general:  $t_{\max} \neq t_E$ .

Without simulation code the only location, where the spatial energy density can be explored quantitatively is at  $z=0$ . At the dump entrance or in a beam window the radial distribution function is simply given by the incoming beam distribution and the multiplicity is 1, i.e.  $\sigma(z=0) = \sigma_{\text{beam}}$  and  $M(z=0) = 1$ . If we assume a round gaussian distributed beam (parameters for  $f_{\text{gs}}$  in that case are:  $\eta_1(z=0) = 1$ ,  $\eta_2(z=0) = 0$  and  $\sigma_1(z=0) = \sigma_{\text{beam}}$ ) carrying  $N_t$  electrons, one can estimate the energy per mass unit generated by this pulse as:

$$N_t \cdot \frac{dE}{dm}(r, z=0) = \frac{N_t}{\rho} \cdot \varepsilon(r, z=0) \approx \left( \frac{1}{\rho} \cdot \frac{dE}{dz} \right)_{\min} \cdot \frac{N_t}{2\pi\sigma_{\text{beam}}^2} \cdot e^{-\frac{r^2}{2\sigma_{\text{beam}}^2}} \quad \text{Equation 46}$$

Since  $\left( \frac{1}{\rho} \cdot \frac{dE}{dz} \right)_{\min}$  is almost constant, it has to be emphasized, that  $dE/dm$  at  $z=0$  does neither depend on the penetrated material nor the energy of the penetrating electrons, as long as they are highly relativistic. It only depends on the number of electrons per unit of transverse area, which they are impinging on. For a gaussian beam profile the maximum electron density is  $N_t / (2\pi\sigma_{\text{beam}}^2)$  at  $r=0$  and thus:

$$N_t \cdot \frac{dE}{dm}(r = z = 0) \approx \left( \frac{1}{\rho} \cdot \frac{dE}{dz} \right)_{\min} \cdot \frac{N_t}{2\pi\sigma_{\text{beam}}^2} \stackrel{1.5 \frac{\text{MeV} \cdot \text{cm}^2}{\text{g}}}{\approx} 40 \frac{\text{J}}{\text{g}} \cdot \frac{N_t}{10^{13}} \cdot \left( \frac{1 \text{mm}}{\sigma_{\text{beam}}} \right)^2 \quad \text{Equation 47}$$

This is a useful figure to illustrate the beam energy independent challenge of e.g. a beam window design for beam pulses of high charge and small spot size.

## B Fundamentals on Dump Heating

In general the time dependent spatial temperature distribution  $T(\vec{r}, t)$  is obtained as the solution of the heat equation:

$$\frac{\partial}{\partial t} T(\vec{r}, t) = \frac{\lambda}{\rho \cdot c} \cdot \nabla^2 T(\vec{r}, t) + \frac{1}{\rho \cdot c} \cdot \frac{dP}{dV}(\vec{r}, t) \quad \text{Equation 48}$$

Where  $\rho$  is the mass density,  $c$  the specific heat and  $\lambda$  the heat conductivity of the material. The heat source  $\frac{dP}{dV}(\vec{r}, t)$  describes how much power is dissipated per unit of volume at the position  $\vec{r}$  and at the time  $t$ . The square of the Nabla operator on the scalar function  $T$  is equivalent to the Laplace operator and can also be written as  $\nabla^2 T = \text{div grad } T$ . The boundary and initial conditions have to be set according to the specific problem. A full quantitative solution of the heat equation can be achieved with finite element codes, e.g. like ANSYS [4]. Nevertheless some analytical solutions can be derived at simple geometries and simplified boundary conditions.

The beam dump layout is a cylindrical problem with rotational symmetry (no azimuthal dependence), in which the position  $\vec{r}$  is adequately described by  $r$  and  $z$ , The Nabla operator in cylinder coordinates is fully expressed as:

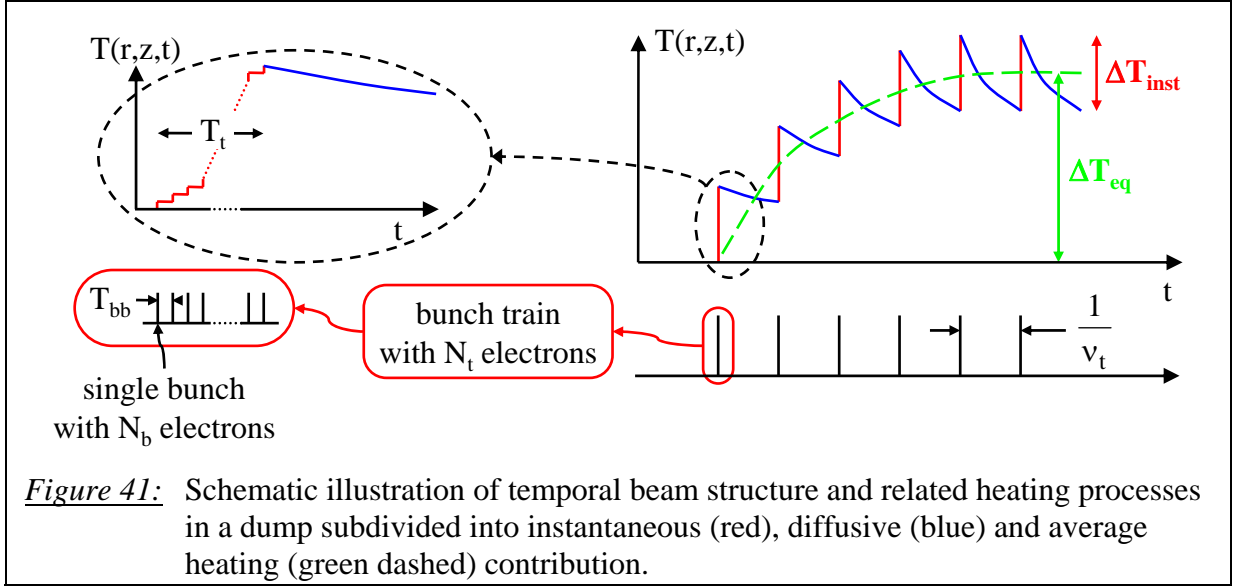
$$\nabla^2 T(r, z) = \frac{1}{r} \frac{\partial}{\partial r} \left( r \frac{\partial T(r, z)}{\partial r} \right) + \underbrace{\frac{\partial^2 T(r, z)}{\partial z^2}}_{=0} + \underbrace{\frac{1}{r^2} \frac{\partial^2 T(r, z)}{\partial \varphi^2}}_{=0} \quad \text{Equation 49}$$

The last two terms are set to zero, because of rotational symmetry and considering pure radial heat flow only. The latter assumption is conservative on the one hand and fairly reasonable on the other hand, since thermal expansion and stress considerations most probably require longitudinal sectioning of an absorber (at least of its core), which interrupts longitudinal heat flow too. Under the given assumptions the heat equation reduces to:

$$\frac{\partial}{\partial t} T(r, z, t) = \frac{\lambda}{\rho \cdot c} \cdot \frac{1}{r} \frac{\partial}{\partial r} \left( r \frac{\partial T(r, z, t)}{\partial r} \right) + \frac{1}{\rho \cdot c} \cdot \frac{dP}{dV}(r, z, t) \quad \text{Equation 50}$$

The next approximation is related to the heat source term, which is driven by a pulsed beam. It is possible to solve the heat equation piecewise within different aspects of time during the pulsed heating process, as will be explained by means of Figure 41. The beam consists of bunch trains carrying a total number of  $N_t$  electrons and repeating with a frequency of  $\nu_t \leq 10\text{Hz}$ . The train itself has a length of  $T_t \leq 0.8\text{ms}$  and consists of sub-picosecond long electron bunches separated in time by  $T_{bb} \geq 200\text{ns}$ .

Starting with an absorber of uniform temperature, the first electron of the beam creates a certain profile of deposited energy in the material. This will immediately, namely instantaneously transform in a temperature profile according to the heat capacity of the material. The spatial gradient of the temperature profile is now responsible, that the deposited heat starts to spread out. It diffuses in the direction of colder regions in order to equalize the temperature profile. The next electron brings in the second portion of energy, which adds to



the energy profile as resulting from the first electron including heat diffusion within the time between the arrival of the first and the second electron. In principle this sum has to be evaluated for all successive electrons of a bunch, a train of bunches and repeating bunch trains.

However heat diffusion is a slow process and broadening of a given temperature profile within the time  $t$  is given by the characteristic thermal diffusion length  $\Lambda$ :

$$\Lambda(t) = \sqrt{a \cdot t} \quad \text{with: } a = \frac{\lambda}{\rho \cdot c} \quad \text{Equation 51}$$

For materials like graphite, aluminium or copper the thermal diffusion length even within the relatively long bunch train passage time  $t = T_t = 0.8\text{ms}$  is only about 0.25mm to 0.3mm and therefore small compared to the width of deposited energy profile in most cases. Thus it is reasonable to neglect thermal diffusion during the passage of a bunch train and consider the related heating as an instantaneous process independent of the temporal bunch structure within the train.

When the bunch structure is not relevant anymore for heating aspects, the heat source  $dP/dV$  can be simplified to be constant in time over the period of the bunch train  $T_t$  and zero between subsequent trains, i.e.:

$$\frac{dP}{dV}(r, z, t) = \begin{cases} N_t \cdot \varepsilon(r, z) / T_t & \text{for } \frac{n}{v_t} \leq t \leq \frac{n}{v_t} + T_t \quad ; n = 0, 1, 2, 3, 4, \dots \\ 0 & \text{for any other time} \end{cases} \quad \text{Equation 52}$$

Where  $N_t$  is the number of electrons within one bunch train,  $v_t$  is the repetition frequency of the bunch trains and  $\varepsilon(r, z)$  is the energy deposition per unit of volume induced by one primary electron impinging on the absorber as extensively discussed in annex A.

Furthermore we can now apply the above considerations on heating to subsequent bunch trains instead of single electrons. We assume an absorber of certain geometry including a heat sink with a constant temperature of  $T_0$ , which defines the temperature at any point in the absorber, when it has not been operated with beam since a long time. When the first train enters, it causes an instantaneous temperature rise  $\Delta T_{\text{inst}}$  at a certain position in the material as shown in Figure 41. Before the next train enters, the temperature decays by diffusion to a certain extend, but not down to the initial value. After the next train, the temperature has increased again by  $\Delta T_{\text{inst}}$  and is now in total higher than after the first train. Train by train the

average temperature level increases up to a quasi steady state situation, in which the temperature growth  $\Delta T_{\text{inst}}$  induced by one bunch train equals to the decay that occurs between subsequent bunch trains due to heat diffusion. The equilibrium temperature rise  $\Delta T_{\text{eq}}$ , around which the saw-tooth like mechanism of instantaneous heating and diffusion oscillates, would actually appear, if the beam was not pulsed, but was constant in time with an amplitude of  $I_{\text{ave}} = N_t \cdot e \cdot v_t$ .

According to this consideration a conservative upper limit of the temperature  $T(r,z)$  at a given position in the absorber, when quasi steady state has reached, is:

$$T(r,z) \leq T_0 + \Delta T_{\text{inst}}(r,z) + \Delta T_{\text{eq}}(r,z) \quad \text{Equation 53}$$

Additionally it has been shown, that the pulsed heating of an absorber can be divided into 3 different time regimes:

1. Instantaneous heating during the bunch train passage
2. Heat diffusion between subsequent bunch trains
3. Average heating due to the average beam current

Each of which will be analyzed in more detail in the following sections B.1 to B.3.

As a result of this analysis  $\Delta T_{\text{inst}}$  and  $\Delta T_{\text{eq}}$  can be evaluated especially when the Grindhammer parameterization is used to describe the radial energy deposition profile. Thus the upper limit of the temperature, as defined by Equation 53 along the axis ( $r=0$ ) of a homogeneous cylindrical absorber can be written as:

$$T(r=0,z) \leq T_0 + \frac{dE}{dz}(z) \cdot \frac{1}{\rho \cdot c} \cdot \frac{N_t}{2\pi \sigma^2(z)} + \frac{dP}{dz}(z) \cdot \frac{1}{4\pi \lambda} \cdot \ln \left( 1 + \frac{R^2}{2\sigma^2(z)} \right)$$

$$\Leftrightarrow \text{since: } \frac{dP}{dz}(z) = \frac{I_{\text{ave}}}{e} \cdot \frac{dE}{dz}(z) = N_t \cdot v_t \cdot \frac{dE}{dz}(z) \quad \text{Equation 54}$$

$$T(r=0,z) \leq T_0 + \frac{dE}{dz}(z) \cdot \frac{N_t}{2\pi} \cdot \left[ \frac{1}{\rho \cdot c \cdot \sigma^2(z)} + \frac{v_t}{2 \cdot \lambda} \cdot \ln \left( 1 + \frac{R^2}{2\sigma^2(z)} \right) \right]$$

Where  $T_0$  is the temperature of the heat sink, which is the cooling water at the circumference of the absorber with outer radius  $R$ . Absorber properties like mass density, specific heat capacity and thermal conductivity are expressed by  $\rho$ ,  $c$  and  $\lambda$ . Bunch train population and repetition rate are given by  $N_t$  and  $v_t$ . The longitudinal energy density  $dE(z)/dz$  per one primary electron and the longitudinal power density  $dP(z)/dz$  as generated by an average beam current  $I_{\text{ave}}$ , are defined in Equation 30 and Equation 36 respectively. The width parameter of the Grindhammer distribution (see Equation 43) is given by  $\sigma(z)$ .

By means of simplified assumptions, namely cylindrical geometry with pure radial heat flow only and separating instantaneous from equilibrium heating, temperatures in a given cylindrical solid dump geometry can be easily calculated. As an input generally EMS simulations have to be carried out in order to get  $\varepsilon(r,z)$  on which basis either everything can be calculated numerically or  $dE(z)/dz$  and  $\sigma(z)$  can be derived to make use of analytical calculations with the Grindhammer distribution.

But as has been shown in annex A.1.1,  $dE/dz$  at  $z=0$  and  $z=t_{\text{max}}$  can be estimated by the material parameters and the incoming beam energy. Since  $\sigma(z=0) = \sigma_{\text{beam}}$ , temperature calculations at the beginning of a shower respectively in beam windows can be done without

an EMS code. Under some conditions, this is also valid for temperature estimations at the shower maximum, e.g. if  $\sigma_{\text{beam}} \gg \sigma_s(t_{\text{max}})$ .

### B.1 Instantaneous Heating

The heating process during the period  $T_t$  of a bunch train passage was approximated to be instantaneous. In that case the diffusion term of the heat equation can be set to zero, i.e.  $\text{div grad } T(r, z, t) = 0$ . The heat source within this period neglects the bunch structure and is expressed as:  $\frac{dP}{dV}(r, z, t) = N_t \cdot \varepsilon(r, z)/T_t$ . Finally the temporal change of temperature is simply obtained by:  $\frac{\partial}{\partial t} T(r, z, t) = \Delta T_{\text{inst}}(r, z)/T_t$ . Writing the heat equation (see Equation 50) with these boundary conditions gives:

$$\frac{\partial}{\partial t} T(r, z, t) = \frac{1}{\rho \cdot c} \cdot \frac{dP}{dV}(r, z, t) \Leftrightarrow \frac{\Delta T_{\text{inst}}(r, z)}{T_t} = \frac{1}{\rho \cdot c} \cdot \frac{N_t \cdot \varepsilon(r, z)}{T_t} \quad \text{Equation 55}$$

$$\Rightarrow \Delta T_{\text{inst}}(r, z) = \frac{N_t}{\rho \cdot c} \cdot \varepsilon(r, z) = \frac{N_t}{\rho \cdot c} \cdot \frac{dE}{dz}(z) \cdot f(r, z) = \frac{N_t}{c} \cdot \frac{dE}{dm}(r, z)$$

This solution just expresses, if thermal diffusion effects are negligible, the temperature rise  $\Delta T_{\text{inst}}$  caused by one bunch train passage is directly proportional to the distribution of deposited energy. If  $f(r, z)$  is replaced by the Grindhammer function  $f_{\text{gh}}$  (see Equation 43) we get:

$$\Delta T_{\text{inst}}(r, z) = \frac{N_t}{\rho \cdot c} \cdot \frac{dE}{dz}(z) \cdot \frac{2 \cdot \sigma^2(z)}{\pi \cdot (r^2 + 2 \cdot \sigma^2(z))^2} \quad \text{Equation 56}$$

respectively on the shower axis at  $r=0$ :

$$\Delta T_{\text{inst}}(r=0, z) = \frac{N_t}{\rho \cdot c} \cdot \frac{dE}{dz}(z) \cdot \frac{1}{2\pi \cdot \sigma^2(z)}$$

The maximum instantaneous temperature rise  $\max(\Delta T_{\text{inst}})$  in the absorber is of course defined by:

$$\max(\Delta T_{\text{inst}}) = \frac{N_t}{c} \cdot \max\left(\frac{dE}{dm}\right) \quad \text{Equation 57}$$

It is located at  $z = t_E$  on the shower axis  $r=0$  between the dump entrance and the shower maximum, depending on the incoming beam size (see explanation on page 65).

Thermal diffusion is not negligible, if the transverse profile of deposited energy has a width in the order of the thermal diffusion length or less, i.e.  $\sigma(z) \leq \Lambda(T_t)$ . In such cases the deposited energy profile spreads significantly within the bunch train passage time and the resulting heating goes less than linearly with  $\varepsilon(r, z)$ . Thus Equation 56 gives a conservative upper limit of the temperature rise induced by the passage of one bunch train.

All given equations here assume, that the specific heat capacity does not depend on the temperature. In some cases, such as graphite, the specific heat capacity varies rather strong with temperature and the exact way to define the instantaneous temperature rise is:

$$\int_{T_i}^{T_i + \Delta T_{\text{inst}}(r,z)} c(T) dT = N_t \cdot \frac{dE}{dm}(r,z) \quad \text{Equation 58}$$

Where  $T_i$  denotes the initial temperature from whose level the instantaneous heating starts.

## B.2 Heat Diffusion

The time period between two bunch trains is characterized by pure heat diffusion in the absence of a heat source, i.e.  $\frac{dP}{dV}(r,z,t) = 0$ . Therefore the temporal development of the temperature profile has to obey the following heat equation:

$$\frac{\partial}{\partial t} T(r,z,t) = \frac{\lambda}{\rho \cdot c} \cdot \frac{1}{r} \frac{\partial}{\partial r} \left( r \frac{\partial}{\partial r} T(r,z,t) \right) \quad \text{Equation 59}$$

We consider an infinite transverse slice of homogeneous material with a thickness of  $dz$ . At the time  $t_0$  the overall energy  $dQ$  in that slice is assumed to have a gaussian radial profile. The temperature profile at time  $t_0$  obviously is then:

$$T(r,z,t_0) = \frac{1}{\rho \cdot c} \cdot \frac{dQ}{dz}(z) \cdot \frac{1}{2\pi\sigma^2(z)} \cdot e^{-\frac{r^2}{2\sigma^2(z)}} \quad \text{Equation 60}$$

At a time  $t_0 + t$  the solution of the pure diffusive heat equation (see Equation 59) with such an initial gaussian temperature profile gives:

$$T(r,z,t_0 + t) = \frac{1}{\rho \cdot c} \cdot \frac{dQ}{dz}(z) \cdot \frac{1}{2\pi(\sigma^2(z) + 2at)} \cdot e^{-\frac{r^2}{2(\sigma^2(z) + 2at)}} \quad \text{with: } a = \frac{\lambda}{\rho \cdot c} \quad \text{Equation 61}$$

In other words under the influence of thermal diffusion, a gaussian temperature profile maintains its gaussian shape, but its width increases in time like:

$$\sigma^2(z,t_0 + t) = \sigma^2(z,t_0) + 2 \cdot a \cdot t = \sigma^2(z,t_0) + 2 \cdot \Lambda^2(t) \quad \text{with: } a = \frac{\lambda}{\rho \cdot c} \quad \text{Equation 62}$$

Here  $\Lambda(t)$  is the thermal diffusion length as defined in Equation 51. The given result enables to study the diffusive development of a variety of differently shaped initial temperature profiles, because in most of the cases they can be approximated as the sum of two or more Gaussians.

## B.3 Average Heating

When asking for the average temperature at a certain position, one has to solve the heat equation for the time independent stationary case, i.e.  $\frac{\partial}{\partial t} T(r,z,t) = 0$ . Solution of an equilibrium situation requires the full knowledge of the geometry of the absorber including its heat sink. Here we assume a cylindrical homogeneous absorber with an outer radius  $R$ , where it is cooled. The beam with an average current of  $I_{\text{ave}} = N_t \cdot e \cdot v_t$  hits the front face of this absorber perpendicular at the center  $r=0$ . In average the beam dissipates power in the material, as given by the heat source  $\frac{dP}{dV}(r,z) = N_t \cdot v_t \cdot \varepsilon(r,z)$ . In equilibrium the dissipated power equals the heat, which flows radially towards the heat sink at the circumference  $r=R$ . As a consequence of this heat flow the temperature drop  $\Delta T_{\text{eq}}(r,z)$ , which builds up between a radius  $r$  in the absorber and its outer radius  $R$ , is the solution of the stationary heat equation:

$$\begin{aligned}
0 &= \frac{\lambda}{\rho \cdot c} \cdot \frac{1}{r} \frac{\partial}{\partial r} \left( r \frac{\partial}{\partial r} \Delta T_{\text{eq}}(r, z) \right) + \frac{1}{\rho \cdot c} \cdot \frac{dP}{dV}(r, z) \\
\Leftrightarrow & \quad - \frac{N_t \cdot v_t}{\lambda} \cdot \varepsilon(r, z) = \frac{1}{r} \frac{\partial}{\partial r} \left( r \frac{\partial}{\partial r} \Delta T_{\text{eq}}(r, z) \right) \quad \text{Equation 63} \\
\Rightarrow & \quad \Delta T_{\text{eq}}(r, z) = \frac{N_t \cdot v_t}{\lambda} \cdot \int_{s=r}^R \frac{ds}{s} \int_{u=0}^s \varepsilon(u, z) \cdot u \cdot du
\end{aligned}$$

This equation may be either integrated numerically or analytically. The later case is possible if  $\varepsilon(r, z)$  is expressed by the Grindhammer parameterization. In that case integration of Equation 63 gives:

$$\Delta T_{\text{eq}}(r, z) = \frac{1}{4\pi \cdot \lambda} \cdot \frac{dP}{dz}(z) \cdot \ln \left[ \frac{1 + \frac{R^2}{2\sigma^2(z)}}{1 + \frac{r^2}{2\sigma^2(z)}} \right] \quad \text{with: } \frac{dP}{dz}(z) = N_t \cdot v_t \cdot \frac{dE}{dz}(z) \quad \text{Equation 64}$$

The maximum equilibrium temperature rise in the absorber will of course establish on the shower axis ( $r=0$ ) at the shower maximum ( $z=t_{\text{max}}$ ), where the dissipated power per unit length peaks, hence:

$$\max(\Delta T_{\text{eq}}) = \Delta T_{\text{eq}}(r=0, z=t_{\text{max}}) = \frac{1}{4\pi \cdot \lambda} \cdot \frac{dP}{dz}(t_{\text{max}}) \cdot \ln \left[ 1 + \frac{R^2}{2\sigma^2(t_{\text{max}})} \right] \quad \text{Equation 65}$$

The term  $\frac{dP}{dz}(t_{\text{max}}) = \max\left(\frac{dP}{dz}\right)$  can be calculated by Equation 38 on page 63.

In some cases it is quite useful to estimate the temperature drop  $\Delta T_{\text{eq}}(r_1, r_2, z)$  across a radial layer between  $r_1$  and  $r_2$  ( $r_1 < r_2$ ), which is out of the shower core and therefore barely influenced by direct energy impact. In other words practically all power  $dP(z)/dz$  is dissipated within  $r_1$ , i.e.  $\varepsilon(r \geq r_1, z) \approx 0$ . For that case the heat equation gives the simple solution:

$$\begin{aligned}
\Delta T_{\text{eq}}(r_1, r_2, z) &= \frac{1}{2\pi \cdot \lambda} \cdot \frac{dP}{dz}(z) \cdot \ln \left( \frac{r_2}{r_1} \right) \\
\text{with: } \frac{dP}{dz}(z) &= N_t \cdot v_t \cdot \int_{r=0}^{\infty} \varepsilon(r, z) \cdot 2\pi r \, dr \approx N_t \cdot v_t \cdot \int_{r=0}^{r_1} \varepsilon(r, z) \cdot 2\pi r \, dr
\end{aligned} \quad \text{Equation 66}$$

In principle this solution could have been derived also from Equation 64 in the approximation of  $2\sigma^2(z) \ll r^2, R^2$ .

This result can be applied for example if the beam is in average distributed (swept) along a circle with radius  $R_s$  across the face of the absorber, instead of hitting its center. If we now neglect the radial extension of the shower, i.e.  $R_s \gg \sigma(z)$ , then a rough upper estimate on the equilibrium temperature drop between the sweep radius  $R_s$  and the outer radius  $R$  of the absorber can be done with Equation 66 like:

$$\Delta T_{\text{eq}}(R_s, R, z) = \frac{1}{2\pi \cdot \lambda} \cdot \frac{dP}{dz}(z) \cdot \ln \left( \frac{R}{R_s} \right) \quad \text{Equation 67}$$

## References

- [1] European XFEL Project Team, *European X-Ray Free Electron Laser Facility, Technical Design Report*, edited by M. Altarelli et al., Deutsches Elektronen Synchrotron, Hamburg, 2006
- [2] N. V. Mokhov, *The MARS Code System Users Guide*, Version 13 (95), Fermilab-FN-628, 1995  
N. V. Mokhov et al., Fermilab-Conf-98/379, 1998  
<http://www-ap.fnal.gov/MARS/>
- [3] L. Issler, H. Ruöß, P. Häfele, *Festigkeitslehre-Grundlagen*, Springer Verlag, Berlin, Dezember 2003
- [4] Awenson Analysis Systems Inc., *ANSYS User Manual*, 1983
- [5] V. Popov, *Heat Exchange in Contact Zones of detachable and non-detachable Units*, Energy Press, Moscow, 1971
- [6] Particle Data Group, *Particle Physics Booklet*, July 1996
- [7] B. Rossi, *High-Energy Particles*, Prentice-Hall, New York, 1952
- [8] G. Grindhammer et al., *The fast Estimation of Electromagnetic Showers*, NIM A290 pages 469-488, 1990